ABSTRACT

ACHINIVU, EZINNE CHIDIEBERE. Isolation and Recovery of Lignin from Lignocellulosic Biomass Using Recyclable Protic Ionic Liquids (PILs) for a Cost-Effective Biomass Processing Technique. (Under the direction of Dr. Wesley A. Henderson).

Effectively partitioning lignocellulosic biomass into its various fractions−cellulose, hemicellulose and lignin−is essential for the implementation of a biofuel/biorefinery-based economy. In particular, an efficient, low-cost technique for the removal and recovery of lignin, the component that largely renders biomass intractable, is necessary to facilitate easier access to the polysaccharides and the production of valuable side-product streams based on lignin. Current separation techniques for lignin removal suffer significant drawbacks such as being energy intensive and environmentally harmful, and need to be optimized to minimize waste generation and resource (lignin) underutilization.

A highly effective method has been developed for the simple extraction of lignin from lignocellulosic biomass using potentially inexpensive protic ionic liquids (PILs). Solubility tests with commercially available biomass components, in conjunction with the physical and chemical properties of the PILs, were correlated with the lignin extraction efficiency of the PILs in actual biomass (cornstover). These results indicate that increasing the xylan (i.e., hemicellulose) solubility in the PILs and dispersing the cellulose results in greater fiber disruption/penetration, which significantly enhances the effectiveness of the lignin extraction. Systematic variations in the cation supported by Raman spectroscopy and force field calculations confirms that PILs from cyclic amines favor xylan solubility as these PILs are more ionic and PILs from alkanolamines are able to participate in hydrogen bonding

with the polysaccharides and disperse the cellulose. In particular, the PIL ethanolammonium acetate, i.e., [Eth][Ac], is able to extract up to 85% of the lignin found in cornstover.

The effect of hydrogen bonding in the PIL is further analyzed in order to design a PIL with increased lignin extraction efficiency. Analysis of lactate-PILs indicates that hydrogen bonds play an important role in the physiochemical properties of the PILs, but the trend in lignin extraction for the PILs still follow the trend in ionicity expected. Therefore, ionic interactions are the dominant factor that contributes to lignin removal–with hydrogen bonding slightly improving the ionic effect. The developed method for lignin extraction was also effectively applied to remove lignin from switchgrass, but woody materials such as pinewood and beech wood were not favorable for this lignin removal process.

After the lignin-extraction step, the PILs are easily recovered using distillation leaving the separated lignin and cellulose-rich residues available for further processing. Complete PIL recovery was hindered by the formation of unwanted side products (amides) in the [Pyrr][Ac] PIL. The [Eth][Ac] PIL, however, showed no formation of amides, but have a PIL lower recovery rate (90%) due to the high temperature requirement for distillation induced by the increased hydrogen bonding in this PIL. Careful selection of the PIL ions is necessary to develop a PIL with balanced properties for the recovery of pure PILs at a high yield.

The lignin extract and the cellulose-rich pulp were physically, chemically, and thermally characterized. Lignin characterization shows that the PILs fragment the lignin molecules during the extraction/dissolution process. The more ionic [Pyrr][Ac] PIL fragments the lignin to smaller sized particles and results in a more homogenous distribution of lignin particle sizes. Cellulose-rich residues are shown to have increased fiber size

(swelling) and the formation of pores on the fiber surface is observed. The crystallinity (phase and amount), however, is largely unchanged. Using PILs, a simple yet effective method has been developed for the removal of lignin from biomass, which should greatly aid in the implementation of an economically viable integrated multi-product biorefinery.

Isolation and Recovery of Lignin from Lignocellulosic Biomass Using Recyclable Protic Ionic Liquids (PILs) for a Cost-Effective Biomass Processing Technique

by
Ezinne Chidiebere Achinivu

A dissertation submitted to the Graduate Faculty of
North Carolina State University
in partial fulfillment of the
requirements for the degree of
Doctor of Philosophy

Chemical Engineering

Raleigh, North Carolina

2014

APPROVED BY:

_____	_____
Dr. Wesley A. Henderson Committee Chair	Dr. Phillip Westmoreland
_____	_____
Dr. Sunkyu Park	Dr. Steven Peretti

DEDICATION

This dissertation is dedicated to my family Dr. Ochi Achinivu, Evangelist. Chinyere Achinivu, Achinivu Achinivu and Chibuzo Achinivu who have supported me through out the course of my life and have jeered me on to succeed in my destined career.

BIOGRAPHY

Ezinne Chidiebere Achinivu was born to parents Ochiabuto and Chinyere Achinivu in Berkeley, California. A couple of years later, the family relocated to Lagos, Nigeria where she completed a majority of her elementary and secondary education, and finally to Abuja Nigeria. After graduating form Vivian Fowler Memorial College for girls (Secondary school) in 2005, she attended the University of Maryland College Park. Soon after (2010) she received her Bachelor of Science in Chemical engineering, and continued her postgraduate education at North Carolina State University where she will be receiving her PhD degree.

ACKNOWLEDGMENTS

I am grateful to God for his grace and favor in directing my footsteps to North Carolina State University where I completed my PhD thesis. It was truly an intricate well thought out design involving multiple situations and circumstances that led me to that chosen path and the successful completion of my thesis. While at NC State, the collegiate atmosphere represented by the Chemical and Biomolecular engineering department was very conducive for academic progress while catering to the physical, financial, social, and moral needs of the students. The faculty, staff (Mrs. Sandra Bailey), and students are all greatly appreciated.

I specifically would like to recognize my research advisor, Dr. Wesley A. Henderson, who I believe was one of the most effective advisors in the department. His organizational skills, attention to detail, determination and rigor towards research were skills I greatly admired, and were also necessary for producing quality academic research. Dr. Henderson, being quite knowledgeable, was a valuable resource in research design and execution, professional writing, and also offered personal guidance with managing the stresses of graduate school. I am deeply grateful for his time and attention during the course of my PhD. I pray for God's blessing to be returned to you in kind (in guidance and even financially for the multiple free lunches/dinners he also provided). I am also very thankful to my committee members (Dr. Philip Westmoreland, Dr. Steven Peretti, and Dr. Sunkyu Park) who provided guidance on my project outside of the required committee meetings. They were quite flexible and interested in me progressing my project, which led to research collaborations.

My research group also played a significant role in my PhD career. Each member consciously kept the lab/office environment favorable for working, and also provided support on various equipments/instrumentation. The ILEET alum are as follows Drs. Xingling Geng, Qian Zhou, Kate Brown, Daniel Seo, Eric Fox, Josh Allen, Sang-Don Han, and Dennis McOwen. I am also indebted to the various research assistants who worked with me and provided invaluable support on my research project. The students were Gouqing Li, Reagan Howard, Drew Williams, George Marshall, and Michael Brews. I wish you all the greatest success as you continue your promising careers and may God reward your time and effort appropriately.

I would also like to recognize all the research groups that allowed me to utilize their instrumentation and were very hospitable while I worked in your lab. The timely completion of my thesis depended heavily on the availability/use of these instruments. The groups and instruments were: Dr. Orlin Velev (UV-Vis), Dr. Gregory Parsons (SEM), Dr. Fanxing Li (TGA) and Dr. Dhana Savithri (HPLC and IC) and Dr. Sunkyu Park (GPC) Dr. Hanna Gracz (NMR).

Finally I would like to thank my family and friends (JCCI and JYAM) for their support prayers and words of encouragement. I would like to express my deep gratitude to my Mum & Dad for your prayers, consistent calls, and financial support, and to Pastor Toyin Tofade for your guidance while I was on the journey of self-discovery.

"Arise, shine, for your light has come, and the glory of the LORD rises upon you … The least of you will become a thousand, the smallest a mighty nation. I am the LORD; in its time I will do this swiftly." Isaiah 60

TABLE OF CONTENTS

LIST OF TABLES xii

LIST OF FIGURES xv

LIST OF SCHEMES xxii

CHAPTER 1: Introduction 1

1.1. Motivation 1

1.2. Lignocellulosic biomass: Biomass components (biopolymers) and structure 6

1.2.1. Cellulose 6

1.2.2. Hemicellulose 7

1.2.3. Lignin 8

1.2.4. Tertiary Structure 12

1.3. Current Methods for Biomass Fractionation (Pretreatment) 13

1.3.1. Ionic Liquids (ILs) 14

1.3.2 PILs and Lignin Dissolution 14

CHAPTER 2: Materials and Methods 24

2.1 Materials 24

2.1.1 Reagents and Solvents Used 24

2.1.2 Biomass/Biopolymer Preparation 24

2.2. Instrumentation 25

2.2.1 Karl Fischer.....25

2.2.2 Differential Scanning Calorimetry (DSC) 25

2.2.3 Thermogravimetric Analysis (TGA).....26

2.2.4 Density/Viscosity Measurements.....26

2.2.5 Conductivity Measurements 26

2.2.6 Nuclear Magnetic Resonance (NMR) Spectroscopy 27

2.2.7 FT–IR Spectroscopy 27

2.2.8 Raman Spectroscopy.....27

2.2.9 Ultraviolet/Visible (UV/VIS) Spectrophotometry.....28

2.2.10 Ion Chromatography (IC) 28

2.2.11 Gel Permeation Chromatography (GPC).....29

2.2.12 X–Ray Diffraction (XRD) 29

2.2.13 Imaging 29

2.3. PIL Synthesis and Characterization.....30

2.4. Biopolymer Solubility Tests 30

2.5. Degree of Cellulose Dispersion 31

2.6. PIL Distillation/Recovery Tests....31

2.7. PIL Heating (Stability) Test....32

2.8. Biomass Dissolution: Pretreatment....32

2.9. Biomass Characterization: Compositional Analysis....33

2.10. Rapid Biomass Treatment and Analysis....34

2.11. Enzymatic Hydrolysis....35

2.12. Determination of Kamlet–Taft Solubility Parameters....36

2.13. Molecular Weight Determination....38

CHAPTER 3: Lignin Extraction from Biomass Using PILs: A Short Study....41

3.1. Introduction....41

3.2. PIL Characterization: Ionicity and Thermal Stability....43

3.3. Solubility of Biopolymers in PILs....46

3.4. Lignin Extractability from Biomass....50

3.5. PIL Recyclability and Characterization of Recovered Materials....55

3.6. Concerns about the Purity of the Recovered PILs....62

3.7. Conclusions....70

CHAPTER 4: Predictors for an Enhanced Lignin Removal from Lignocellulosic Biomass

....75

4.1. Introduction 75

4.2. Effect of Structural Changes in the Cation of Acetate PILs on Biopolymer Solubility Tests 80

4.2.1. Solubility of Microcrystalline Cellulose in PILs 85

4.2.2. Solubility of Kraft Lignin and Organosolv Lignin in PILs 85

4.2.3. Solubility of Xylan in PILs 86

4.3. Energy Minimization 90

4.4. Raman Spectroscopy 96

4.5. Cellulose Dispersion 97

4.6. Monomer Solubility Tests 100

4.7. Conclusions 101

CHAPTER 5: [Eth][Ac] as a model solvent for lignin removal from biomass 107

5.1. Introduction 107

5.2. PIL Characterization 109

5.3. Solubility of Biopolymers in PILs 112

5.4. Lignin Extractability From Biomass 117

5.5. Recyclability and Concerns About Purity Readdressed 120

5.6. Viscosity Reduction 126

5.7. Lignin Removal from Multiple Biomass Sources 130

5.8. Conclusions.....133

CHAPTER 6: Lignin Characterization Commentary 137

6. 1. Introduction.....137

6. 2. Elemental Analysis 138

6. 3. Molecular Weight Distribution.....140

6. 4. Lignin FT-IR Analyses 143

6. 5. Energy Minimization 148

6. 6. Effect of the Solvent Type on Lignin Regeneration 153

6. 7. Conclusions.....159

CONCLUSIONS 161

APPENDICES 163

Appendix A.....164

Appendix B 165

Appendix C 167

Appendix D.....175

Appendix E 193

LIST OF TABLES

CHAPTER 1

Table 1. 1 Typical chemical composition of various lignocellulosic materials 4

Table 1. 2. Typical composition of the common linkages found in lignin.....9

CHAPTER 3

Table 3. 1. Solubility of Kraft lignin, cellulose and xylan (% w/w) in the reagents and PILs (after heating/stirring at 90 °C for 24 h).....50

Table 3. 2. Composition (% w/w) of EF-CS and PIL-CS after pretreatment (90 °C for 24 h) 51

Table 3. 3. Composition of corn stover components after pretreatment with [Pyrr][Ac]—amount recovered, g (% w/w of initial component in EF-CS) 52

Table 3. 4. PIL yield after recovery from each PIL, distillation conditions and mole ratio of acid-to-base from NMR analysis 56

CHAPTER 4

Table 4. 1. ΔpK_a values for the reagents used to synthesize PILs.....80

Table 4. 2. Solubility of Kraft lignin, cellulose and xylan (% w/w) in the reagents and PILs from noncyclic aliphatic amine bases (after heating/stirring at 90 °C for 24 h)...81

Table 4. 3. Solubility of Kraft lignin, cellulose and xylan (% w/w) in the reagents and PILs from cyclic aliphatic amine bases (after heating/stirring at 90 °C for 24 h) 82

Table 4. 4. Solubility of Kraft lignin, cellulose and xylan (% w/w) in the reagents and PILs from aromatic amine bases (after heating/stirring at 90 °C for 24 h) 83

Table 4. 5. Solubility of Kraft lignin, cellulose and xylan (% w/w) in the reagents and PILs from oxygenated aliphatic amine bases (after heating/stirring at 90 °C for 24 h) 84

Table 4. 6. Solubility of Kraft lignin, cellulose and xylan (% w/w) in the reagents and PILs from hybrid (oxygenated-cyclic-aliphatic) amine bases (after heating/stirring at 90 °C for 24 h) 84

CHAPTER 5

Table 5. 1. Solubility of Kraft lignin, cellulose and xylan (% w/w) in the OAA PILs and reagents mixtures (after heating/stirring at 90 °C for 24 h) 114

Table 5. 2. Composition (% w/w) of EF-CS and PIL-CS after pretreatment (90 °C for 24 h). 118

Table 5. 3. Qualitatively determined solubility of Kraft lignin, cellulose and xylan (% w/w) in the the DMSO/[Eth][Ac] mixtures (after heating/stirring at 90 °C for 24 h) ...129

CHAPTER 6

Table 6. 1. Elemental analysis and C_{900} empirical formula of the lignins 139

Table 6. 2. Weight-average (M_w) and number-average (M_n) molecular weights (g mol^{-1}) and polydispersity (M_w / M_n) of the Kraft lignin recovered from PIL dissolution and the lignin extracted from CS using the [Pyrr][Ac] PIL 142

Table 6. 3. Absorption peak assignment in FT-IR spectra of Kraft lignin recovered from PIL dissolution and the lignin extracted from CS using the [Py][Ac] PIL.....147

LIST OF FIGURES

CHAPTER 1

Figure 1. 1. Geographic locations (in the U.S.) of lignocellulosic biomass resources 2

Figure 1. 2. Fossil energy ratio (FER) for cellulosic ethanol production in comparison to conventional energy sources 2

Figure 1. 3. Pretreatment of biomass showing the effect of lignin removal and resulting reduction in cellulose crystallinity 4

Figure 1. 4. Representative structures that give rise to the biopolymers cellulose, hemicellulose, and lignin in nature 8

Figure 1. 5. Common phenyl propane linkages in lignin 9

Figure 1. 6. Representation of a lignin polymer model 10

Figure 1. 7. Microscopic to macroscopic view of a typical representation of lignocellulosic biomass 11

Figure 1. 8. Image describing the integrated multi-product biorefinery concept as biomass is being processed to biofuels and bioproducts 12

CHAPTER 2

Figure 2. 1. Solvatochromic dye molecules used to determine the Kamlet-Taft solubility parameters 37

CHAPTER 3

Figure 3. 1. PIL ions and their abbreviations: pyridinium $[Py]^+$, 1-methylimidazolium $[Mim]^+$, pyrrolidinium $[Pyrr]^+$ and acetate $[Ac]^-$. 43

Figure 3. 2. Walden Plot as a measure of ionicity for PILs used in this study 44

Figure 3. 3. Variable-temperature TGA heating traces (5 °C min^{-1}) of reagents and PILs ..45

Figure 3. 4. Images depicting the solubility of 5% w/w commercially available biomass components (Kraft lignin, microcrystalline cellulose and xylan) in the PILs: (a) after stirring for 30 min at room temperature (25 °C) and (b) after stirring for 24 h at 90 °C (sample sizes were 10.0 g) 48

Figure 3. 5. Images depicting the solubility of 5% w/w commercially available biomass components (Kraft lignin, microcrystalline cellulose and xylan) in reagents used to synthesize the PILs: (a) after stirring for 30 min at room temperature (25 °C) and (b) after stirring for 24 h at 90 °C (sample sizes were 10.0 g). 49

Figure 3. 6. Images depicting the CS fibers before and after PIL treatment and the recovered lignin from CS after PIL treatment: (a) EF-CS, (b) [Py][Ac]-CS, (c) [Mim][Ac]-CS and (d) [Pyrr][Ac]-CS 53

Figure 3. 7. XRD of CS recovered from PIL pretreatment.....54

Figure 3. 8. Rate of lignin removal (% e is percent extracted) from CS with the [Pyrr][Ac] PIL using UV/VIS analysis (absorbance data shown on left, compositional analysis data shown on right) 54

Figure 3. 9. Photographic images (a) 2x and (b) 10x of original (Kraft lignin) and recovered lignin from PIL dissolution 57

Figure 3. 10. Variable-temperature TGA heating traces of PILs before and after recycling 58

Figure 3. 11. Variable-temperature TGA heating traces of original (Kraft lignin) and recovered lignin from PIL dissolution 58

Figure 3. 12. XRD of cellulose recovered from PIL dissolution 60

Figure 3. 13. Images of cellulose recovered from PIL dissolution (500X and 3000X).....60

Figure 3. 14. Variable-temperature TGA heating traces of Kraft lignin and the recovered lignin from CS after PIL treatment 61

Figure 3. 15. Photos of PILs: (a) before and (b) after heating for 24 h at 90 °C 62

Figure 3. 16. Variation in ^{1}H-NMR spectra (δ_{solv} = 4.75 ppm) of PIL ([Pyrr][Ac]) with heating time showing: (a) full NMR spectrum, (b) d = 3.1-3.7 ppm and (c) d = 1.7-2.2 ppm 64

Figure 3. 17. Effect of changing water content on the chemical shifts of the acidic protons in PILs ([Pyrr][Ac]) 66

Figure 3. 18. Rate of formation of amide from UV/Vis and NMR analyses 67

Figure 3. 19. Isothermal TGA heating traces (90 °C) of PILs. Note that the biomass processing with the PILs occurs in sealed containers, in contrast to the TGA measurements 68

Figure 3. 20. ^{1}H-NMR spectra (δ_{solv} = 4.75 ppm) of [Pyrr][Ac] to determine the amount of amide left over in the recovered PIL.....69

CHAPTER 4

Figure 4. 1. PIL ions used in this study.....79

Figure 4. 2. Orbitals present in the pyridinium anion 88

Figure 4. 3. Minimum energy structures of primary NAA PILs using one ionic couple 91

Figure 4. 4. Minimum energy structures of secondary NAA PILs using one ionic couple..92

Figure 4. 5. Minimum energy structures of CAA PILs using one ionic couple 93

Figure 4. 6. Minimum energy structures of the AA PILs [Py][Ac] and [Mim][Ac] using one ionic couple.....94

Figure 4. 7. Minimum energy structures of the OAC PIL [Eth][Ac] using one ionic couple 95

Figure 4. 8. Minimum energy structures of the hybrid PIL [PipOH][Ac] using one ionic couple.....95

Figure 4. 9. Comparison of the Raman spectra (2500-3500 cm^{-1}) of PILs, as well as, their amine reagent (red) depicting the nature of the N-H peak in amines before and after protonation 97

Figure 4. 10. Image showing the effect of different cation structures in the PIL on their ability to disperse cellulose after heating/stirring at 90 °C for 24 h) 99

Figure 4. 11. Images depicting the solubility of 5% w/w sugars in the PILs: after stirring for (a) after stirring for 30 min at room temperature (25 °C) and (b) after stirring for 24 h at 90 °C (sample sizes were 5.0 g).....101

CHAPTER 5

Figure 5. 1 Chemical structures of OAA PILs discussed in this chapter.....109

Figure 5. 2. Minimum energy structures of OAA lactate-based PILs using one ionic couple 110

Figure 5. 3. Variable-temperature TGA heating traces (5 °C min^{-1}) of OAC PILs.....110

Figure 5. 4. Walden Plot as a measure of ionicity for PILs used in this study 111

Figure 5. 5 Images depicting the solubility of 5% w/w microcrystalline cellulose in the reagents: (a) after stirring for 30 min at room temperature (25 °C) and (b) after stirring for 24 h at 90 °C (sample sizes were 10.0 g).....115

Figure 5. 6. Images depicting the solubility of 5% w/w xylan in the PILs: (a) after stirring for 30 min at room temperature (25 °C) and (b) after stirring for 24 h at 90 °C (sample sizes were 10.0 g) 116

Figure 5. 7. Images depicting the solubility of 5% w/w microcrystalline cellulose and xylan in the reagents: (top) after stirring for 30 min at room temperature (25 °C) and (bottom) after stirring for 24 h at 90 °C (sample sizes were 10.0 g).....117

Figure 5. 8. Images depicting the effect of the PIL treatment on the CS fibers.....118

Figure 5. 9. XRD of CS recovered from PIL pretreatment.....119

Figure 5. 10. Effect of heating on the [Eth][Ac] PIL showing (a) the absorption spectra of the PIL after heating for 24 h at 90 °C, (b) the time dependent rate of discoloration in the PIL and (c) images showing the effect of heating on the PIL's observed color.....121

Figure 5. 11. ^{1}H-NMR spectra (δ_{solv} = 4.75 ppm) of PIL ([Eth][Ac]): (a) after synthesis and (b) after distillation from the CS-Lignin solution (Liquor 1) 122

Figure 5. 12. Isothermal (90 °C) TGA heating traces (5 °C min^{-1}) of OAC PILs 123

Figure 5. 13. XRD of cellulose recovered from PIL dissolution 124

Figure 5. 14 Images of cellulose recovered from PIL dissolution (500X and 3000X).....125

Figure 5. 15. Variable temperature viscosity OAC of PIL 126

Figure 5. 16. Molecular solvents used to reduce the PIL's viscosity.....126

Figure 5. 17. Images depicting the solubility of 5% w/w commercially available biomass components (Kraft lignin, microcrystalline cellulose and xylan) in the various concentrations of DMSO mixtures,: (a) after stirring for 30 min at room temperature (25 °C) and (b) after stirring for 24 h at 90 °C (sample sizes were 10.0 g).....130

Figure 5. 18. Images depicting the biomass fibers before and after PIL treatment 132

Figure 5. 19 XRD of the biomass fibers recovered from PIL pretreatment.....133

CHAPTER 6

Figure 6. 1. The basic units of lignin; *p*-coumaryl (hydroxyphenyl), coniferyl (guaiacyl), and sinapyl (syringyl) alcohol 138

Figure 6. 2. Size exclusion chromatograph of acetylated Kraft lignin recovered from PIL dissolution and CS lignin from the [Pyrr][Ac] PIL 142

Figure 6. 3. FT-IR spectra for Kraft lignin recovered from PIL dissolution and the lignin extracted from CS using the [Pyrr][Ac] PIL.....144

Figure 6. 4. FT-IR spectra for the [Py][Ac] PIL and the reagents used to synthesize it (pyridine and acetic acid).....146

Figure 6. 5. Energy minimization of the lignin model compound (LigM), LigM-LigM.....150

Figure 6. 6. Energy minimization for LigM-PIL for the [Py][Ac] PIL, LigM-[Py][Ac], and LigM-Py 151

Figure 6. 7. Energy minimization for LigM-PIL for the [Pyrr][Ac] and [Eth][Ac] PILs and LigM-Pyrr 152

Figure 6. 8. Solvents used for lignin dissolution and regeneration study 153

Figure 6. 9. (a) The solubility of lignin in some common solvents after (b) stirring for 24 h at 90 °C, recovering the supernatant, solvent evaporation, and re-dissolution in 0.1M NaOH as determined by: (c) the Kraft lignin calibration curve at (d) the wavelength of maximum absorbance.....156

Figure 6. 10. Images (10X) of lignin recovered from solvent and PIL dissolution after heating at 90 °C and 24 h.....157

Figure 6. 11. FTIR spectra of lignin regenerated from solvent dissolution after heating at 90 °C and 24 h 158

Figure 6. 12. Images (10X) of lignin showing the lignin extracted from CS using the [Pyrr][Ac] PILs: (a) the solids recovered after the PIL removal, and (b) solids after passing the solids form (a) through a water wash step 158

LIST OF SCHEMES

CHAPTER 2

Scheme 2. 1. Lignin-extraction process for CS using a PIL with labeled process streams...34

CHAPTER 3

Scheme 3. 1. Formation reaction for PILs.....42

Scheme 3. 2. Formation of the amide 1-(pyrrolidin-1-yl)ethanone, a possible side product that is found in recycled [Pyrr][Ac] 63

CHAPTER 1: Introduction

1.1. Motivation

Liquid biofuel (e.g., ethanol) use for transportation in the U.S. has grown tremendously in recent years, displacing significant amounts of petroleum consumption.[1] The driving force for this change is largely due to energy security/independence, with concerns over climate change and sustainability accelerating this change. However, such fuels are largely derived from feed corn resulting in the rapid increase of world food prices and other unanticipated consequences.[1–3] Furthermore, life-cycle analyses of the biofuel production processes indicate that the net energy gain (fuel energy out minus energy input) from corn is almost negligible and achieves (relative to petroleum) only a 22% reduction in CO_2 emissions, one of the major greenhouse gases believed to contribute to climate change.[4] This barrier calls for the diversification to alternative biofuel feedstocks and an improvement in the efficiency of current production methods.

The exploitation of second- and third-generation biofuels that are derived from the whole plant matter of dedicated energy crops or agricultural residues, forest harvesting residues or wood processing waste,[5] rather than from food crops (first-generation biofuels), is an emergent area of research.[1–6] These resources, collectively known as lignocellulosic biomass, have the potential to serve as low-cost and renewable feedstocks for biofuel production.[4] It is estimated that there are over one billion tons of renewable biomass available for conversion into biofuels.[5] The multiple categories for the classification of lignocellulosic biomass results in different biomass resources that can be considered for the

Figure 1. 1. Geographic locations (in the U.S.) of lignocellulosic biomass resources.[55]

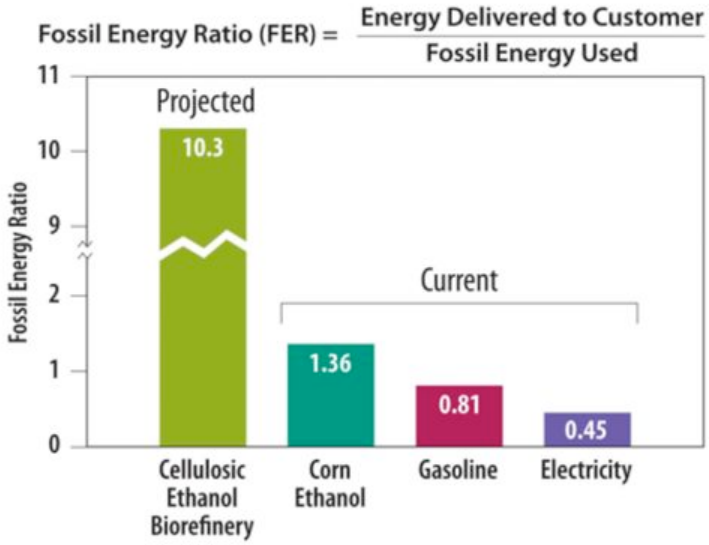

Figure 1. 2. Fossil energy ratio (FER) for cellulosic ethanol production in comparison to conventional energy sources.[56]

production of fuels and this creates the opportunity for the region-specific production of biofuels (Figure 1. 1), which will mitigate the costs associated with energy transportation. Therefore, the use of lignocellulosic biomass for the production of biofuels could displace a substantial portion of the fossil fuels currently consumed within the transportation sector, especially if integrated with plug-in hybrid electric vehicles (PHEVs) and the Smart Grid.[6] Furthermore, there is a net fuel energy production of 2 to 36 times the energy input (depending on the feedstock) with a 90% reduction in CO_2 emissions, which gives fuel production from biomass a fossil energy ratio that surpasses that of the conventional energy sources that are currently being utilized (Figure 1. 2). In addition to utilizing lignocellulosic biomass for bioenergy/biofuels, there is also the possibility of producing bioproducts such as bioplastics and biochemicals.[2–3] This is an appealing feature that may well be crucial for improving the total cost of production of biofuels from lignocellulosic biomass.

Unlike food-based sources, lignocellulosic materials are comprised mainly of cellulose, hemicellulose, and lignin; extractives like waxes and proteins are also present in smaller quantities (Table 1. 1).[7] These three main fractions exhibit different physical and chemical structures, which influences the biomass processing methods utilized. For biofuel production, the polysaccharides (cellulose and hemicellulose) need to be broken down to liberate monomeric sugars. In cellulose, for example, enzymes can be used to break the α-(1,4)-glycosidic linkages, thus liberating glucose, which can then be fermented into ethanol.[8] Lignin, on the other hand, is a polyaromatic compound rich in benzene rings, which has been

identified as a precursor to some valuable aromatic chemical compounds, such as vanillin,[9–10] in addition to fuels.[11]

Table 1. 1 Typical chemical composition of various lignocellulosic materials.[2]

raw material	lignin (%)	cellulose (%)	hemicellulose (%)
Softwoods	25-35	45-55	24-40
Hardwoods	18-25	45-50	25-35
Grasses	10-30	25-40	25-50

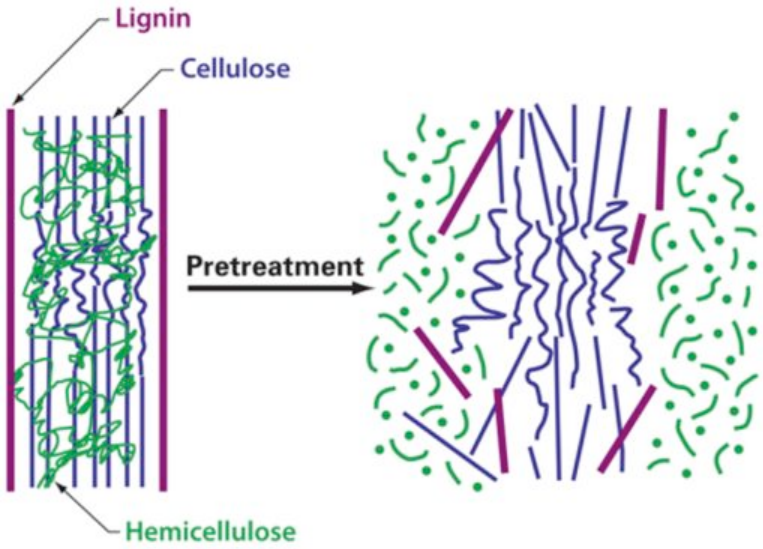

Figure 1. 3. Pretreatment of biomass showing the effect of lignin removal and resulting reduction in cellulose crystallinity.[54]

In order to access each of these components for further processing, biomass needs to be fractionated. To successfully do this, the cross-linked matrix of lignin and hemicelluloses that embeds the cellulose fibers needs to be perturbed and/or removed (Figure 1. 3). Specifically, effective removal (depolymerization) of lignin is necessary to facilitate easier access to the cellulose.[12] In addition, most of the cellulose in lignocellulosic biomass is highly crystalline, which makes it difficult to dissolve or hydrolyze under natural conditions.[13–16] For biofuel production, the intra- and inter-molecular hydrogen bonds in cellulose need to be disrupted, which consequently increases the porosity and surface area of the cellulose available for subsequent enzymatic hydrolysis.[13] Such a process, known as biomass pretreatment, is most efficient when all of these goals can be accomplished in a single step. Pretreatment is essential for the effectiveness (in terms of both yield and cost) of further downstream processes.[13,15]

A variety of pretreatment methods have been developed, with alkali pretreatment being the most effective for lignin removal.[13,17–22] These methods have shown some promise for the cost-effective pretreatment of lignocellulosic biomass for the conversion of biomass to fuels and chemicals.[10] However, the majority of these pretreatment methods tend to be costly, energy intensive, and involve the use of harsh chemicals such as caustic bases (e.g., sodium hydroxide and sodium hydrosulfide) or strong acids (e.g., sulfuric acid).[13, 19–22] Furthermore, upon sufficient removal of the lignin, the chemicals initially used cannot be easily separated and recycled, resulting in the generation of large amounts of waste that may require neutralization depending upon the pretreatment method used. As this waste is

disposed of, there is a substantial loss of lignin, a highly functional natural product that comprises 20-35% of the mass of lignocellulosic biomass. [2-3, 23-24]

Lignin may prove to be a useful raw material for conversion to functional polymers or as a starting point for catalytic transformation into liquid hydrocarbons.[23–24] Currently, lignin is unproductively degraded and burned for energetic utilization in an attempt to recover the chemicals used (as in Kraft pulping).[25–26] Efficient recycling techniques need to be employed to recover the extracted lignin, as well as the pretreatment chemicals. This research project introduces the use of protic ionic liquids (PILs)–salts which melt below ambient temperature formed from acid and base reagents–that can be easily synthesized and recovered, as an alternative to conventional lignin removal methods for biomass processing. Subsequent to demonstrating the lignin removal process, rigorous experimental and computational techniques were employed to understand the molecular-level interactions that predict each PIL's effectiveness for lignin removal. The results obtained were then utilized to select the PIL ions with favorable characteristics for increasing the lignin removal from the biomass fibers and these PILs were applied for lignin removal from a variety of biomass sources. The extracted lignin was also characterized in order to develop a deeper understanding of the mechanism for lignin dissolution.

1.2. Lignocellulosic biomass: Biomass components (biopolymers) and structure

Lignocellulosic materials are comprised mainly of cellulose, hemicelluloses, and lignin; extractives like waxes and proteins are also present in smaller quantities.[27-29] The chemical composition of plants differs considerably and is influenced by both genetic and

environmental factors (Table 1. 1).[14] The three main fractions of lignocellulosic materials exhibit different physical and chemical structures (Figure 1. 4).

1.2.1. Cellulose

Cellulose, the most abundant of the three principal biopolymers, is a polysaccharide of glucose linked through α-(1,4)-linkages. Cellobiose, a dimer of glucose, is the repeat unit established through this linkage, which forms cellulose chains (Figure 1. 4). The high molecular weight cellulose polymer chains are linked together by hydrogen bonds, which cause the cellulose to be packed into microfibrils.[31] Naturally occurring cellulose is a semi-crystalline material that contains highly crystalline nanofibrillar domains. These nanofibrils are connected through amorphous regions, which naturally assemble into the three-dimensional structure (composite) known to give many trees, plants, and marine animals their strength and structural integrity. For biofuel production, sugars need to be produced from the polysaccharides. For cellulose, for example, fermentable D-glucose can be produced through the action of either acid or enzymes to break the α-(1,4)-glycosidic linkages.

1.2.2. Hemicellulose

Hemicellulose is a heteropolysaccharide composed of different hexoses, pentoses, and glucoronic acid.[32] The main feature that differentiates hemicellulose from cellulose is that hemicellulose has branches with short lateral chains consisting of different sugars. Xylan (Figure 1. 4) is the most common hemicellulose component for grasses and hardwoods, while glucomannan is the most prevalent component for softwoods[33] Hemicellulose serves as a connection between the lignin and the cellulose fibers and gives the whole cellulose-

hemicellulose-lignin network more rigidity.[33-34] Sugars can also be liberated from hemicellulose by hydrolysis.[32-32]

1.2.3. Lignin

Lignin, after cellulose and hemicellulose, is one of the most abundant polymers in nature and is present in the plant cell walls. Lignin is a highly irregular and insoluble polymer consisting of three different phenyl propane units (*p*-coumaryl, coniferyl and sinapyl alcohol) that are held together by different kinds of linkages (Table 1. 2, Figure 1. 5–1.6). The main purpose of lignin is to give the plant structural support, impermeability, and resistance against microbial attack and oxidative stress. Unlike polysaccharides, no chains containing repeating subunits are present in lignin (Figure 1. 6), thereby making the enzymatic hydrolysis of this polymer extremely difficult. In general, herbaceous plants such as grasses have the lowest contents of lignin, whereas softwoods have the highest lignin content (Table 1. 1).[30] Lignin can also serve as a renewable source of chemicals that could be utilized to produce high-value chemicals such as dyes, pigments, or resins that could be developed to supplement the cost of running the biorefinery.

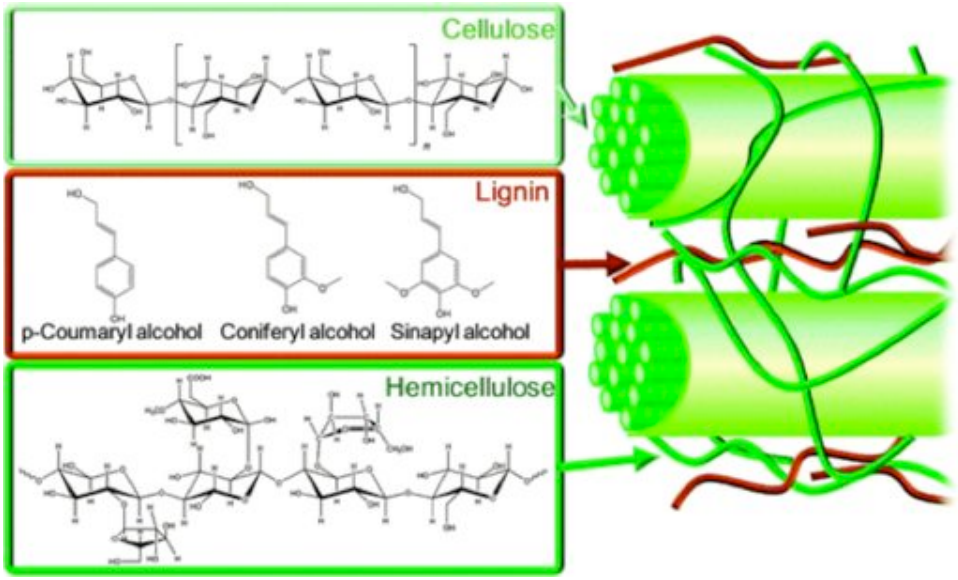

Figure 1. 4. Representative structures that give rise to the biopolymers cellulose, hemicellulose, and lignin in nature.[57]

Table 1. 2. Typical composition of the common linkages found in lignin.[59–61]

Linkage type	Dimer structure	Percent of total linkages	
		Softwood	Hardwood
β-O-4'	Arylglycerol-β-aryl ether	50	60
α-O-4'	Noncyclic benzyl aryl ether	2-8	7
β-5'	Phenylcoumaran	9-12	6
5-5'	Biphenyl and Dibenzodioxocin	10-11	5
4-O-5'	Diaryl ether	4	7
β-1'	1,2-Diaryl propane	7	7
β−β	Pinoresinol/lignan type	2	3

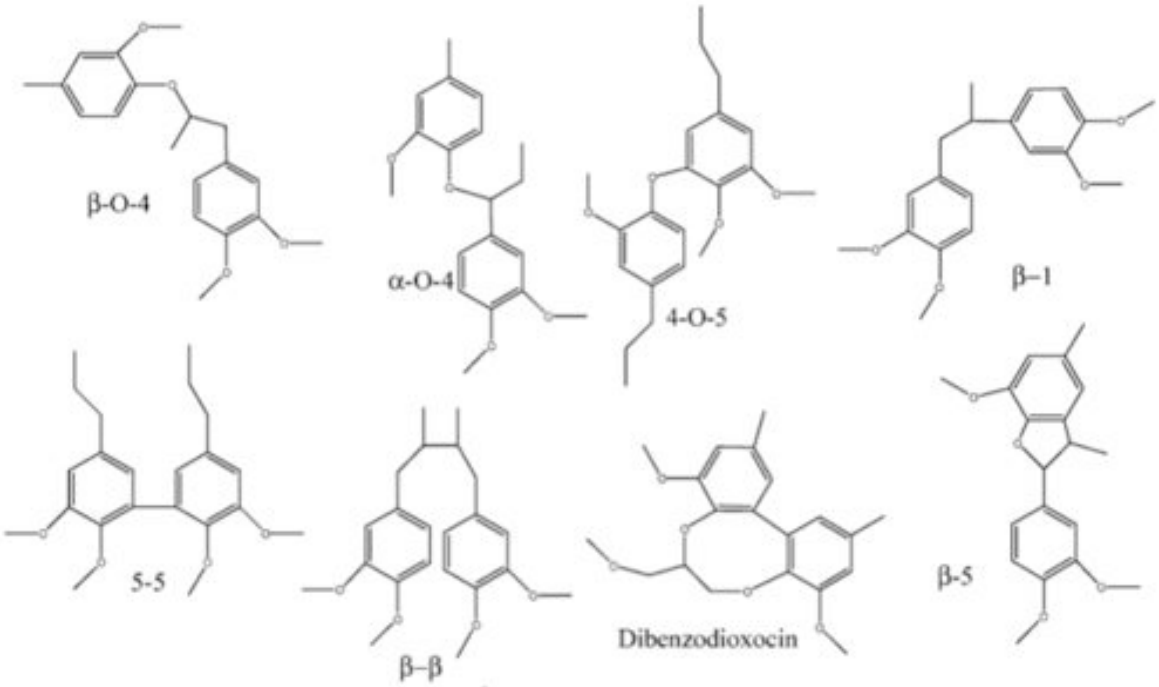

Figure 1. 5. Common phenyl propane linkages in lignin.

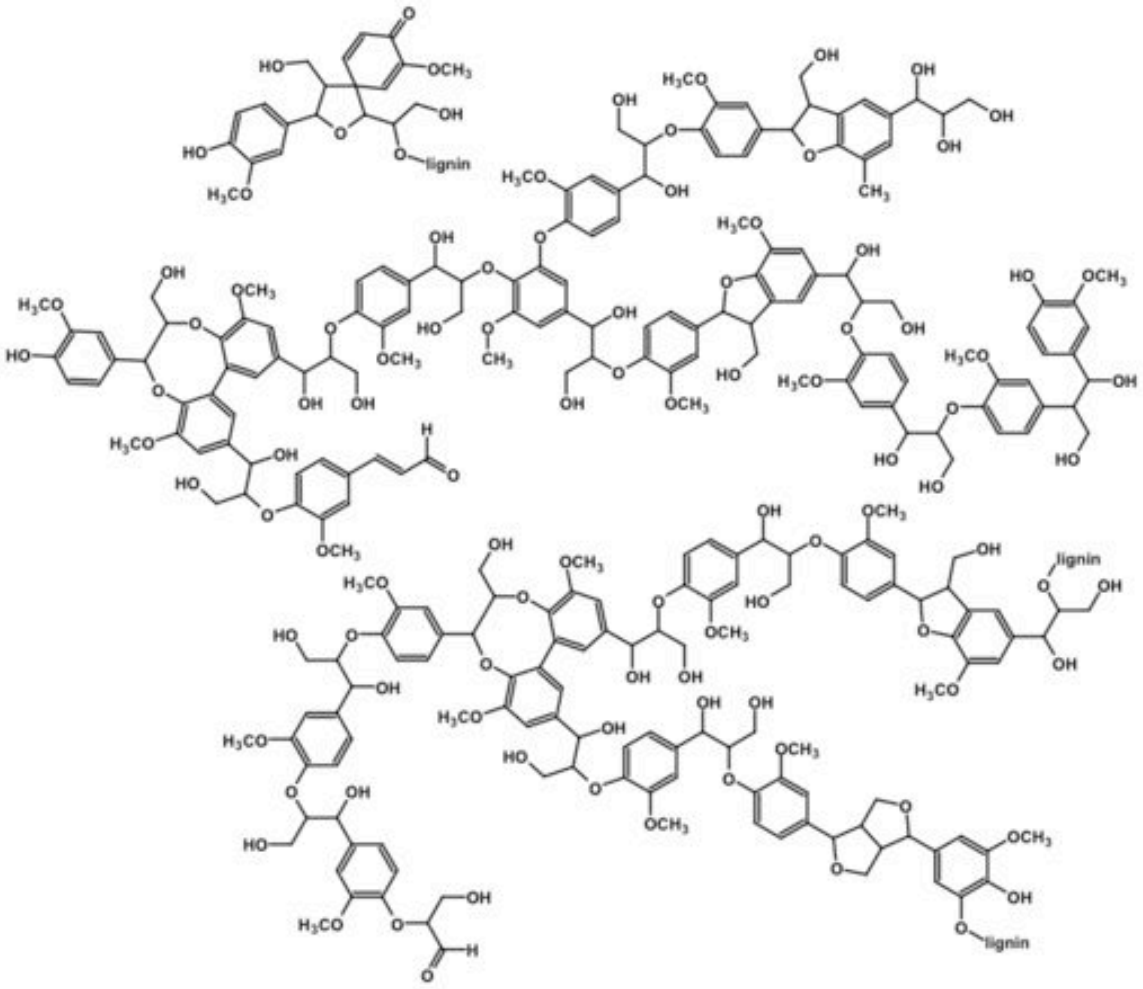

Figure 1. 6. Representation of a lignin polymer model.[58]

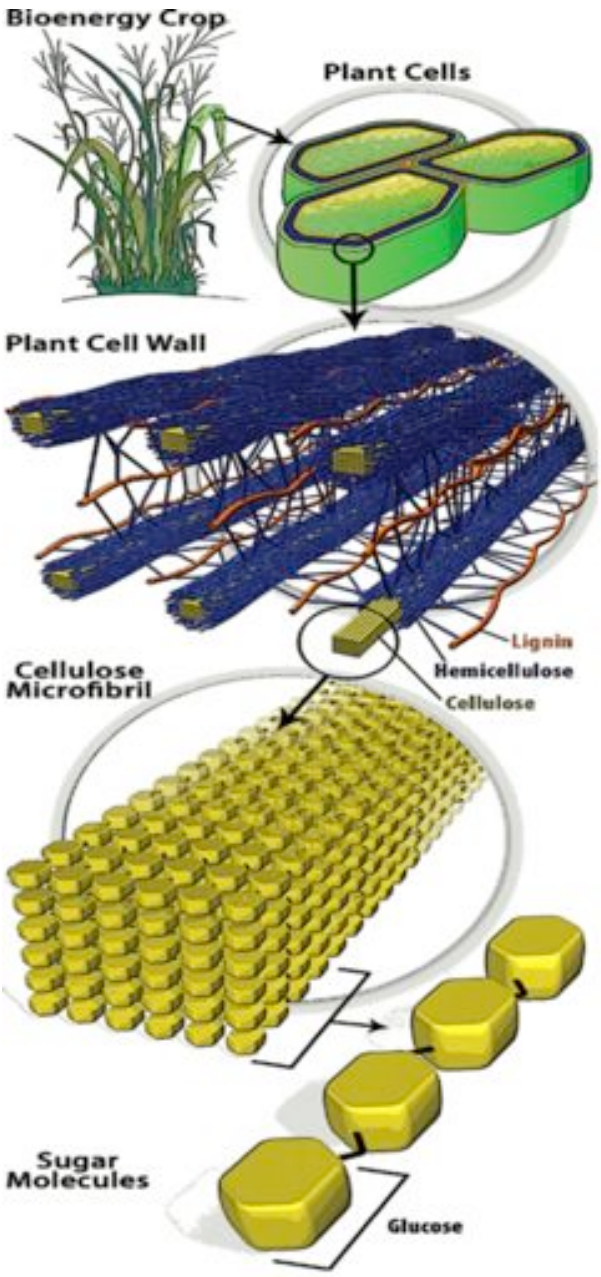

Figure 1. 7. Microscopic to macroscopic view of a typical representation of lignocellulosic biomass.[54]

1.2.4. Tertiary Structure

The tertiary structure of lignocellulosic materials is directed by a variety of covalent and non-covalent linkages between the various constituents (Figure 1. 7). Cellulose is complexed with hemicellulose, lignin, and other components (Figures 1. 7), and it is this complicated association that shields cellulose and hemicellulose from direct enzymatic hydrolysis.[35–37] In order to make cellulose more accessible and thus improve the enzymatic hydrolysis efficiency, lignocellulosic biomass is pretreated to potentially remove (much of the) lignin and reduce the cellulose crystallinity to facilitate the downstream processing of the polysaccharides (Figure 1. 8).

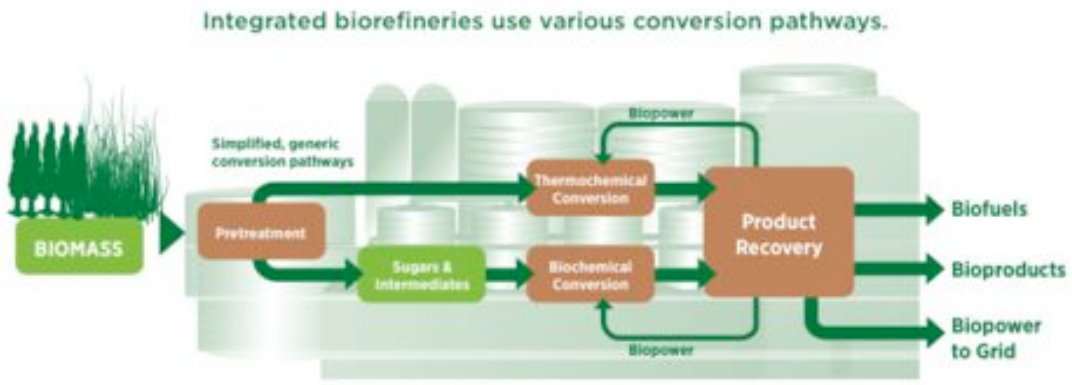

Figure 1. 8. Image describing the integrated multi-product biorefinery concept as biomass is being processed to biofuels and bioproducts.[54]

1.3. Current Methods for Biomass Fractionation (Pretreatment)

Despite the potential for lignocellulosic biomass to be a fuel source, there are still limitations that prevent it from reaching economic levels of development. The total process of biofuel production–including pretreatment, solvent and by-products recovery, and production of derivatives from by-products–needs to be optimized to make the process of producing biofuels more economic. Typical pretreatment methods can be roughly divided into five different categories: physical (milling and grinding), physicochemical (steam pretreatment/auto hydrolysis, hydrothermolysis, and wet oxidation), chemical (alkali, dilute acid, oxidizing agents, organic solvents, and ionic liquids), biological, electrical, or a combination of these[13,17–22] A number of these methods have promise for cost-effective pretreatment of lignocellulosic biomass for the conversion of biomass to fuels and chemicals. However, the current representative pretreatment pattern for lignocellulosic materials is usually based solely on product streams that contain separated polysaccharides in which cellulose is enzymatically hydrolyzed to produce cellulosic bioethanol or other bio-based products. Any other residues, including lignin and the remaining cellulose and hemicelluloses, are usually discarded or inefficiently burned to generate power.[38] This biorefinery pattern causes environmental pollution from waste generation and resource underutilization. To overcome these drawbacks, an economically viable and environmentally friendly integrated multi-product biorefinery is necessary to accelerate effective biomass fractionation routes for complete and total lignocellulose utilization.[39]

1.3.1. Ionic Liquids (ILs)

Lignin removal from biomass has been previously demonstrated with conventional ionic liquids (ILs),[28] but this typically requires high-temperature processing (≥ 100 °C) and extracts only a moderate fraction of the lignin in the biomass (< 50%).[28] The greater lignin removal only occurs when the polysaccharides are simultaneously solubilized, thus resulting in decreased sugar yield. Production of value-added co-products alongside biofuels demands the need for streamlined selectivity (better partitioning of the biomass components) during pretreatment.

Additionally, the high cost of the ILs necessitates their complete recovery, which is difficult to achieve due to small IL losses during processing, minor amounts of thermal degradation of the IL ions, and the build up of extractants in the IL.[28] Although the extracted lignin can be precipitated from IL/lignin mixtures,[28] the amount of lignin, which is retained in the IL remains significant, therefore, hindering their application for large-scale processes. The use of low-cost ILs instead (i.e., PILs)–which can be completely recovered–for biomass pretreatment, could potentially improve the overall economics of biofuel production.

1.3.2 PILs and Lignin Dissolution

In contrast to conventional ILs, PILs are simply formed by a proton transfer from a Brönsted acid to a Brönsted base.[410] A distinguishing characteristic is the presence of one or more acidic protons in the resulting PIL. A typical reaction for the formation of PILs is illustrated below (where A-acid, and B-base):

$$B:_{(l)} + A-H_{(l)} \longleftrightarrow [B-H^+][A^-]_{(l)}$$
$$B:_{(l)} \longleftrightarrow B:_{(g)}\ ,\ A-H_{(l)} \longleftrightarrow A-H_{(g)}$$

The low cost of these reagents (acid and base), as well as the simplicity of the PIL synthesis, render the production of PILs more cost friendly than their aprotic counterparts. Furthermore, by taking advantage of the reversible exothermic reactions for PIL synthesis and the large difference in volatility between the PIL reagents and lignin, a procedure for the facile recovery/recycling of the PIL is available (i.e., once the lignin has been extracted from the biomass using a PIL, further separation via simple distillation is employed to recover the PIL leaving the non-volatile extracted lignin available for further processing).[41]

Recent studies with lignin model compounds suggest that PILs could act as acid-catalysts in the cleavage of the β-O-4 bonds found in lignin due to the acidic proton present in the PIL. A mechanism for the acid-catalyzed hydrolysis of phenolic and non-phenolic lignin model compounds in a PIL, i.e., methylimidazolium chloride [Mim][Cl], has been proposed.[18,43] A high conversion of the model compounds is achieved resulting in the conclusion that PILs may have some catalytic function.[43] This is expected, as studies have shown that PILs can be used in place of inorganic acids in many conventional acid-catalyzed reactions.[44–45] In addition to this conclusion, it was also demonstrated that the reactivity of the model compounds in the PILs is dependent not only on the acidity of the PIL (catalyst-function), but also on the nature of the ions present and their interaction with the model compounds (solvent-function).[18] Variations in the anion indicate that the reactivity also depends on the anion that is present during the reaction.[18] Their findings conclude that the

ability of the anion to interact with the hydroxyl groups on the model compounds through hydrogen bonding affects the conversion of the model compounds achieved in this reaction.[18] Based on this new mechanism that has been proposed, PILs may present a catalyst function which can be advantageous for the removal of lignin from lignocellulosic materials.[46]

It is important to note, however, that these reactions were carried out at relatively high temperatures (130-200 °C).[47–53] PILs, in general, are not thermally stable under these processing conditions; the PILs will be largely dissociated into the amines and acid (i.e., HCl or H_2SO_4) reagents rather than existing as discrete ions. Using the proposed PIL (i.e., [Mim][Cl] or 1-methylimidazolium chloride), HCl–a strong acid–could be liberated and this can explain the high efficiency observed for the acid-catalyzed reaction. The presence of small amounts of water or ethanol in these processes resemble to some extent the well-known Organosolv pretreatment process with ethanol/water mixtures and the addition of a strong acid H_2SO_4 as a catalyst.[45-57] The process described in this thesis, however, does not utilize the strong acids (pKa values: HCl -8.0, H_2SO_4 -3.0/1.9 and HAc 4.8) necessary for lignin depolymerization. In addition, the high temperatures and acids employed by these other processes degrade the polysaccharides into a variety of chemicals,[52] whereas the reported process results in little to no degradation of the polysaccharides.

References:

1. Gomez, L. D.; Steele-King, C. G.; McQueen-Mason, S. J. Sustainable liquid biofuels from biomass: The writing's on the walls. *New Phytol.* **2008**, *178*, 473.
2. Zhang, Y. H. P. Reviving the carbohydrate economy via multi-product lignocellulose biorefineries. *J. Indus. Microbiol. Biotechnol.* **2008**, *35*, 367.
3. Schwietzke, S.; Ladisch, M.; Russo, L.; Kwant, K.; Mäkinen, T.; Kavalov, B.; Maniatis, K.; Zwart, R.; Shahanan, G.; Sipila, K.; Grabowski, P.; Telenius, B.; White, M.; Brown, A. Analysis and identification of gaps in research for the production of second-generation liquid transportation biofuels. IEA Bioenergy [Online] 2008, *1*.
4. Bourne, J. K. Green Dreams. *National Geographic,* October 2007.
5. Simmons, B.; Loque, D.; Blanch, H. Next-generation biomass feedstocks for biofuel production. *Genome Biol.* **2008**, *9*, 242.
6. Luke Tonachel, E.; Hwang, R. The Next Generation of Hybrid Cars: Plug-in Hybrids Can Help Reduce Global Warming and Slash Oil Dependency. Natural Resources Defense Council: Climate facts [Online] 2007 http://www.nrdc.org/energy/plugin.pdf (accessed Nov 5, 2011).
7. Perez, J.; Muñoz-Dorado, J.; de la Rubia, T.; Martínez, J. Biodegradation and biological treatments of cellulose, hemicellulose and lignin: An overview. *Int. Microbiol.* **2002,** *5*, 53.
8. *Kirk-Othmer Encyclopedia of Chemical Technology*, 4th ed.; Wiley: New York, 1993; Vol. 5, p 476.

9. Voitl, T.; Rudolf, v. R. P. Oxidation of lignin using aqueous polyoxometalates in the presence of alcohols. *ChemSusChem* **2008**, *1*, 763.
10. Bozell, J. J.; Holladay, J. E.; Johnson, D.; White, J. F. Results of Screening for Potential Candidates from Biorefinery Lignin, Volume II, Pacific Northwest National Laboratory, Richland, WA, 2007.
11. Yan, N.; Zhao, C.; Dyson, P. J.; Wang, C.; Liu, L.; Kou, Y. Selective degradation of wood lignin over noble-metal catalysts in a two-step process. *ChemSusChem* **2008**, *1*, 626.
12. Chang, M.C. Harnessing energy from plant biomass. *Curr. Opin. Chem. Biol.* **2007**, *11*, 677.
13. Kumar, P.; Barrett, D. M.; Delwiche, M. J.; Stroeve, P. Methods for pretreatment of lignocellulosic biomass for efficient hydrolysis and biofuel production. *Ind. Eng. Chem. Res.* **2009**, *48,* 3713.
14. Leonowicz, A.; Matuszewska, A.; Luterek, J.; Ziegenhagen, D.; Wojtas-Wasilewska, M.; Cho, N. S.; Hofrichter, M.; Rogalski, J. Biodegradation of lignin by white rot fungi. *Fungal Genet. Biol.* **1999**, *27*, 175.
15. Tomme, P.; Warren, R. A.; Gilkes, N. R. Cellulose hydrolysis by bacteria and fungi. *Adv. Microb. Physiol.* **1995**, *37*, 1.
16. Perez, J.; Muñoz-Dorado, J.; de la Rubia, T.; Martínez, J. Biodegradation and biological treatments of cellulose, hemicellulose and lignin: An overview. *Int. Microbiol.* **2002,** *5*, 53.

17. Béguin, P.; Aubert, J. P. The biological degradation of cellulose. *FEMS Microbiol. Rev.* **1994**, *13*, 25.

18. Hsu, T. A.; Ladisch, M. R.; Tsao, G. T. Alcohol from cellulose. *Chem. Technol.* **1980**, *10* 315.

19. Lloyd, T. A.; Wyman, C. E. Combined sugar yields for dilute sulfuric acid pretreatment of corn stover followed by enzymatic hydrolysis of the remaining solids. *Bioresour. Technol.* **2005**, *96*, 1967.

20. Dale, B. E.; Moreira, M. J. A freeze-explosion technique for increasing cellulose hydrolysis. *Biotechnol. Bioeng. Symp.* **1982**, *31*, 43.

21. Lau, M. W.; Dale, B. E.; Balan, V. Ethanolic fermentation of hydrolysates from ammonia fiber expansion (AFEX) treated corn stover and distillers grain without detoxification and external nutrient supplementation. *Biotechnol. Bioeng.* **2008,** *99*, 529.

22. Chang, V.; Burr, B.; Holtzapple, M. T Lime pretreatment of switchgrass. *Appl. Biochem. Biotechnol.* **1997**, *63-65*, 3.

23. Li, Y.; Sarkanen, S. Miscible blends of kraft lignin derivatives with low-T_g polymers. *Macromolecules* **2005**, *38*, 2296.

24. Li, Y.; Sarkanen, S. Alkylated kraft lignin-based thermoplastic blends with aliphatic polyesters. *Macromolecules* **2002**, *35*, 9707.

25. Amen-Chen, C.; Pakdel, H.; Roy, C. Production of monomeric phenols by thermochemical conversion of biomass: a review. *Bioresour. Technol*. **2001**, *79,* 277.

26. Chakar, F. S.; Ragauskas, A. J. Current and Future Softwood Kraft Lignin Process Chemistry. *Ind. Crops Prod.* **2004**, *20*, 131.

27. Clark, J. H. Green chemistry for the second generation biorefinery-Sustainable chemical manufacturing based on biomass. *J. Chem. Technol. Biotechnol.* **2007**, *82*, 603.
28. Tan, S. S. Y.; MacFarlane, D. R.; Upfal, J.; Edye, L. A.; Doherty, W. O. S.; Patti, A. F.; Pringle, J. M.; Scott, J. L. Extraction of lignin from lignocellulose at atmospheric pressure using alkylbenzenesulfonate ionic liquid. *Green Chem.* **2009**, *11*, 339.
29. Malherbe, S.; Cloete, T. E. Lignocellulose biodegradation: Fundamentals and applications. *Rev. Environ. Sci. Biotechnol.* **2002**, *1*, 105.
30. Kuhad, R.; Singh, A.; Eriksson, K. E. Microorganisms and enzymes involved in the degradation of plant fiber cell walls. In *Biotechnology in the Pulp and Paper Industry*, Eriksson, K., Babel, W., Blanch, H., Cooney, C., Enfors, S., Fiechter, A., Klibanov, A., Mattiasson, B., Primrose, S., Rehm, H., Rogers, P., Sahm, H., Schügerl, K., Tsao, G., Venkat, K., Villadsen, J., von Stockar, U., Wandrey, C. Eds. Springer Berlin / Heidelberg: 1997; Vol. 57, p 45.
31. Taherzadeh, M.; Karimi, K. Pretreatment of lignocellulosic wastes to improve ethanol and biogas production: A review. *Int. J. of Mol. Sci.* **2008**, *9*, 1621.
32. Manter, D. K. Manual of Environmental Microbiology, third edition. *Soil Sci. Soc. Am. J.* **2008**, *72*, 566.
33. Hendriks, A. T. W. M.; Zeeman, G. Pretreatments to enhance the digestibility of lignocellulosic biomass. *Bioresour. Technol.* **2009**, *100*, 10.
34. Jia, S.; Cox, B. J.; Guo, X.; Zhang, Z. C.; Ekerdt, J. G. Cleaving the β-O-4 bonds of lignin model compounds in an acidic ionic liquid, 1-H-3-methylimidazolium chloride: An optional strategy for the degradation of lignin. *ChemSusChem* **2010**, *3*, 1078.

35. Fengel, D.; Wegener, G. *Wood: Chemistry, Ultrastructure, Reactions*. De Gruyter, Berlin. **1984**.

36. Leonowicz, A.; Matuszewska, A.; Luterek, J.; Ziegenhagen, D.; Wojtas-Wasilewska, M.; Cho, N. S.; Hofrichter, M.; Rogalski, J. Biodegradation of lignin by white rot fungi. *Fungal Genet. Biol.* **1999**, *27*, 175.

37. Tomme, P.; Warren, R. A.; Gilkes, N. R. Cellulose hydrolysis by bacteria and fungi. *Adv. Microb. Physiol.* **1995**, 37, 1.

38. Zhang, Y. H. P. Reviving the carbohydrate economy via multi-product lignocellulose biorefineries. J. Ind. *Microbiol. Biotechnol*. **2008**, *35*, 367.

39. Reviews in chemical engineering. *App. Cat.* **1983,** *6* ,382

40. MacFarlane, D. R.; Pringle, J. M.; Johansson, K. M.; Forsyth, S. A.; Forsyth, M. Lewis base ionic liquids. *Chem. Comm.* **2006,** 42, 1905.

41. NREL. Technical report. Biomass analysis technology team laboratory analytical procedure. **1996** Golden, CO: National Renewable Energy Laboratory.

42. Cox, B. J.; Jia, S.; Zhang, Z. C.; Ekerdt, J. G. Catalytic degradation of lignin model compounds in acidic imidazolium based ionic liquids: Hammett acidity and anion effects. *Polym. Degrad. Stab.* **2011,** *96*, 426.

43. Li, C.; Knierim, B.; Manisseri, C.; Arora, R.; Scheller, H. V.; Auer, M.; Vogel, K. P.; Simmons, B. A.; Singh, S. Comparison of dilute acid and ionic liquid pretreatment of switchgrass: Biomass recalcitrance, delignification and enzymatic saccharification. *Bioresour. Technol.* **2010,** *101*, 4900.

44. Cole, A. C.; Jensen, J. L.; Ntai, I.; Tran, K. L. T.; Weaver, K. J.; Forbes, D. C.; Davis, J. H. Novel brønsted acidic ionic liquids and their use as dual solvent-catalysts. *J. Am. Chem. Soc.* **2002,** *124*, 5962.

45. Zhao, G.; Jiang, T.; Gao, H.; Han, B.; Huang, J.; Sun, D. Mannich reaction using acidic ionic liquids as catalysts and solvents. *Green Chem.* **2004,** *6*, 75.

46. Tan, S. S. Y.; MacFarlane, D. R.; Upfal, J.; Edye, L. A.; Doherty, W. O. S.; Patti, A. F.; Pringle, J. M.; Scott, J. L. Extraction of lignin from lignocellulose at atmospheric pressure using alkylbenzenesulfonate ionic liquid. *Green Chem.* **2009,** *11*, 339.

47. B. J. Cox, S. Jia, Z. C. Zhang and J. G. Ekerdt, *Polym. Degrad. Stab.*, 2011, **96**, 426-431.

48. S. Jia, B. J. Cox, X. Guo, Z. C. Zhang and J. G. Ekerdt, *ChemSusChem*, 2010, **3**, 1078-1084.

49. B. J. Cox and J. G. Ekerdt, *Biores. Technol.*, 2012, **118**, 584-588.

50. B. J. Cox and J. G. Ekerdt, *Biores. Technol.*, 2013, **134**, 59-65.

51. J. Long, B. Guo, J. Teng, Y. Yu, L. Wang and N. Zhang and X. Li, *Biores. Technol.*, 2011, **102**, 10114-10123.

52. J. Long, X. Li, B. Guo, F. Wang, Y. Yu and L. Wang, Green Chem. 2012, 14, 1935-1941.

53. J. Long, X. Li, B. Guo, L. Wang and N. Zhang, *Catal. Today*, 2013, **200**, 99-105.

54. U.S. DOE. 2006. Breaking the Biological Barriers to Cellulosic Ethanol: A Joint Research Agenda, DOE/SC/EE-0095, U.S. Department of Energy Office of Science and Office of Energy Efficiency and Renewable Energy, http://genomicscience.energy.gov/biofuels/.(accesed February, 28th 2011).

55. The Future of Ethanol Cellulosic http://web.extension.illinois.edu/ethanol/cellulosic.cfm

56. Alonso. D. M.;. Wettstein, S. G.; Dumesic, J. A. *Chem. Soc. Rev*. **2012**, *41*, 8075–8098

57. Why Cellulosic Ethanol? http://www.facstaff.bucknell.edu/mvigeant/thermo_demos/Team_Kyoto/celluloseproject/Whycelletoh.html.

58. Adler, E.; Lignin - Past, Present and Future. *Wood Science and Technology* **11** (3). p. 169-218. (1977).

59. Argyropoulos, D.S.; Jurasek, L.; Kristofova, L.; Xia, Z.; Sun, Y. and Palus, E.; Abundance and reactivity of dibenzodioxocins in softwood lignin. *Journal of Agricultural and Food Chemistry* **50** (4). p. 658-666. (2002).

60. Froass, Peter M.; Ragauskas, Arthur J.; Jiang, Jian-er. Chemical structure of residual lignin from kraft pulp**.** *Journal of Wood Chemistry and Technology,* **16**(4), 347-365 (1996).

Kukkola, E.M.; Koutaniemi, S.; Poellaenen, E.; Gustafsson, M.; Karhunen, P.; Lundell, T.K.; Saranpaeae, P.; Kilpelaeinen, I.; Teeri, T.H. and Fagerstedt, K.V.; The dibenzodioxocin lignin substructure is abundant in the inner part of the secondary wall in Norway spruce and silver birch xylem. *Planta* **218** (3). p. 497- 500. (2004).

CHAPTER 2: Materials and Methods

2.1 Materials

2.1.1 Reagents and Solvents Used

Ethylamine (Et), propylamine (Prop), butylamine (But), diethylamine (DiEt), dipropylamine (DiProp), dibutylamine (DiBut), pyrrolidine (Pyrr), *N*-methylpyrrolidine (mPyrr), Piperidine (Pip), *N*-methylpiperidine (mPip), hexaneneamine (Hex), pyrrole (Pyr), *N*-methylpyrrole (mPyr), imidazole (Im), *N*-methylimidazole (Mim), 1, 2-dimethylimidazole (mMim), pyridine (Py), pyrimidine (Pyri), ethanolamine (Eth), 3-amino-1-propanol (3A1P), 1-amino-2-propanol (1A2P), 2-(ethylamino)ethanol (EtAmOH), 2-methoxyethanamine (MeOx), morphopline (Morph), *N*-methylmorpholine (mMorph), 4-Morpholineethanol (MorphOH), 1-piperidineethanol (PipOH), and 4-pyridinemethanol (PyMe) of at least 99% purity, were purchased from Sigma-Aldrich and used as-received. High purity acetone (ACTN), acetonitrile (ACN), ethyl acetate (EtAc), diethyl ether (Et_2O), hexane (HEX), glacial acetic acid (HAc), ethanol (EtOH) and sulfuric acid solution (H_2SO_4, 72% w/w) were purchased from Fisher Scientific and used as-received. Triple-distilled water was used for the preparation of all aqueous solutions and for CS washes.

2.1.2 Biomass/Biopolymer Preparation

Corn stover (CS) and switch grass (SG) were supplied by Novozymes North America, Inc. (Franklinton, NC), while pinewood (PW) and beechwood (BW) were provided by NC State University's Wood and Paper Science Department (Raleigh, NC). All the biomass fibers were ground with a Wiley knife mill (model 4, Thomas–Wiley Co., Philadelphia, PA) using a

2 mm screen. The ground biomass fibers were subsequently size-partitioned and extracted using benzene/ethanol (2:1 v/v) according to the standard NREL procedures LAP–021[1] and LAP–010[2] respectively, to produce extractive-free biomass fibers (EF-CS, EF-SG, EF-PW and EF-BW). The biomass fibers were then air-dried for 72 h.

Kraft lignin (i.e., Indulin-AT) (pine lignin, 93% w/w total solids (TS), 6% w/w ash) (Mead West Vaco, Glen Allen, VA), Organosolv Lignin (Lignol's HP-L™ High Purity Lignin), microcrystalline cellulose powder (particle size 20 mm, Sigma product number 310697) and xylan from beechwood (Sigma product number X4252) were used as-received.

2.2. Instrumentation

2.2.1 Karl Fischer

The water content of the PILs was determined using a Mettler Toledo DL39 Karl Fischer coulometer. The anolyte and catholyte, coulomat AG, was purchased from Hydranal (Sigma product number 34836).

2.2.2 Differential Scanning Calorimetry (DSC)

DSC analysis was performed on a TA Instruments Q2000 differential scanning calorimeter. The instrument was calibrated with cyclohexane (solid–solid phase transition at -87.06 °C, melt transition at 6.54 °C) and indium (melt transition at 156.60 °C). Typically, sample pans were slowly cooled (5 °C min^{-1}) to -150 °C and then heated (5 °C min^{-1}) to 50 °C. In cases where a melting peak was observed, it was necessary to hold or cycle the samples extensively at various temperatures in the instrument prior to the final measurements to confirm complete crystallization (where possible).

2.2.3 Thermogravimetric Analysis (TGA)

TGA measurements were performed using a TA Instruments Q5000 thermogravimetric analyzer. The thermal stability of the PILs was analyzed by heating (5 °C) the PILs in a Pt pan from ambient temperature to 400 °C. Separate samples of each PIL were also analyzed isothermally at 90 °C for 24 h. All TGA experiments were performed under a N_2 atmosphere (> 99.99% N_2, H_2O concentration 2–5 ppm).

2.2.4 Density/Viscosity Measurements

Density and viscosity measurements were performed using an Anton–Paar SVM 3000 Stabinger viscometer (with an internal density meter). Calibration of the instrument was performed with Cannon certified viscosity standards. Isopropanol and N_2 gas (> 99.99%, H_2O concentration 2–5 ppm) were used to clean the instrument before and after the measurements. The instrument was sealed during use to prevent water contamination. The water content was checked before and after the measurements using the Karl Fischer coulometer to ensure that no increase in the water content occurred during the measurements. Density and viscosity values were recorded from 0 to 50 °C in 5 °C increments.

2.2.5 Conductivity Measurements

The conductivity of the PILs was measured with electrochemical impedance spectroscopy using a Solartron 1287A potentiostat and 1260A impedance analyzer. Spectra were collected from 106 to 20 Hz with a 10 mV ac perturbation. The hermetically-sealed conductivity cells consisted of two parallel Pt electrodes. The cell constants were determined using aqueous KCl standard solutions. Samples were equilibrated in a Binder environmental

chamber at temperatures between 0 and 50 °C in 5 °C increments with at least 45 min allowed for equilibration after each temperature change before the measurements were taken.

2.2.6 Nuclear Magnetic Resonance (NMR) Spectroscopy

Combinations of homonuclear ^{1}H– and ^{13}C–NMR analysis were applied to study the structure of the synthesized PILs. All of the pulsed–field NMR experiments were performed on a Bruker Avance 500 MHz spectrometer with an Oxford Narrow Bore magnet. The NMR sample tubes were prepared by transferring samples of approximately 0.6 ml of the PILs into 5 mm NMR tubes with an external D_2O capillary for lock purpose. All spectra were acquired at a temperature of 21 °C. DSS was used as an internal standard. The NMR probe was tuned to the ^{13}C frequency, which is 125.75 MHz in the 500 MHz spectrometer (^{1}H frequency-500.128 MHz). A single frequency carbon probe was used to run the 1–D ^{13}C spectra (δ_H 2.6 for DMSO-d6). For measurements in Chapter 4 (Appendix D), a 400MHz spectrometer was used, and the sample sizes were also 0.6 ml with 0.2 % v/v PIL in the reference solvent.

2.2.7 FT–IR Spectroscopy

IR spectroscopy was performed using a Perkin–Elmer Spectrum 2000 FT–IR spectrophotometer. Spectra were recorded as a thin film between KRS-5 plates, in the range 400 – 4000 cm^{-1} and were accumulated for 32 scans at a resolution of 4 cm^{-1}. The spectra were baseline corrected and processed using the available software.

2.2.8 Raman Spectroscopy

Raman spectroscopy measurements were performed on a Horiba-Jobin Yvon LabRAM HR VIS high-resolution confocal microscope using a 632 nm^{-1} He-Ne laser as the

excitation source. Specimens were deposited onto glass microscope slides and were illuminated through a 50X optical objective. Linkam heating/cooling stage was utilized for temperature control and protection from ambient moisture when volatile samples were used. A 50X long-distance optical objective was necessary for use with the Linkam stage. Samples were added to a stainless steel microscope slide with a well milled into the slide. The slide was then sealed in the Linkam stage and transferred to the spectrometer. The instrument was calibrated with a two-point calibration of the Raman laser line at 0.0 nm and a monocrystalline Si wafer at 520.7 cm^{-1}. Raman spectra were collected over the spectral range 400 – 4000 cm^{-1} and were typically collected at room temperature, where most samples are liquid, using a 10–30 s exposure time and 20 accumulations to ensure high resolution spectra.

2.2.9 Ultraviolet/Visible (UV/VIS) Spectrophotometry

UV/Vis spectra were acquired using a JASCO spectrophotometer (V-550) in a quartz cuvette (1 cm path length) at room temperature 25 °C. A reference cuvette containing the pure PIL was used in all measurements. All the spectra were measured at a resolution of 0.05 nm per data point.

2.2.10 Ion Chromatography (IC)

The IC (Dionex ICS–5000, Dionex Corporation, Sunnyvale, CA) was equipped with a pulsed electrochemical detector. The column used was a CarboPac PA1 (4 x 250 mm) column which was operated at 18 °C with 0.018M KOH as the mobile phase at a flow rate of 0.9 ml. All of the above measurements were performed in duplicate to ensure reproducibility.

2.2.11 Gel Permeation Chromatography (GPC)

The gel permeation chromatography (GPC) system consisted of a Shimadzu LC-20AD pump, a Shimadzu CTO-20A oven (35C) equipped with two Waters Styragel column (HR1 & HR5E, molecular range 0~4M), a Shimadzu SPD-20A UV/vis detector (dual wavelength, 235 nm and 254 nm were used for all experiment) and a Shimadzu RID-10A reflective index detector were used to analysis the samples. The THF was used as the mobile phase with a flow rate of 0.7 mL/min. A calibration curve was created based on 12 polystyrene (PSS ReadyCal-Kit Poly) from molecular weight of 266 to 2.52 x 106 g/mol. Data collection and processing were done by Shimadzu LCsolution software.

2.2.12 X–Ray Diffraction (XRD)

Dry biomass samples (extractive–free, e.g., EF–CS and PIL–treated, i.e., PIL–CS) were passed through a 0.5 mm screen and then randomly picked for XRD measurements. The measurements were performed using a Rigaku SmartLab X–ray diffractometer with a Cu target-ray tube (operating at 40 kV and 44 mA) as the source. The diffraction patterns were taken in a 2θ range between 10° and 40° using 1° increments.

2.2.13 Imaging

The morphology of the untreated and treated biomass fibers was examined with a scanning electron microscope (SEM) (Phenom, FEI). Before imaging, all biomass samples were sputter-coated in a Quorum Technologies mini sputter coater (Model SC7620) with a Au/Pd target for 120 s at 20 mA. All images were obtained at acceleration voltages of 5 kV

and a magnification of 500X. Photographic images of up to 10X magnification were also taken using a Canon Rebel T3i EOS 600D 18.0 MP Digital SLR Camera.

2.3. PIL Synthesis and Characterization

High-purity PILs were synthesized by adding the acid and bases as neat reagents to eliminate both the need for solvent and the introduction of incidental water. Similar to previous studies,[3–4] the PILs were synthesized using a round-bottom flask equipped with two addition funnels—one for the acid and one for the base. The reagents were slowly added into the flasks and homogenized with a magnetic stirring bar. The flasks were mounted in an ice/water bath to prevent heat buildup during the reactions. Stirring was continued for 24 h at room temperature to obtain a clear liquid. The water content of the PILs was measured and then they were hermetically sealed in crimp-top vials to prevent moisture contamination. See Appendix A for the PIL synthesis set up. The purity of the PILs was also determined via NMR analysis (see Appendices C and D).

2.4. Biopolymer Solubility Tests

The solubility of the commercially available biopolymer (lignin, xylan and cellulose) in the PILs was determined by initially adding 1% w/w of the biomass components to glass vials containing 5 g of the solvents (i.e., PILs and reagents). The vials were hermetically-sealed to prevent loss of the solvent and stirred for 24 h at 90 °C in an Al heating block. The solutions were then visually checked to determine whether dissolution had occurred. If a given solution was transparent with no undissolved solids, the amount of the biomass component was incrementally adjusted to increase the mass fraction to 2, 5 or 10% w/w and

stirred for another 24 h at 90 °C. The addition was continued until the solution appeared to be heterogeneous.

To determine the exact amount dissolved, the mixtures were centrifuged to separate any undissolved solids. The supernatants were then carefully transferred to other vials and sealed. Needles were then inserted into the septum tops and the vials were placed in a vacuum oven to remove the PILs or reagents. The amount of solid remaining after solvent removal, determined gravimetrically, is indicative of the amount of the biopolymer that went into solution. From this information, the final solubility of each component in the solvent was calculated. This technique is particularly useful for determining lignin solubility due to the dark color of lignin solutions, which make visual observations or optical microscopy ineffective.

2.5. Degree of Cellulose Dispersion

The degree of cellulose dispersion was determined qualitatively by physically comparing the cellulose/PIL mixtures before and after the solubility tests. At the end of each solubility run (see above), heating and stirring was discontinued and the mixtures were left undisturbed for 24 hrs for any undissolved solids to settle. Images were the taken and compared with the original cellulose/PIL mixtures before the solubility tests were run.

2.6. PIL Distillation/Recovery Tests

To support the recyclability trends observed (using TGA), mixtures consisting of 5% w/w lignin dissolved in each PIL were prepared and stirred for at least 30 min at 90 °C to ensure that all of the lignin dissolved. These mixtures were then connected to the vacuum distillation

line to separate the PILs from the lignin (See Appendix B for the distillation set up). Yields of the recovered material were determined, as well as, their purity via NMR analysis and thermal stability (TGA).

2.7. PIL Heating (Stability) Test

Heating tests were run to determine the effect of extended heating on the PILs. The pure PILs were hermetically sealed in crimp-top vials (to prevent loss of the PILs) and stirred for 24 h at 90 °C in an Al heating block. Color changes in the PILs were used to initially assess the effect of heating on the PILs and possible impurity formation. For further characterization, UV/VIS analysis was employed to relate the rate of discoloration to the rate of impurity (amide) formation at different times, while NMR analysis was also used to track the formation of impurities and to determine the possible chemical structure of the impurity(ies).

2.8. Biomass Dissolution: Pretreatment

Dried EF–biomass fibers was added to round-bottom flasks containing PILs that had been equilibrated for 30 min at 90 °C (5% w/w solids loading rate). The mixtures were stirred for 24 h and finally separated using a vacuum filtration line. The filtrate (Liquor 1) was collected for lignin recovery/PIL distillation tests (Liquor 2 is the water-wash on the recovered lignin after distillation of the PIL from Liquor 1). The leftover biomass solid was washed to remove any remaining PIL/lignin using a two-step wash sequence. This involved an initial rinse with 1 L of ethanol (Liquor 3) followed by a rinse with at least 2 L of water (Liquor 4) until a clear filtrate was observed and no ethanol was detected using UV/VIS analysis. The

recovered solids were left to equilibrate overnight in the refrigerator, after which, the moisture content was calculated using NREL Laboratory Analytical Procedure LAP−002,[1,5] to determine the amount of total solids recovered. The collected materials, referred to as PIL–treated biomass fibers (PIL–), were separated into two fractions: one was air-dried, passed through a 0.5 mm screen and stored in a parafilm-sealed vial in a desiccator for subsequent compositional analysis and XRD measurements, while the other was utilized for the SEM analysis (see the process flow diagram–Scheme 2.1.–for the definition of the various fractions).

2.9. Biomass Characterization: Compositional Analysis

Extractive-free (EF–), PIL treated (PIL–), extracted solids and lignin were analyzed for their lignin, carbohydrate, and ash content using NREL Laboratory Analytical Procedure LAP−002.[5] Dried samples (TS of at least 90%) were treated with 72% w/w H_2SO_4 at 30 °C for 1 h, followed by dilute acid (4% w/w) at 121 °C for 1 h. The acid-hydrolyzed samples were separated with a filtering crucible after cooling to near room temperature. The residues were used to measure the acid-insoluble lignin and ash content. The filtrate was used to determine the acid-soluble lignin using a UV/VIS spectrophotometer at 320 nm (CS) 240 nm (SG, PW, BW) with an extinction coefficient value of 30 L g^{-1} cm^{-1} (CS) and for analysis of the monosaccharide concentrations using the IC system described above. The cellulose and xylan contents were calculated from the glucose (5-carbon) and xylose (4-carbon) content multiplied by conversion factors of 0.90 and 0.88, respectively, to account for the water released during the hydrolysis.

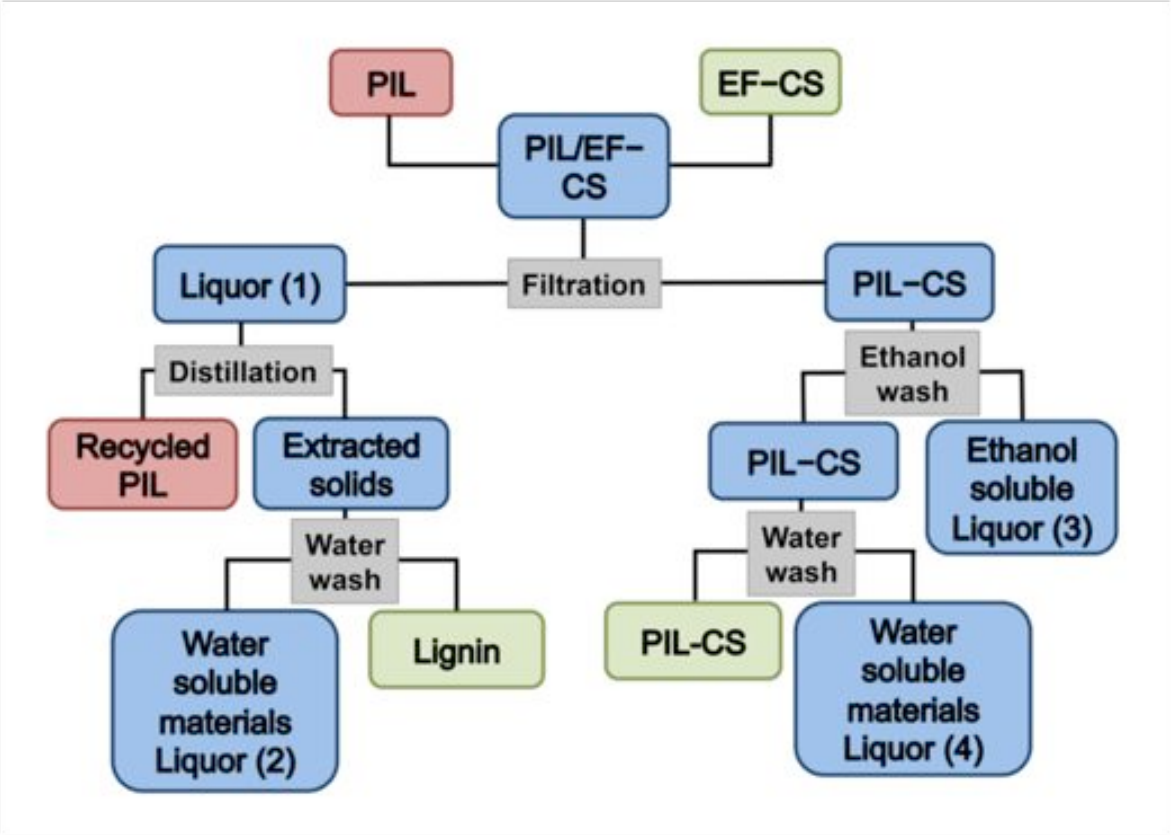

Scheme 2. 1. Lignin-extraction process for CS using a PIL with labeled process streams.

2.10. Rapid Biomass Treatment and Analysis

The following method was developed to swiftly predict the lignin extraction efficiency for each PIL with biomass. EF–biomass fibers were added to 20 ml crimp-top vials containing PILs that had been equilibrated for 30 min at 90 °C (5% w/w solids loading rate). The vials were hermetically sealed and the mixtures were stirred for 24 h and finally separated for analysis. Two (2) ml aliquots of the PIL–biomass mixtures were taken and

centrifuged to separate the solids from the liquids. In the case of PILs with a high viscosity, when the PIL–biomass mixture forms a gel, water was added to reduce the viscosity. The amount of lignin extracted was determined using UV/Vis analysis on the supernatant collected. Each spectra collected is blanked with the pure PIL spectra, which has undergone similar heat treatment. The complete visible spectrum (200–800 nm) of each sample was collected to determine the wavelength of the maximum absorbance, which is indicative of the amount of extracted species from biomass. This method gives relative idea of each PIL's efficiency for lignin removal from biomass. This procedure was also utilized for the time–dependent measurements.

2.11. Enzymatic Hydrolysis

Enzyme digestibility tests were performed on extractive-free (EF–) and PIL treated (PIL–) biomass samples according to the NREL Laboratory Analytical Procedure LAP–009.[6] Samples were prepared in 50 ml Erlenmeyer flasks using a solids loading of 1.5% (w/v) and to each flask, 50 μL penicillin [10 mg/ml] was used as an antibiotic. Enzymes were loaded at a rate of 10 mg protein/mg cellulose of the enzyme cocktail [10 mg protein/ml] and the final volume was adjusted to 10 ml using deionized water. Enzyme cocktail was a generous gift from Novozymes North America, Inc. (Franklinton, NC). These tests were performed at 50 °C and pH 4.8 maintained by a 0.1 M sodium citrate buffer.

The Erlenmeyer flasks containing the enzyme hydrolysis preparations were transferred into a Thermo Scientifique MaxQ Mini 4450 Shaker (Dubuque, Iowa) and agitated at 200 rpm. Samples were taken periodically (2, 4, 6, 8, 10, 12, 24, 36, 48, and 96 h) and analyzed for glucose and xylose. At the specified time, 0.4 ml of each sample was taken

and centrifuged with 40 μl (4% H_2SO_4) in order to reach a final pH ≤ 2 and quench the reaction. The supernatant was then filtered through a 0.2 mm membrane and analyzed using the IC system as described above. Total released glucose (or xylose) after 96 h of hydrolysis was used to calculate the enzymatic digestibility. Untreated biomass fibers were taken through the same procedure as a reference.

2.12. Determination of Kamlet–Taft Solubility Parameters

Measurement of the Kamlet–Taft solubility parameters of a series of PILs was carried out as follows. The solvatochromic dyes, (2,6-Diphenyl-4-(2,4,6-triphenyl-1-pyridinio)-phenolate) Reichardt's dye (RD) (from Sigma Aldrich), 4-nitroaniline (NA) (from Acros Organics), and *N*,*N*-diethyl-4-nitroaniline (NNDE) (from Oakwood Products Inc., Columbia, SC), were used as-received (Figure 2.1.). Solutions of each dye in methanol were prepared at concentrations between 10^{-5} to 10^{-4} M to ensure the absorbance was between 0.4-0.8 units. For each PIL to be tested, 2 ml of each dye's solution was transferred into three separate vials, sealed, and the methanol was then carefully removed by vacuum drying at room temperature. After the solvent was removed, 2 ml of the PIL was added into the vials and homogenized with the left over dye particles in the vial.

The absorbance spectrum of each PIL/dye solution was measured between 350 and 800 nm. Four spectra of each probe were measured, and the average peak maximum (λ_{max}) was calculated. From the wavelength at the maximum absorption, the α, β and π* values were calculated.

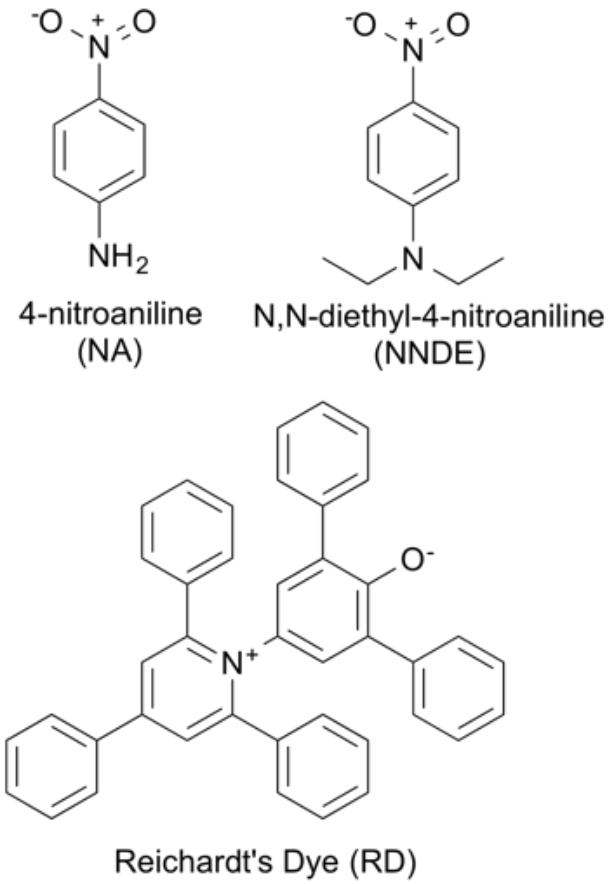

Figure 2. 1. Solvatochromic dye molecules used to determine the Kamlet-Taft solubility parameters.

The normalized E_T^N polarity is obtained by measuring the corresponding maximum absorption[7] of Reichardt's dye (RD) in the chemical of choice:

$$E_T^N = \frac{E_T(30) - 30.7}{32.4},\ E_T(30) = \frac{28591}{\lambda(RD)_{max}}$$

The Kamlet-Taft parameter π* provides a measure of a solvent's dipolarity/polarizability ratio. It is obtained by measuring the wavelength of maximum absorbance, ν_{max} in kK (kilokeyser, 10^{-3} cm^{-1}), of the dye *N*,*N*-diethyl-4-nitroaniline (NNDE):

$$\pi^* = \frac{\nu(NNDE)_{max} - \nu_0}{s}$$

where ν_0: 27.52 kK and *s*: -3.182. The parameter α provides a measure of a solvent's hydrogen-bond-donating acidity (HBD),[8] while the parameter β provides a measure of a solvent's hydrogen-bond-accepting basicity (HBA)[8]:

$$\alpha = \frac{E_T(30) - 14.6\,(\pi^* - 0.23) - 30.31}{16.5}$$

$$\beta = \frac{1.035\,\nu(NA)_{max} - \nu(NNDE)_{max} + 2.64}{16.5}$$

Note: Equations were adopted from the simplifications of Lee *et. al.*[9]

2.13. Molecular Weight Determination

The lignin samples were fully dried under vacuum at 40 °C. Approximately 25 mg of each of the lignin samples was dissolved in pyridine (1.5 ml) followed by acetic anhydride (1.5 ml). The acetylation was carried out overnight in the dark for 24 h. The resulting solutions were then poured in an excess (50 ml) of ethanol and centrifuged/washed 3 times. The solvent was removed using a rotary evaporator. After this, the lignin samples were fully dried under vacuum at 40 °C. The obtained acetylated samples were dissolved in tetrahydrofuran (THF). The molecular weight was then characterized by a GPC using seize exclusion chromatography (SEC).

References:

1. Hames, B.; Ruiz, R.; Scarlata, C.; Sluiter, A.; Sluiter J.; and Templeton, D. *Preparation of Samples for Compositional Analysis*; NREL Analytical Procedure LAP-021, Technical Report NREL/TP-510-42620: National Renewable Energy Laboratory (NREL), Golden, CO, 2008.

2. Sluiter, A.; Ruiz, R.; Scarlata, C.; Sluiter J.; and Templeton, D. *Determination of Extractives in Biomass*; NREL Analytical Procedure LAP-010, Technical Report NREL/TP-510-42619: National Renewable Energy Laboratory (NREL), Golden, CO, 2008.

3. Burrell, G. L.; Burgar, I. M.; Separovic F.; Dunlop, N. F. Preparation of Protic Ionic Liquids with Minimal Water Content and ^{15}N NMR Study of Proton Transfer. *Phys. Chem. Chem. Phys.* **2010**, *12*, 1571–1577.

4. Pinkert, A.; Marsh, K. N.; Pang, S. Alkanolamine Ionic Liquids and their Inability to Dissolve Crystalline Cellulose. *Ind. Eng. Chem. Res.* **2010**, 49, 11809–11813

5. A. Sluiter, B. Hames, R. Ruiz, C. Scarlata, J. Sluiter, D. Templeton and D. Crocker, *Determination of Structural Carbohydrates and Lignin in Biomass*; NREL Analytical Procedure LAP-002, Technical Report NREL/TP-510-42619: National Renewable Energy Laboratory (NREL), Golden, CO, 2010.

6. Selig, M.; Weiss, N.; Ji, Y. *Enzymatic Saccharification of Lignocellulosic Biomass*; NREL Analytical Procedure LAP-009: Technical Report NREL/TP-510-42629, National Renewable Energy Laboratory (NREL), Golden, CO, 2008.

7. Reichardt, C. Solvatochromic Dyes as Solvent Polarity Indicators. *Chem. Re*v. **1994**, *94*, 2319–2358.

8. (a) Kamlet, M. J.; Taft, R. W. The Solvatochromic Comparison Method. I. The .beta.-Scale of Solvent Hydrogen-Bond Acceptor (HBA) Basicities *J. Am. Chem. Soc*. **1976**, *98*, 377-383. (b) Taft, R.; Kamlet, M. J. The Solvatochromic Comparison Method. 2. The .alpha.-Scale of Solvent Hydrogen-Bond Donor (HBD) Acidities. *J. Am. Chem. Soc*. **1976**, *98*, 2886–2894. (c) Kamlet, M. J.; Abboud, J. L.; Abraham, M. H.; Taft, R. W. Linear Solvation Energy Relationships. 23. A Comprehensive Collection of the Solvatochromic Parameters, .pi.*, .alpha., And .beta., and some Methods for Simplifying the Generalized Solvatochromic Equation. *J. Org. Chem*. **1983**, *48*, 2877.

9. Lee, J. M.; Ruckes, S.; Prausnitz, J. M. Solvent Polarities and Kamlet–Taft Parameters for Ionic Liquids Containing a Pyridinium Cation. *J. Phys. Chem. B* **2008**, 112, 1473–1476.

CHAPTER 3: Lignin Extraction from Biomass Using PILs: A Short Study

Abstract

This study demonstrates an effective method that has been developed for the simple extraction of lignin from lignocellulosic biomass using PILs. After the lignin-extraction step, the PIL is easily recovered using distillation leaving the separated lignin and cellulose-rich residues available for further processing. Biopolymer solubility tests indicate that increasing the xylan (i.e., hemicellulose) solubility in the PIL results in greater fiber disruption/penetration, which significantly enhances the effectiveness of the lignin extraction. The physical and thermal properties of the PIL depict that the xylan solubility depends on the PIL's ionicity. One of the PILs studied, pyrrolidinium acetate ([Pyrr][Ac]), is able to selectively extract up to 75% of the lignin found in cornstover, leaving up to 93% of the polysaccharides recovered in the cellulose-rich pulp.

3.1. Introduction

Effectively partitioning lignocellulosic biomass into its various fractions—cellulose, hemicellulose and lignin—is essential for the implementation of a bio-based economy that depends on the production of biofuels, biomaterials and bioproducts from naturally occurring biopolymers.[1-5] In particular, an efficient, low-cost technique for the removal and recovery of lignin, the component that largely renders biomass intractable,[6-12] is necessary to facilitate easier access to the polysaccharides (cellulose and hemicellulose) and the production of valuable side-product streams based on each component.[13-15]

Current separation techniques for lignin removal suffer significant drawbacks such as being energy intensive and environmentally harmful, and these need to be optimized to minimize waste generation and resource underutilization (lignin). Here it is demonstrated that PILs can be used as an alternative to conventional (chemically intensive) lignin removal methods for biomass processing. The low cost of these reagents (acid and base), as well as the simplicity of the PIL synthesis, render the production of PILs more cost friendly than their aprotic counterparts.[16] Furthermore, by taking advantage of the reversible exothermic reaction for PIL synthesis (Scheme 3. 1) and the high decomposition temperature ($T_{decomp} \geq$ 200 ºC) for lignin, a procedure for the facile recovery/recycling of the PIL is available. Once the lignin has been extracted from the biomass using a PIL, further separation via simple distillation is employed to recover the PIL leaving the non-volatile extracted lignin available for further processing. Three PILs with different cations (Figure 3. 1**)** were utilized to demonstrate this method and explore the properties of the PIL that result in superior lignin extraction efficiency.

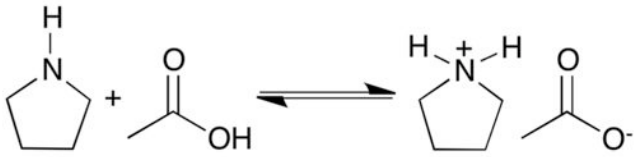

Scheme 3. 1. Formation reaction for PILs.

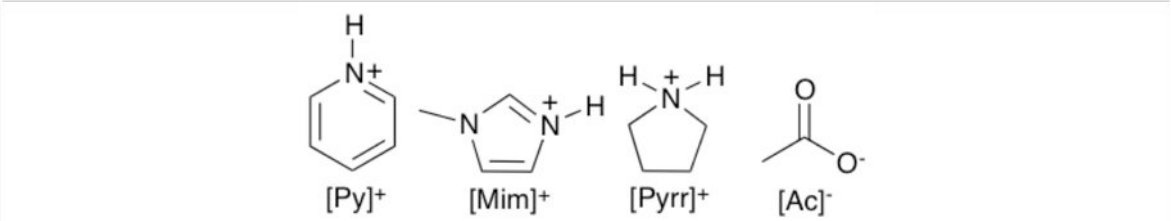

Figure 3. 1. PIL ions and their abbreviations: pyridinium $[Py]^+$, 1-methylimidazolium $[Mim]^+$, pyrrolidinium $[Pyrr]^+$ and acetate $[Ac]^-$.

3.2. PIL Characterization: Ionicity and Thermal Stability

PIL synthesis occurs via a reversible proton exchange (Scheme 3. 1.), however, in certain cases, the reaction could favor the formation of the reagents instead of the PILs depending on the combination of acid/base used, resulting in a low ionicity.[17] The extent of this proton transfer (i.e., ion formation) has been linked to the difference in the pK_a values for the acid and base (ΔpK_a), which is typically determined in dilute aqueous solutions. The greater the difference, the more the reaction is driven to the right in Scheme 3. 1. and serves as one indication of the completeness of proton transfer.[18] Given that the pK_a values for the reagents are Py 5.14, Mim 7.50, Pyrr 11.27, and HAc 4.76,[19-20] this suggests that the ionicity (fraction of amine-acid mixture present as ions) should increase in the order:

$$[Py][Ac] < [Mim][Ac] << [Pyrr][Ac]$$

Another measure of ionicity is to categorize the PILs based on the Walden rule.[18, 21–23] The Walden rule relates the ionic mobilities (represented by the molar conductivity Λ) to the fluidity (ϕ) (inverse viscosity) of the medium through which the ions move.[21] Ideally, the

slope should be unity for ions with independent mobility. [18, 21–23] The position of the ideal line is established using aqueous KCl solutions at high dilution. [18, 23] PILs with data points below the ideal line are classified as "poor" ILs (i.e., low ionicity), while those that are close to the line are "good" ILs and above the line are "super" ILs.[18, 23] Most PILs are classified as poor ILs, as they fall below the ideal line (Figure 3. 2),[21–23] however, the Walden plot shows an increasing trend in ionicity between the three PILs used that closely matches the trend observed with the ΔpK_a values (Figure 3. 2).

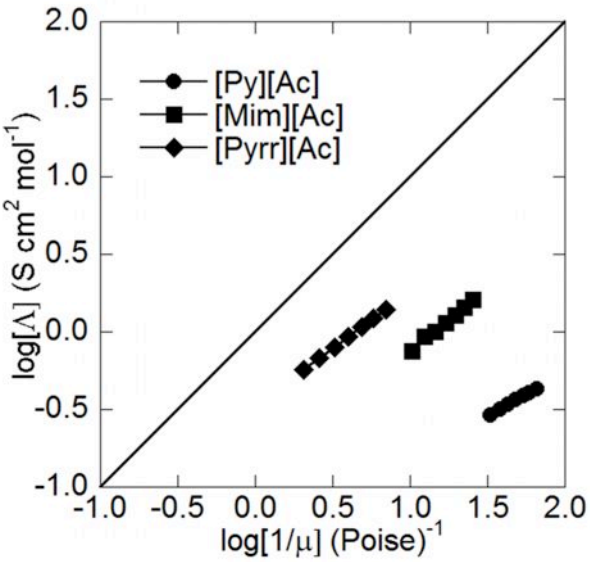

Figure 3. 2. Walden Plot as a measure of ionicity for PILs used in this study.

$$\Lambda = \frac{\sigma * \mathrm{M.M}}{\rho}$$

$$\phi = \eta^{-1}$$

where:

σ = ionic conductivity

M. M = molecular mass

ρ = density

η = viscosity

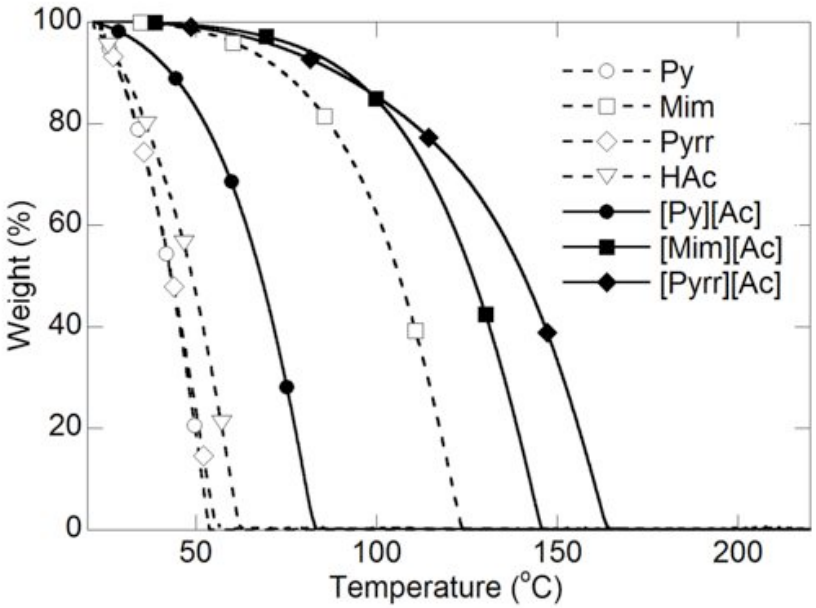

Figure 3. 3. Variable-temperature TGA heating traces (5 °C min^{-1}) of reagents and PILs.

Mass loss at elevated temperature for the PILs occurs due to the formation and subsequent loss of volatile reagents (i.e., the reversal of the proton exchange reaction - Scheme 3. 1). Therefore, it is important to monitor the thermal stability of the PILs in order to predict the ease of recyclability (via distillation). The thermal stability of the PILs follows the trend in ionicity established above (Figure 3. 2). For the [Py][Ac] and [Mim][Ac] PILs, mass loss occurs at temperatures only moderately higher than that for the amines from which the salts are formed. However, in the [Pyrr][Ac] PIL, mass loss does not occur until a substantially higher temperature than for the highly volatile pyrrolidine (Pyrr) or acetic acid (HAc) (Figure 3. 3). This suggests that in the [Pyrr][Ac] PIL, proton transfer in the amine is largely complete and the N-H bond formed is quite stable. This is expected as the thermal stability of ionized species are usually higher than their neutral complements.[18,24] When ILs are synthesized, charged species are attracted and strongly interact to balance their effective charge, therefore, producing highly stable aggregates that are typically more difficult to separate—resulting in the increased thermal stability that is observed.[18,24]

3.3. Solubility of Biopolymers in PILs

The solubility of biomass components in the PILs was determined initially using commercially available model biopolymers: lignin (Kraft lignin-Indulin AT), cellulose (microcrystalline cellulose) and hemicellulose (xylan from beech wood). Figures 3. 4 and 3. 5 show the solubility of the commercially available lignin, cellulose and xylan (biomass components) in the PILs and reagents, respectively, with 5% w/w of the biomass components

added to the glass vials. The vials were hermetically-sealed to prevent loss of the reagents and stirred for 24 h at 90 °C in an Al heating block.

The pictures (Figures 3. 4–3. 5) are helpful for visualizing the relative solubility of the biomass components and approximating the saturation concentrations, which was also determined quantitatively using the method previously described. The PILs, as well as the reagents used to synthesize them, are able to dissolve large amounts of Kraft lignin (Table 3. 1)—with the exception of Pyrr and HAc. Furthermore, a negligible solubility of cellulose in t he reagents and PILs is noted. Xylan (the principal component of corn stover hemicellulose),[25] on the other hand, has widely varying solubility in the different reagents and PILs (Table 3. 1). Notably, xylan is largely insoluble in Py, Pyrr, HAc, and [Py][Ac]; is moderately soluble in Mim and [Mim][Ac]; and has a relatively high solubility in [Pyrr][Ac]. Given that [Pyrr][Ac] is more "ionic" than the other PILs, this suggests that the xylan and lignin solubility in this PIL may originate from interactions with the salt ions (as the solubility of these biopolymers in both Pyrr and HAc is quite low), leading to the conclusion that the trend in xylan solubility (and cellulose solubility to a lower extent) is proportional to the PILs ionicity. These results provide verification that PILs are able to dissolve large amounts of (Kraft) lignin and little to no cellulose, which is necessary for the selective extraction (partitioning) of lignin for lignocellulosic biomass fractionation. These results, however, do not indicate that a PIL is a much more favorable lignin extraction agent than the reagents, but this will be demonstrated below for lignin extraction from corn stover (CS).

Figure 3. 4. Images depicting the solubility of 5% w/w commercially available biomass components (Kraft lignin, microcrystalline cellulose and xylan) in the PILs: (a) after stirring for 30 min at room temperature (25 °C) and (b) after stirring for 24 h at 90 °C (sample sizes were 10.0 g).

Figure 3. 5. Images depicting the solubility of 5% w/w commercially available biomass components (Kraft lignin, microcrystalline cellulose and xylan) in reagents used to synthesize the PILs: (a) after stirring for 30 min at room temperature (25 °C) and (b) after stirring for 24 h at 90 °C (sample sizes were 10.0 g).

Table 3. 1. Solubility of Kraft lignin, cellulose and xylan (% w/w) in the reagents and PILs (after heating/stirring at 90 °C for 24 h)

	lignin	cellulose	xylan
Py	> 50	0.10 ± 0.00	0.02 ± 0.02
Mim	> 50	0.24 ± 0.02	6.34 ± 0.17
Pyrr	7.98 ± 0.10	0.63 ± 0.00	1.44 ± 0.07
HAc	0.7	0.07 ± 0.01	0.90 ± 0.04
[Py][Ac]	> 50	0.12 ± 0.03	0.82 ± 0.00
[Mim][Ac]	> 50	0.20 ± 0.05	5.60 ± 0.77
[Pyrr][Ac]	> 50	0.79 ± 0.04	> 15[a]

[a] Solubility limited by viscosity.

3.4. Lignin Extractability from Biomass

The structure and properties of Kraft lignin differ markedly from that of biomass lignin. Therefore, the PILs were then employed to remove lignin from extractive-free corn stover (EF-CS). After heating and stirring the EF-CS in the PILs (90 °C for 24 h), the insoluble solids (i.e., PIL-CS) were separated by filtration from the liquid PIL filtrate (i.e., Liquor 1) (Scheme 2. 2). Compositional analysis of the solids (Table 3. 2) revealed that the lignin extraction efficiency increased in the order:

$$[Py][Ac] < [Mim][Ac] << [Pyrr][Ac]$$

The [Pyrr][Ac] PIL was able to extract greater than 70% of the lignin in the EF-CS, leaving a polysaccharide-rich stream (PIL-CS) (Tables 3. 3). Despite the high Kraft lignin solubility in all three PILs (Table 3. 1), the amount of CS-lignin extracted varied significantly

for the three PILs (Table 3. 2). The trend in lignin removal followed the trend in xylan solubility previously established (Table 3. 1). Using the same processing conditions (stirring at 90 °C for 24 h), the neat reagents were found to be ineffective at extracting lignin from corn stover–% lignin after pretreatment: Py (15.6%), Mim (13.9%), Pyrr (15.0%) and HAc (16.5%) (compare with results in Table 3. 2). Note that the Mim reagent, which is able to dissolve some hemicellulose (xylan) (Table 3. 1), is able to extract more lignin than the Py and Pyrr, but these reagents still does not extract a significant amount of the lignin from the CS.

Table 3. 2. Composition (% w/w) of EF-CS and PIL-CS after pretreatment (90 °C for 24 h)

	EF-CS	[Py][Ac]-CS	[Mim][Ac]-CS	[Pyrr][Ac]-CS
lignin	16.6	15.7	14.3	6.2
glucan	38.2	42.6	44.5	52.8
xylan	20.0	20.8	22.1	22.0
arabinan	2.5	1.3	1.8	2.9
galactan	1.1	0.9	0.8	0.8
mannan	0.1	0.0	0.2	0.2
ash	0.9	1.1	2.0	0.4
total	61.9	65.6	69.4	78.7

Table 3. 3. Composition of corn stover components after pretreatment with [Pyrr][Ac]—amount recovered, g (% w/w of initial component in EF-CS)

	lignin	glucan	xylan	arabinan	galactan	mannan	ash
EF-CS	0.833 (100)	1.913 (100)	1.000 (100)	0.126 (100)	0.053 (100)	0.005 (100)	0.040 (100)
extracted solids from [Pyrr][Ac] (Lignin)	0.606 (72.81)	0.067 (3.50)	0.009 (0.85)	0.006 (5.00)	0.001 (1.00)	0.000 (6.00)	0.029 (71.25)
water wash-lignin (Liquor 2)	0.025 (3.00)	0.204 (10.66)	0.311 (31.07)	0.028 (22.55)	0.026 (49.18)	0.004 (77.84)	-
[Pyrr][Ac]-CS (PIL-CS)	0.185 (22.19)	1.572 (82.17)	0.656 (65.53)	0.087 (68.95)	0.023 (43.32)	0.001 (12.52)	0.010 (25.00)
ethanol wash-CS (Liquor 3)	0.010 (1.20)	~ 0	~ 0	~ 0	~ 0	~ 0	-
water wash-CS (Liquor 4)	0.005 (0.60)	~ 0	~ 0	~ 0	~ 0	~ 0	-
total	0.831 (99.80)	1.834 (96.33)	0.975 (97.45)	0.122 (96.50)	0.050 (93.50)	0.005 (96.00)	0.039 (96.25)
Liquor 2 + PIL-CS	0.210 (25.19)	1.776 (92.83)	0.967 (96.60)	0.115 (91.50)	0.049 (92.50)	0.005 (90.36)	0.010 (25.00)

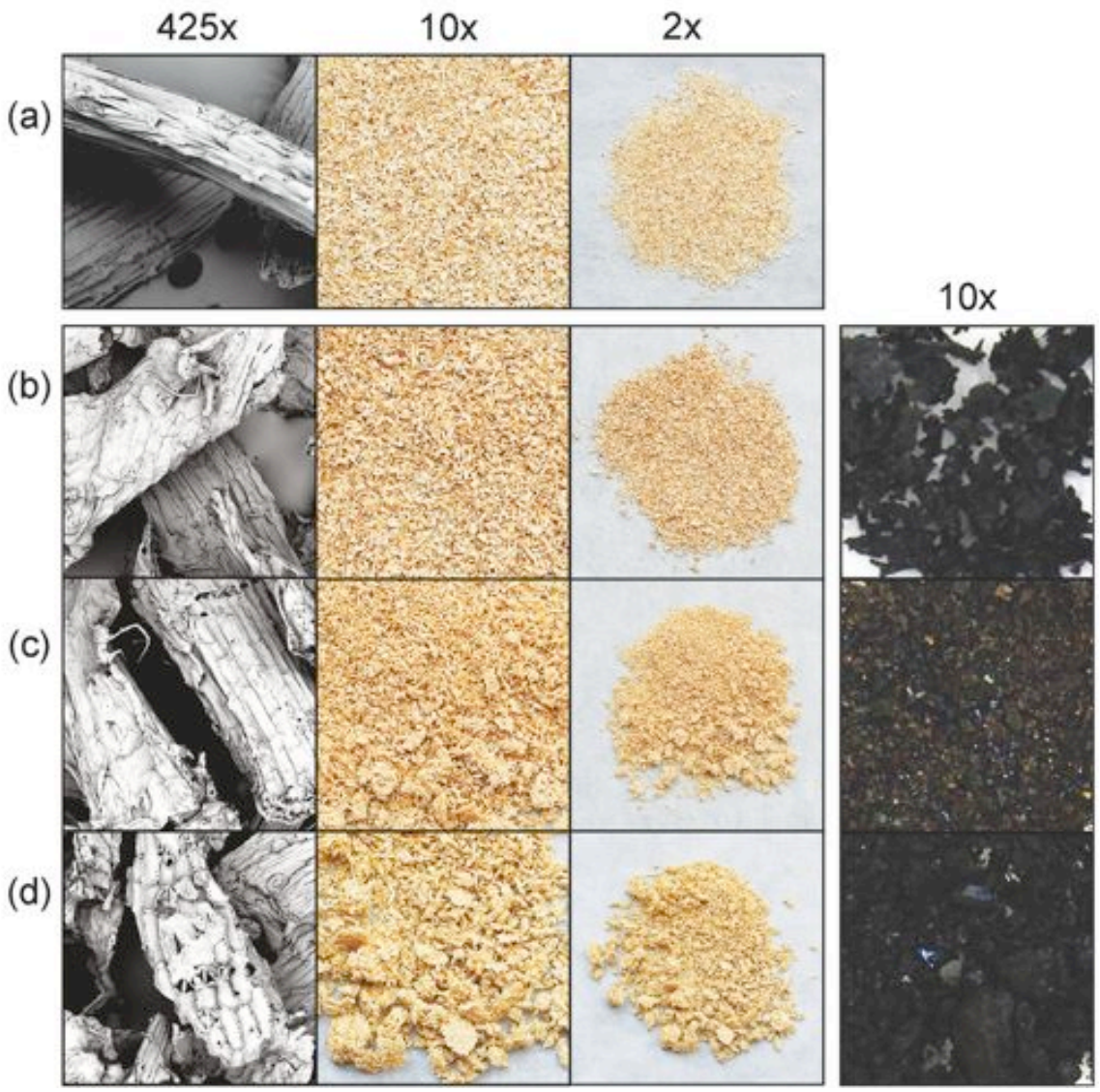

Figure 3. 6. Images depicting the CS fibers before and after PIL treatment and the recovered lignin from CS after PIL treatment: (a) EF-CS, (b) [Py][Ac]-CS, (c) [Mim][Ac]-CS and (d) [Pyrr][Ac]-CS.

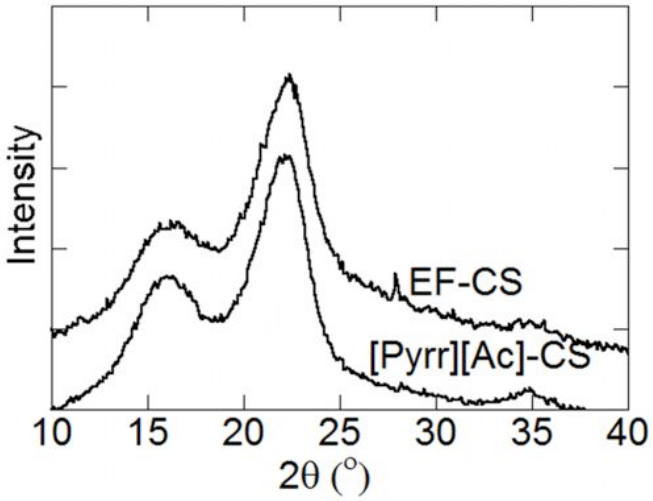

Figure 3. 7. XRD of CS recovered from PIL pretreatment.

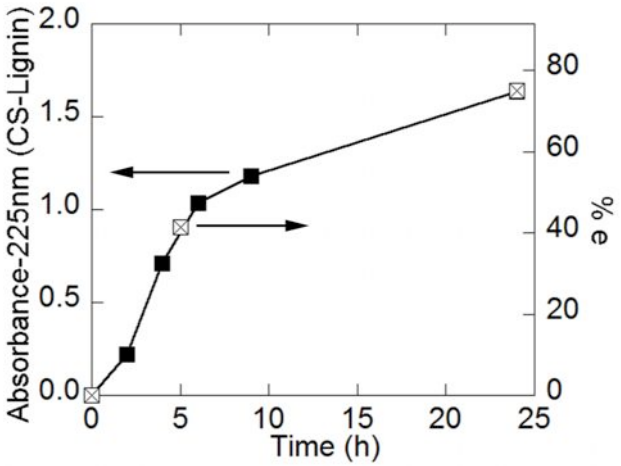

Figure 3. 8. Rate of lignin removal (% e is percent extracted) from CS with the [Pyrr][Ac] PIL using UV/VIS analysis (absorbance data shown on left, compositional analysis data shown on right).

SEM analysis of the CS fibers before and after the PIL pretreatment confirmed that an increase in lignin removal does correspond with an increased disruption of the CS fibers (increase in the size of the fibers, as well as the formation of pores on the fiber surface- Figure 3. 6)–indicating that penetration of the CS fibers by the PILs has occurred as both more lignin and hemicellulose are removed. Lignin found in the outer plant cell wall accounts for only about 20% of the lignin in biomass.[26] In order to access the remainder of the lignin, one or more of the polysaccharides needs to be partially soluble in the PIL. The crystallinity of the PIL-CS fibres was determine using XRD analysis, which indicated a sharpening of the peaks after PIL processing due to the retention of the cellulose structure (cellulose-I) and removal of the lignin (Figure 3. 7).

A study of the time-dependent pretreatment of CS with the [Pyrr][Ac] PIL shows that an increased reaction time is optimal for high lignin removal (Figure 3. 8). Using UV/Vis spectroscopy, the absorbance of the liquid portion was measured at various time increments to access the amount of lignin removed after various pretreatment times. The compositional analyses for three samples are also included to support this data (0 h, 5 h and 24 h) (Figure 3. 8).

3.5. PIL Recyclability and Characterization of Recovered Materials

To demonstrate the separation/recyclability technique, mixtures of the PILs with Kraft lignin were made and then separated using vacuum distillation. The distillation temperature increased in the same order as the thermal stability trends observed from the TGA data (Figure 3. 3, Table 3. 4) and the process does not require a high distillation

temperature, especially with the application of a partial vacuum (Table 3. 4). The amount of PIL recovered and its purity and yield were determined both gravimetrically and via NMR analysis (Table 3. 4 and Figures C. 5–C. 7). The recovered PILs and lignin exhibit similar thermal stability trends to those found for the initial PILs and Kraft lignin used (Figures 3. 9–3. 11). Greater than 90% of the PILs were recovered, but small amounts of the PILs remained with the lignin. (Table 3. 4) Changes in the physical appearance of the lignin are noted which is most likely due to differences in particle size of the lignin upon re-precipitation (Figure 3. 9). The loss in yield of the PILs may be due to some amount of PIL that is strongly coordinated to the lignin and/or due to amides formed from the degradation side reaction (see below); it was found that further mass loss occurred with additional periods of drying in a vacuum oven, or by washing the lignin with a solvent (water/ethanol).

Table 3. 4. PIL yield after recovery from each PIL, distillation conditions and mole ratio of acid-to-base from NMR analysis

PIL used	% recovered	mole fraction (acid:base) (NMR)	distillation conditions (T, P)
[Py][Ac]	98.15	0.49:0.51	50, 0.1 torr
[Mim][Ac]	96.75	0.50:050	70, 0.1 torr
[Pyrr][Ac]	93.18	0.51:0.49	100, 0.1 torr

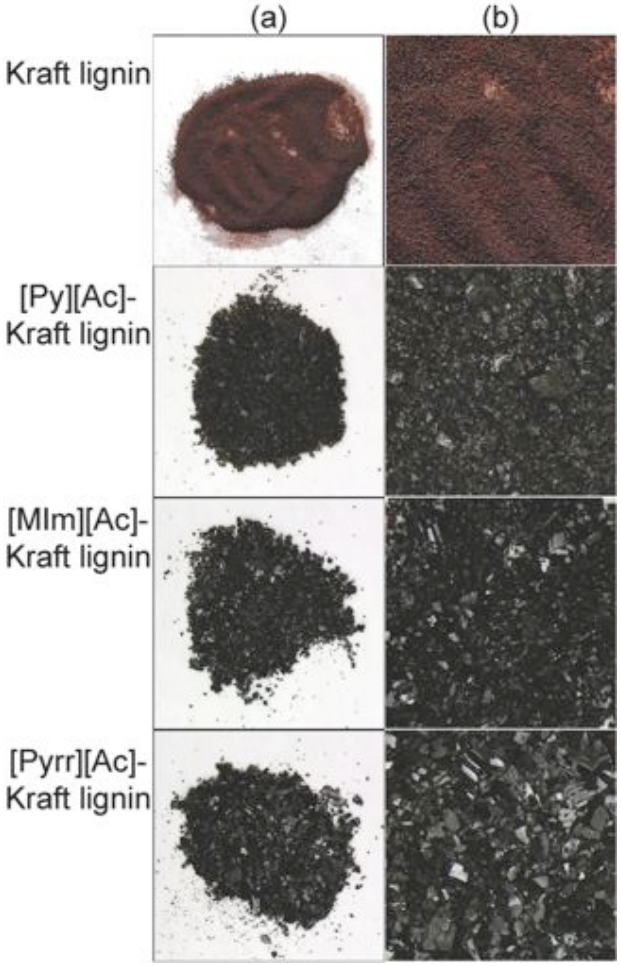

Figure 3. 9. Photographic images (a) 2x and (b) 10x of original (Kraft lignin) and recovered lignin from PIL dissolution.

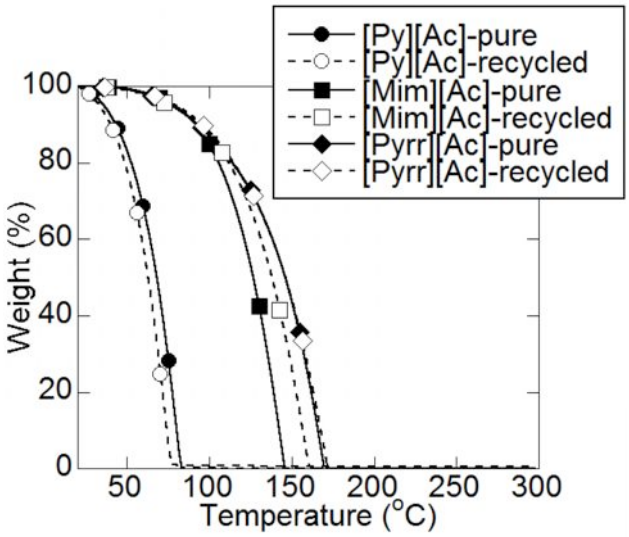

Figure 3. 10. Variable-temperature TGA heating traces of PILs before and after recycling.

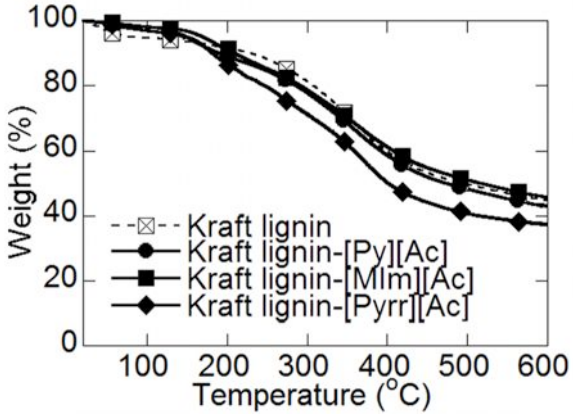

Figure 3. 11. Variable-temperature TGA heating traces of original (Kraft lignin) and recovered lignin from PIL dissolution.

Similar dissolution experiments were also performed using cellulose in order to observe any changes in the morphology of the polysaccharides after PIL dissolution. This may be important for the downstream processing of cellulose into glucose via enzymatic hydrolysis. Since the PILs dissolve only a very small amount of cellulose (less than 1% w/w cellulose), undissolved cellulose remained after heating at 90 °C for 24 h. The liquids were separated from the solids using vacuum filtration, after which the undissolved solids were washed with solvent (ethanol, and then water), using vacuum filtration to separate the solvent. The detailed procedure is described above with cellulose used instead of EF-CS.

XRD data was used to determine the crystal structure of this material for comparison with that of the initial cellulose powder (Figure 3. 12). The recovered cellulose is highly crystalline and the data closely matches that of the original material (i.e., with the cellulose-I structure). A small peak may be present after treatment with the [Pyrr][Ac] PIL, however, indicating a different crystal structure (i.e., cellulose-II) (Figure 3. 12). Nevertheless, one can conclude that the recovered cellulose largely maintains its original crystallinity and crystal structure. Since the [Pyrr][Ac] PIL only dissolves about 0.8% w/w cellulose (the maximum of the three PILs) (Table 3. 1), there is almost no allowance for interaction between the PIL and cellulose, which results in little to no modification of the cellulose. SEM analysis shows no major changes in the cellulose fibers after PIL treatment (Figure 3. 13).

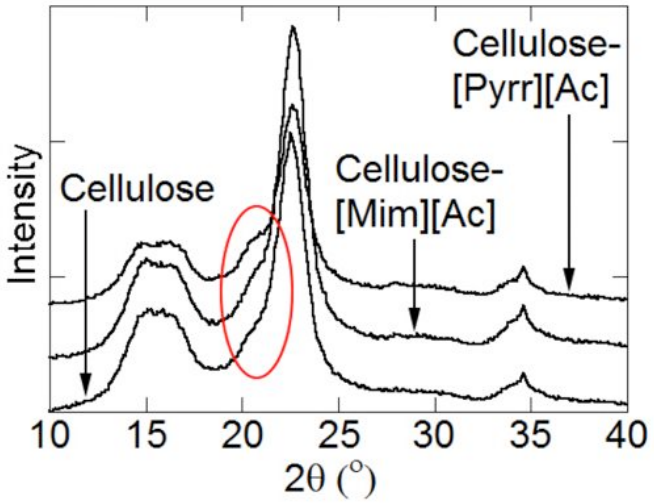

Figure 3. 12. XRD of cellulose recovered from PIL dissolution.

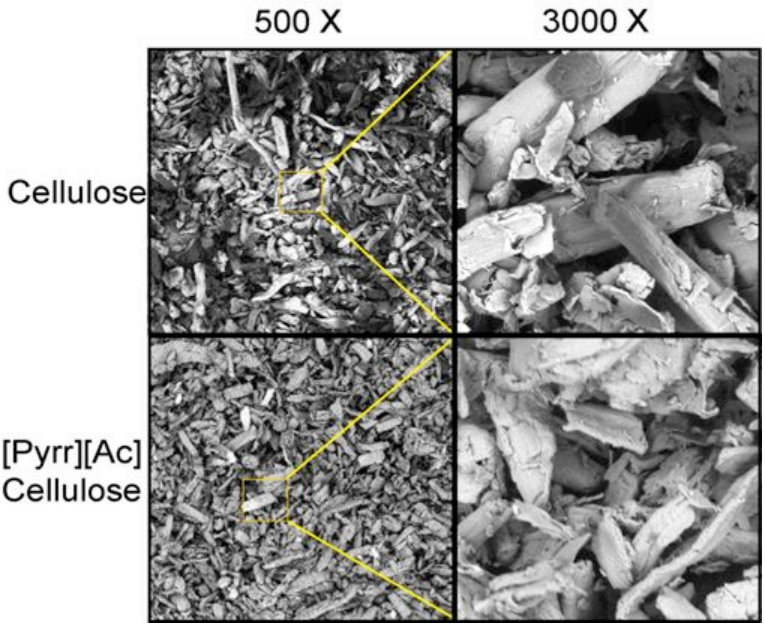

Figure 3. 13. Images of cellulose recovered from PIL dissolution (500X and 3000X).

These results demonstrate the ease of recyclability of the PILs and the distillation techniques was applied to recover the PILs from the filtrate mixture containing the extracted materials (lignin with a lesser amount of hemicellulose and other components) (Liquor 1). The recovered PILs were characterized using ^{1}H-NMR analysis (Figure C. 8–C. 10). The [Py][Ac] and [Mim][Ac] PILs were recovered as essentially pure PILs, but the [Pyrr][Ac] PIL contained some amide impurity (Figures C. 8–C. 10) due to the extensive pretreatment time at elevated temperature.[27] Note that the shift in the peak associated with the protons bonded to the cation nitrogen atom was verified to be due to the presence of small amounts of water (see below). The recovered lignin extracts exhibit similar thermal stability trends to that of Kraft lignin (Figure 3. 14).

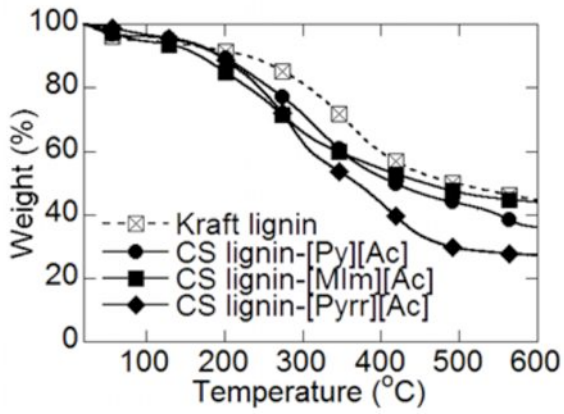

Figure 3. 14. Variable-temperature TGA heating traces of Kraft lignin and the recovered lignin from CS after PIL treatment.

3.6. Concerns about the Purity of the Recovered PILs

Heating the PILs at 90 °C for 24 h resulted in the discoloration of the [Mim][Ac] and [Pyrr][Ac] PILs (Figure 3. 15). No significantly different peaks were observed in the NMR analysis of the [Mim][Ac] PIL after the heating tests (Figure C. 9). For the [Mim][Ac] PIL, this change in color is likely a result of amine discoloration of Mim (the base used to synthesize PIL).[28] Oxidation reactions are common in aromatic amines when they are left standing or exposed to air/water and this is increased upon heating, but the amounts are small and undetectable by NMR spectrometry.[28]

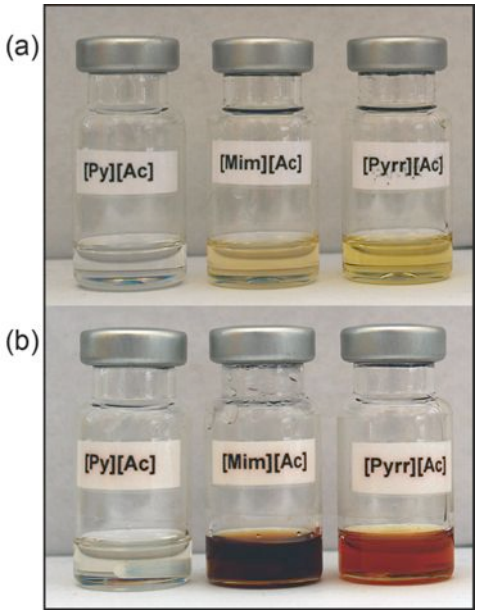

Figure 3. 15. Photos of PILs: (a) before and (b) after heating for 24 h at 90 °C.

^{1}H-NMR analysis of the [Pyrr][Ac] PIL, on the other hand, displayed new peaks after the heating tests, which indicates the formation of a substantial amount of a side product/impurity (Figure C. 10). Combinations of saturated amines and carboxylic acids are susceptible to the formation of amides when given enough energy input (Scheme 3. 2).[27] Energy, in the form of heat, is input during the dissolution process and could therefore lead to the formation of amides.

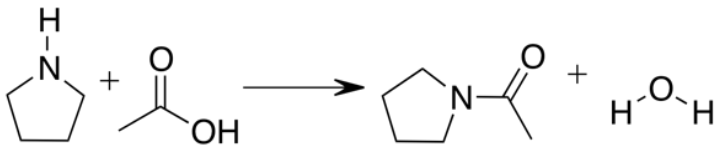

Scheme 3. 2. Formation of the amide 1-(pyrrolidin-1-yl)ethanone, a possible side product that is found in recycled [Pyrr][Ac].

In order to further understand the effect of heating on these PILs, NMR analysis of the [Pyrr][Ac] PIL after different heating times was carried out (Figure 3. 16 a). Looking at the chemical shifts of the resultant NMR spectra, there is the development of new peaks in the recovered PIL at δ = 2.08, 3.38 and 3.56 ppm (Figure 3. 16 b, c).

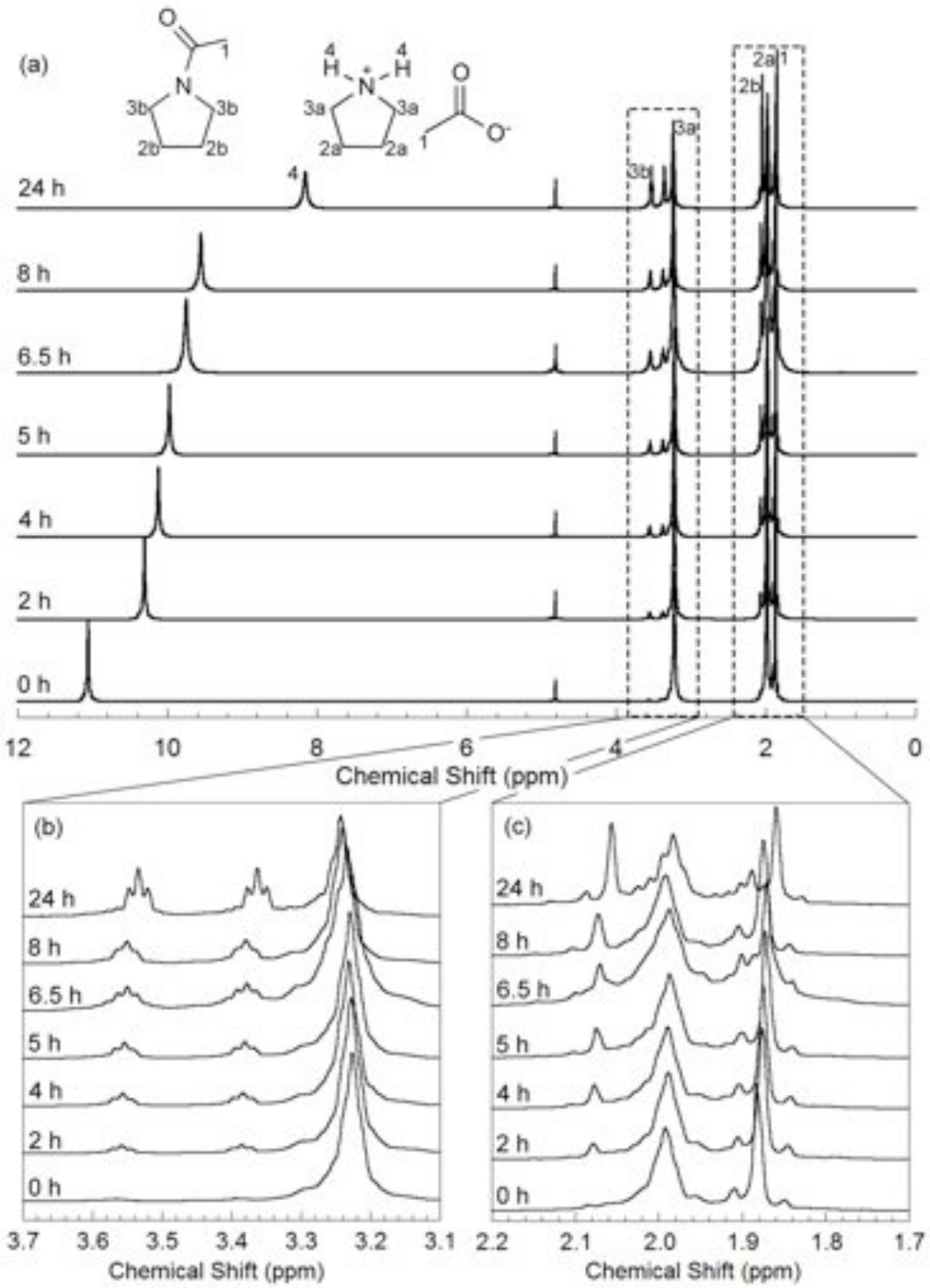

Figure 3. 16. Variation in ^{1}H-NMR spectra (δ_{solv} = 4.75 ppm) of PIL ([Pyrr][Ac]) with heating time showing: (a) full NMR spectrum, (b) δ = 3.1-3.7 ppm and (c) δ = 1.7-2.2 ppm.

The two distinct peaks at δ = 3.38 to 3.56 ppm can be accredited to the protons on the cation α carbon atom next to the nitrogen atom (Scheme 3. 2, Figure 3. 16 b). When the amide forms, there is hindered rotation at that C-N bond that removes the symmetry of those two protons, causing the splitting pattern observed (doublet of triplets). This effect is weaker on the β protons, but a

clear peak at δ = 2.08 ppm is also observed to increase as the heating time increases (Figure 3. 16 c).

There is also shifting in the N-H peak [δ ≈ 8-12 ppm], which is believed to be due to the presence of water that is formed with the amides (Scheme 3. 2). The proton on the nitrogen is the most acidic proton and so will be most affected by the presence of water molecules (see below). As the heating time increases, the water content increases and the position of the N-H peak changes. Recovered PILs from distillation always show a shift in the N-H peak that was suspected to be due to small amounts of water introduced upon exposure to the atmosphere or from interactions with biomass and biopolymers (Figure C. 5–C. 10). To examine this further, different samples were prepared by introducing various amounts of water into the [Pyrr][Ac] PIL (measured by Karl Fisher). The NMR analysis of each sample confirms that small changes in water content do affect the chemical shift of the N-H peak, which is likely due to changes in the H-bonding network as water is added into the system (Figure 3. 17).

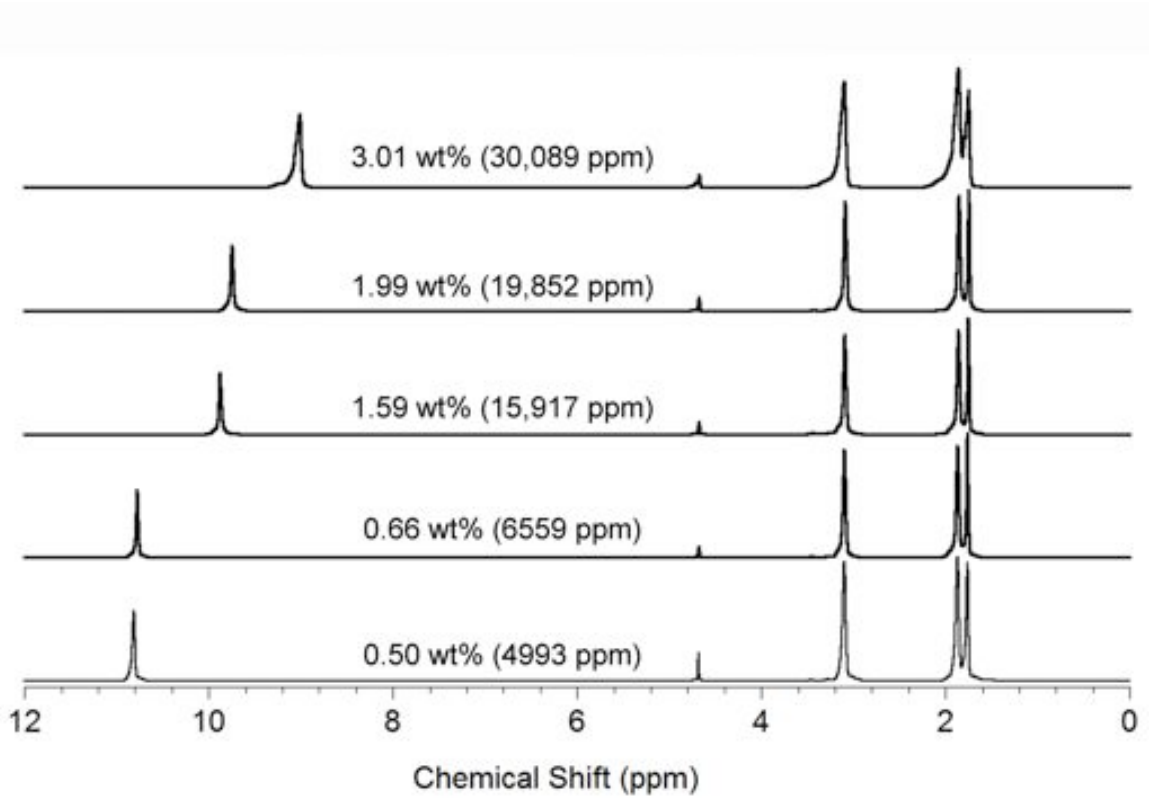

Figure 3. 17. Effect of changing water content on the chemical shifts of the acidic protons in PILs ([Pyrr][Ac]).

Quantification of the amide content using UV/Vis and NMR analyses indicates the amount of amide formed with increasing heating time (Figure 3. 18). The NMR analysis was used to determine the ratio of impurity to the pure PIL with time. The increasing linear trend observed (Figure 3. 18) indicates that the impurity will continue to form providing pure reagents (starting material) are present in the system and enough energy is introduced to excite them. The trend observed from the UV/Vis spectra, however, is exponential and starts to level off after 8 h (Figure 3. 18) indicating that the effect of the amide (impurity) on the

absorbance is negligible after a certain amide concentration. The PILs have a relatively low thermal stability, which implies that the reagents are continuously released when the PIL is heated for extended times (Figure 3. 19). This could feed the reaction for the formation of amides.

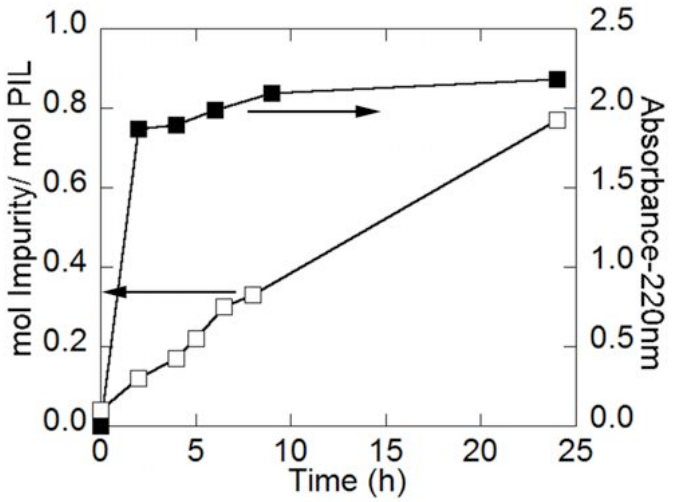

Figure 3. 18. Rate of formation of amide from UV/Vis and NMR analyses.

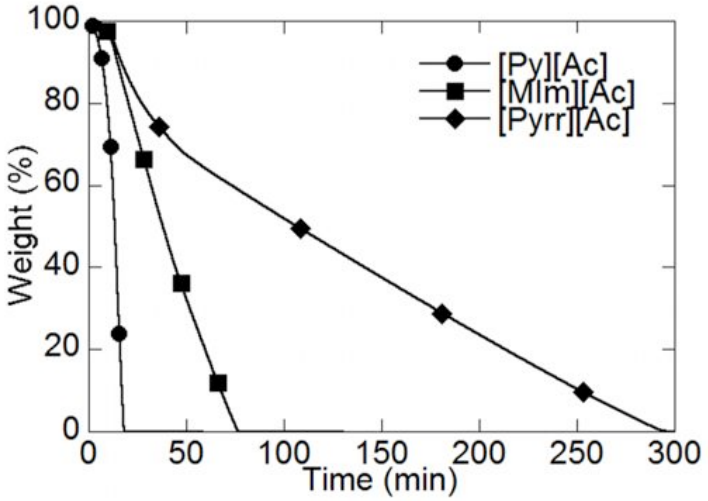

Figure 3. 19. Isothermal TGA heating traces (90 °C) of PILs. Note that the biomass processing with the PILs occurs in sealed containers, in contrast to the TGA measurements.

After the heating tests, an attempt was made to separate the amide impurity from the pure PIL ([Pyrr][Ac]) by distillation. However, NMR peaks for the amide are observed in the recovered material (Figure 3. 20). In addition, a residue remained in the distilling flask that could not be recovered. The presence of amide impurity in the recovered PIL is likely due to the fact that the amide has similar volatility characteristics as the PIL reagents (Pyrr and HAc). This prevents selective separation of the PILs from the amide degradation product by simple distillation.

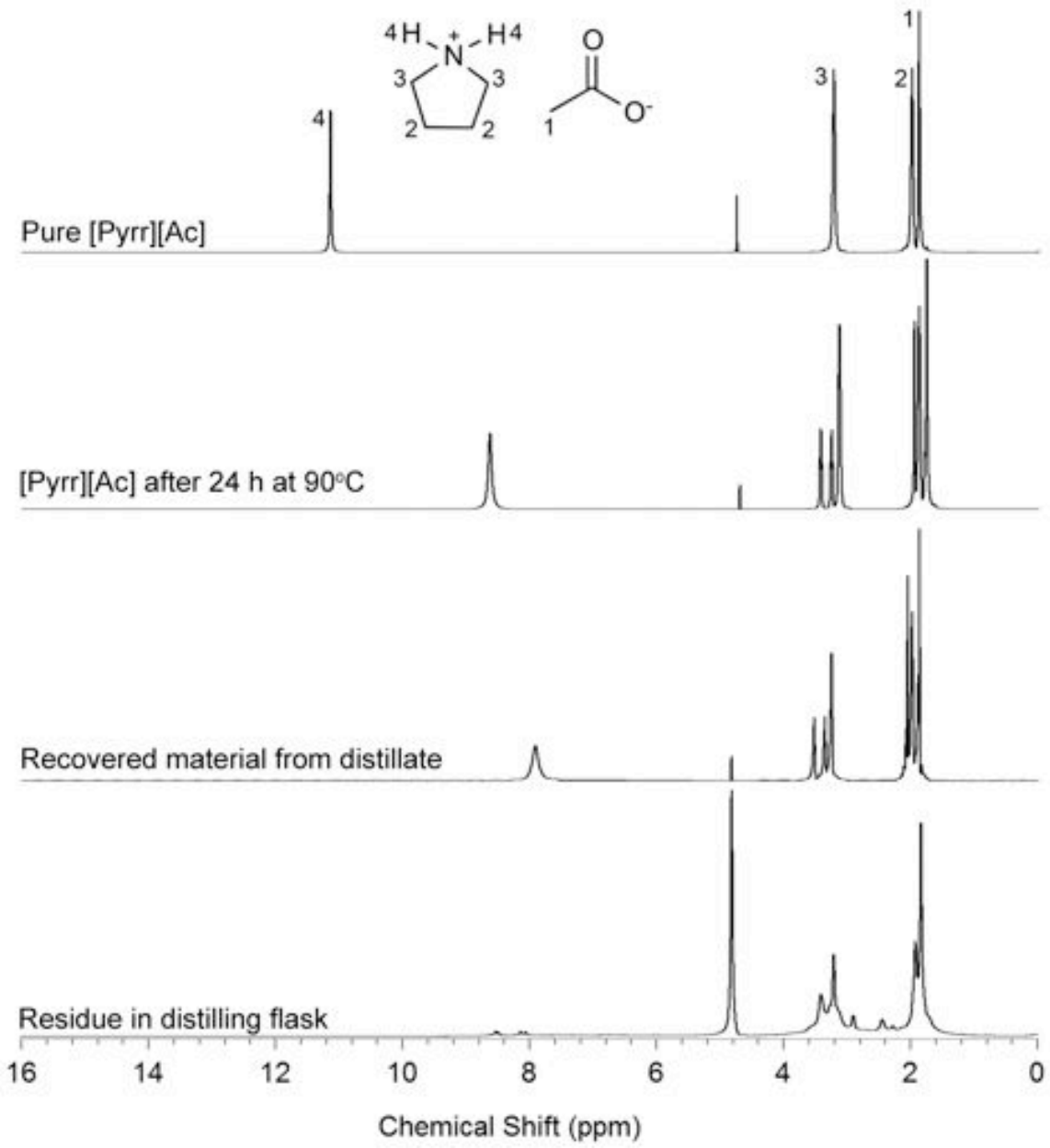

Figure 3. 20. ^{1}H-NMR spectra (δ_{solv} = 4.75 ppm) of [Pyrr][Ac] to determine the amount of amide left over in the recovered PIL.

3.7. Conclusions

The results reported demonstrate that PILs are able to extract large amounts of lignin from biomass. The dissolution, to some extent, of one or more of the polysaccharides, however, is necessary to enable PIL penetration of the biomass fibers and full access to the lignin. Partial dissolution of xylan, the major hemicellulose component in CS, disrupts the fibers enough to attain a very high amount of lignin extraction. This preliminary work with three PILs suggests that the solubility of xylan in the PILs may be directly proportional to the salt ionicity. Further work systematically varying the structure of ions will confirm this.

Pure PILs can be recovered at yields approaching 100% using relatively mild distillation conditions (with a partial vacuum). For full PIL recovery, however, a careful selection of the anions/cations used to synthesize the PIL is necessary to avoid PILs that are susceptible to the formation of amide by-products due to thermal degradation.[27] This reaction is thought to be minimized by increasing the number of substituents on the amine group. This slight increase in steric hindrance on the cation could reduce the reactivity of the reagents and select for the lower energy state–the PIL.[27] PILs, which do not undergo this side reaction, but extract even greater amounts of lignin from CS have, however, been identified and will be discussed in subsequent chapters.

The functionality/composition of the lignin extracted by the PILs appears to be largely retained. It is crucial to note that, after the PIL distillation step leaving the lignin-rich solids, the polysaccharides and sugars extracted by the PIL may be readily separated from the lignin by a simple water wash step (Liquor 2 in Scheme 2. 2), as the lignin is insoluble in

water. If this wash is then combined with the polysaccharide-rich solids, well over 90% of the polysaccharides/sugars may be recovered with removal of approximately 75% of the lignin in the EF-CS (Table 3. 3). Therefore, the use of potentially inexpensive PILs to selectively extract lignin from lignocellulosic biomass with high extraction efficiency and low waste generation is a quite promising means for the total utilization of lignocellulosic biomass—a necessary requirement for the implementation of a biofuel/biorefinery-based economy.

References:

1. Zhang, Y.-H. P. *J. Indus. Microbiol. Biotechnol.* **2008**, *35*, 367–375.
2. Bozell, J. J. *Clean*, **2008**, *36,* 641–647.
3. Clark, J. H. *J. Chem. Technol. Biotechnol.* **2007**, *82*, 603–609.
4. Clark, J. H.; Deswarte, F. E. I.; Farmer, T. J., *Biofuels Bioprod. Biorefin.* **2009**, *3*, 72–90.
5. Clements L. D.; Van Dyne, D. L. In *Biorefineries-Industrial Processes and Products: Status Quo and Future Directions*; Kamm, B., Gruber, P. R., Kamm, M. Eds.; Wiley-VCH Verlag: GmbH, Weinheim, Germany, 2008; 115–128.
6. Hendriks, A. T. W. M.; Zeeman, G. *Bioresour. Technol.* **2009**, *100*, 10–18.
7. Taherzadeh, M.; Karimi K *Int. J. Mol. Sci.* **2008**, *9*, 1621–1651.
8. Kumar, P.; Barrett, D. M.; Delwiche M. J.; Stroeve, P. *Ind. Eng. Chem. Res.* **2009**, 48, 3713–3729.
9. Fu, D.; Mazza, G.; Tamaki Y. J. *J. Agric. Food Chem.* **2010**, *58,* 2915–2922.
10. Lee, S. H.; Doherty, T. V.; Linhardt R. J.; Dordick, J. S. *Biotechnol. Bioeng.* **2009**, *102*, 1368–1376.
11. Tan, S. S. Y.; MacFarlane, D. R.; Upfal, J.; Edye, L. A.; W. O. S Doherty, W. O. S.; Patti, A. F.; Pringle J. M.; Scott, J. L. *Green Chem.* **2009**, *11*, 339–XX.
12. Li, C.; Knierim, B.; Manisseri, C.; Arora, R.; Scheller, H. V.; Auer, M.; Vogel, K. P.; Simmons, B. A.; Singh, S. *Biores. Technol.* **2010**, *101*, 4900–4906.

13. Holladay, J. E.; White, J. F.; Bozell J. J.; Johnson, D. *Top Value-Added Chemicals from Biomass. Volume II–Results of Screening for Potential Candidates from Biorefinery Lignin*. Pacific Northwest National Laboratory, PNNL-16983, 2007.

14. Voitl T.; von Rudolf, P. R.; *ChemSusChem* **2008**, *1*, 763–769.

15. Yuan, T.-Q.; Xu F.; Sun, R.-C. *J. Chem. Technol. Biotechnol.* **2013**, *8*8, 346–352.

16. Greaves, T. L.; Drummond, C. *J. Chem. Rev*. **2008**, *108*, 206–237.

17. MacFarlane, D. R.; Pringle, J. M.; Johansson, K. M.; Forsyth S. A.; Forsyth, M. *Chem. Comm.* **2006**, 42, 1905–1917.

18. Yoshizawa, M.; Xu, W.; Angell, A. C. *J. Am. Chem. Soc.* **2003**, *125*, 15411–15419.

19. Brown, H. C.; McDaniel D. H.; Häflinger, O. *Determination of Organic Structures by Physical Methods*; Braude, E. A., Nachod, F. C., Eds.; Academic Press: New York, 1955.

20. H. K. Hall. *J. Am. Chem. Soc.*, **1957**, *79*, 5441–5444.

21. P. Z. Walden, *Physik Chem.*, **1906**, *55*, 207 and 246.

22. Angell, C. A.; Byrne, N.; Belieres, J.-P. *Acc. Chem. Res.* **2007**, *40*, 1228–1236.

23. Xu, W.; Angell, C. A. *Science*. **2003**, *302*, 422–425.

24. Belières, J. -P.; Angell, C. A. Protic Ionic Liquids: Preparation, Characterization, and Proton Free Energy Level Representation *J. Phys. Chem. B* **2007**, 111, 4926–4937.

25. Mäki-Arvela, P.; Anugwom, I.; Virtanen, P.; Sjöholm R.; Mikkola, J. P. *Ind. Crop. Prod.* **2010**, *32*, 175–201.

26. Scott, J. A. N.; Procter, A. R.; Fergus B. J.; Goring, D. A. I. *Wood Sci. Technol.* **1969**, *3*, 73–92.

27. Greaves, T. L.; Weerawardena, A.; Fong, C.; Krodkiewska, I.; Drummond, C. J. J. *Phys. Chem. B* **2006**, *110*, 22479–22487.

28. Weidig, C. F. Discoloration inhibitor for aromatic amines. U.S. Patent 4,861,914, August 29, 1989.

29. Gugumus, F. Photooxidation of Polymers and Its Inhibition. In *Oxidation Inhibition in Organic Materials*; Pospíšil, J., Klemchuk, P. P., Eds.; CRC Press: Boca Raton, 1989-1990; Vol. 2, pp 144–146.

CHAPTER 4: Predictors for an Enhanced Lignin Removal from Lignocellulosic Biomass

Abstract

Careful selection of the cations/anions present in PILs is essential for their utilization in many applications especially in the biofuel industry. Increasing the xylan (i.e. hemicellulose) solubility in the PILs and dispersing the cellulose in a stable suspension results in greater fiber disruption/penetration, which significantly enhances the effectiveness of the lignin extraction. Solubility tests with commercially available biomass components, in conjunction with the physical and chemical properties of the PILs, identified trends in xylan solubility. Systematic variations in the cation of acetate-based PILs, supported by force field energy minimizations, confirm that PILs from cyclic amines and alkanolanimes, which favor increased xylan solubility, also support cellulose dispersion. These PILs are more ionic due to the ability of the PIL ions to form hydrogen bonds with ideal bond lengths**,** thereby strengthening the interaction of the PIL ions.

4.1. Introduction

There are several reports in the scientific literature on the ability of ILs to dissolve lignin in order to enable the extraction of lignin form lignocellulosic biomass. However, little is known about the mechanism that supports high lignin dissolution or the physicochemical parameters of the ILs that promote effective lignocellulosic biomass pretreatment. The capability to predict an ILs ability to remove lignin from biomass is essential for the rapid selection and optimization of ILs for biomass applications. The near infinite potential to

combine anions and cations in order to tailor solvent properties has led to ILs typically being called "designer solvents".[1] Varying the ion type and exploiting the structural and chemical variability of each ion can tune the properties of the ILs, thereby, designing task-specific ILs.[2-9]

Previous work in chapter 3 has established that PILs with a high ionicity dissolve larger amounts of xylan allowing for an increase in the penetration of the biomass fibers and enhancing the extraction of large amounts of lignin from biomass (cornstover). The PILs' ionicity is typically estimated using a combination of physical, chemical and thermal properties.[10–16] These techniques, however, are largely qualitative and suffer from drawbacks that prevent their application to a large group of PILs. Additionally, these studies are typically designed for electrochemical applications and the specific properties identified in the correlations (*e.g.*, conductivity) are most applicable to the field of research.

Angell *et al.* have related the molar conductivity to the fluidity of PILs using a Walden plot.[11–13] Although this relationship has been used to classify a wide array of ILs, the Walden rule is inapplicable when there is the formation of aggregates (neutral or charged). PIL reagents containing large bulky end groups (such as hydroxyl groups) can aggregate via weak bonds such as hydrogen bonds (H–bonds) resulting in an increase in the measured viscosity. This increase in viscosity is not directly related to the formation of ionic species; thus, the effective conductivity will not increase as predicted.[19-24] PILs are also susceptible to the formation of ion complexes that do not match the ideal PIL stoichiometry, which also

leads to inaccuracies in the predictions of the viscosity and conductivity of the PIL. Therefore, the Walden rule may be invalid for such PILs.[14-18]

Similarly, the aqueous pK_a values for the acids and base reagents have been employed to provide an estimate of how complete the proton transfer is (ionicity)−where a large ΔpK_a is indicative of extensive proton transfer. Researchers suggest that PILs with $\Delta pK_a > 8$ have nearly ideal Walden behavior.[11-13] This technique could be useful as pK_a values are derived from equilibrium constants, which give us the ratio of concentrations of reactant to products when equilibrium is reached in a reversible reaction (when the rate of the forward reaction equals the rate of the reverse reaction). This information should help in the prediction of the degree of protonation by determining the concentration of ionic species (products) vs. reagents (reactants) present in solution. However, these approximations cannot be used as a definite means of predicting ionicity, as pK_a values (Table 4. 1) are determined in aqueous solutions, which is not representative of the actual pure IL in solution. Other correlations have been made that include the PIL's thermal properties (boiling point, ΔT_{bp}), however, they also suffer from similar drawbacks.[11-13]

The purpose of this study is to develop an effective means for predicting the lignin extraction efficiency of PILs in biomass that can be applied to a variety of ILs with differing structures. The preliminary work done in Chapter 3 needs to be developed further to confirm the trends that have been observed, in order to suggest a more rigorous method for predicting a PIL's ionicity−specifically for the application of lignin dissolution (and biopolymer dissolution as a whole). Biopolymer solubility tests were run on a series of acetate-based

PILs with varying cations and were used to determine the PILs' ability to dissolve xylan (as well as lignin and cellulose). This has been shown to correlate well with the PILs' ionicity and the subsequent lignin extraction efficiency.

The properties of the PILs also depend greatly on the presence of H–bonds as these bonds often lead to the development of an extended three-dimensional network within the PIL.[24] Although this can represent a small portion of the total interaction, hydrogen bonding energies have been shown to have a significant influence on the structure and properties of the PILs. The behavior of the PIL ions was modeled using molecular mechanics modeling (MM2-Chem 3D Pro).[25–26] Utilizing the inbuilt force field functions, energy minimizations were carried out for each PIL to minimize the bond stretching energy of each molecule. This will identify what molecular-level interactions are present in the PILs with high ionicity and clarify the influence of H–bonding on the PILs' properties. The Raman spectra of the PILs were also compared to that of their reagents. In the case of PILs with high ionicity, a change in the spectra due to the formation of ionic species is expected.[27–29]

Monomer solubility tests were also run to elucidate the mechanism behind xylan/cellulose solubility. PILs are slightly acidic and could act as acid-catalysts for a hydrolysis reaction. However, the tightly packed crystalline nature of cellulose prevents this reaction from occurring while, xylan, the branched amorphous polymer may permit this reaction. Looking on a smaller scale at the monomer molecules for these biopolymers, an indication of this reaction type could be identified. The lignin extractability of a representative PIL from each section identified will also be utilized to support the

information derived from the methods established to predict lignin removal. These results will enable the design of PILs with optimal characteristics that will favor high lignin removal from biomass.

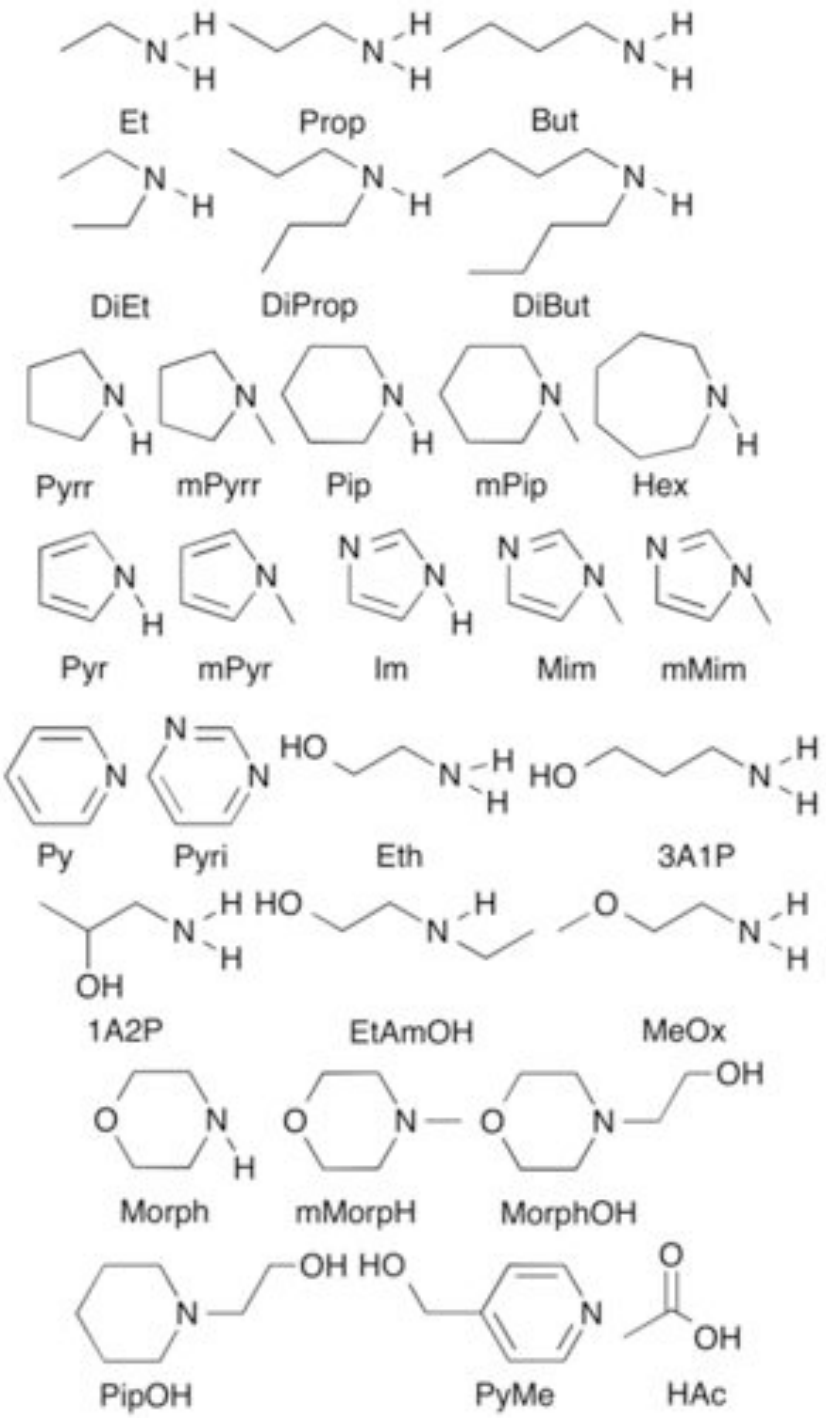

Figure 4. 1. PIL ions used in this study.

Table 4. 1. ΔpK_a values for the reagents used to synthesize PILs

ΔpK_a	HAc	ΔpK_a	HAc
Et	5.9	Im	1.7
Prop	5.8	mMim	–[a]
But	5.8	Pyr	6.5
DiEt	6.3	mPyr	–[a]
DiProp	6.2	EtAmOH	3.2
DiBut	6.5	Eth	4.7
Pyrr	6.5	1A2P	4.1
Pip	6.5	3A1P	4.6
Hex	6.3	MoxEt	0.2
mPyrr	5.7	Morph	3.6
mPip	5.3	mMorph	2.7
Py	0.4	PyMe	0.1
Pyri	3.7	PipOH	–[a]
Mim	2.7	MorphOH	2.75

[a] No data found for these reagents.

4.2. Effect of Structural Changes in the Cation of Acetate PILs on Biopolymer Solubility Tests

The biopolymer solubility test results, using acetate-based PILs, greatly depend on the cation structure. Definite trends were observed as the cation was modified from noncyclic aliphatic ammonium PILs (NAA), cyclic aliphatic ammonium PILs (CAA), aromatic ammonium PILs (AA) and to oxygenated aliphatic ammonium PILs (OAA). (Figure 4. 1) Control experiments were run using the reagents (base) in order to determine the effectiveness for lignin extraction of each PIL in comparison to that of the reagents. This will give us an indication of the ionicity of each PIL. The ΔpK_a values of the PIL, listed in Table

4. 1, were also compared to the results obtained to determine the accuracy of using pK_a values for predicting a PIL's ionicity.

Table 4. 2. Solubility of Kraft lignin, cellulose and xylan (% w/w) in the reagents and PILs from acyclic aliphatic amine bases (after heating/stirring at 90 °C for 24 h).

	lignin	cellulose	xylan
Et	–[a]	–[a]	–[a]
Prop	–[a]	–[a]	–[a]
But	7.52 ± 0.03	0.2 ± 0.08	0.15 ± 0.09
[Et][Ac]	> 50[b]	0.42 ± 0.01	5.24 ± 0.31
[Prop][Ac]	> 50[b]	0.44 ± 0.09	6.51 ± 0.83
[But][Ac]	> 50[b]	0.39 ± 0.13	5.49 ± 0.66
DiEt	1.42 ± 0.05	0.14 ± 0.10	0.07 ± 0.04
DiProp	1.32 ± 0.10	0.13 ± 0.05	0.04 ± 0.02
DiBut	1.60 ± 0.05	0.04 ± 0.01	0.05 ± 0.02
[DiEt][Ac]	> 50[b]	0.27 ± 0.02	5.73 ± 0.38
[DiProp][Ac]	> 50[b]	0.38 ± 0.09	1.50 ± 0.06
[DiBut][Ac]	> 50[b]	0.45 ± 0.02	0.38 ± 0.04

[a] Vapor pressure too low for solubility tests [b] Solubility limited by viscosity

Table 4. 3. Solubility of Kraft lignin, cellulose and xylan (% w/w) in the reagents and PILs from cyclic aliphatic amine bases (after heating/stirring at 90 °C for 24 h).

	lignin	cellulose	xylan
Pyrr	7.98 ± 0.10	0.63 ± 0.44	1.44 ± .07[cite]
Pip	6.88 ± 0.04	0.37 ± 0.03	0.25 ± 0.08
Hex	6.44 ± 0.07	0.34 ± 0.08	0.27 ± 0.02
mPyrr	3.09 ± 0.57	0.54 ± 0.05	0.74 ± 0.20
mPip	2.11 ± 0.63	0.59 ± 0.04	0.63 ± 0.20
[Pyrr][Ac]	> 50[a]	0.79 ± 0.04	> 15[a]
[Pip][Ac]	> 50[a]	0.33 ± 0.03	> 15[a]
[Hex][Ac]	> 50[a]	0.98 ± 0.03	> 15[a]
[mPyrr][Ac]	> 50[a]	1.44 ± 0.04	1.31 ± 0.47
[mPip][Ac]	> 50[a]	0.72 ± 0.01	3.07 ± 0.92

[a] Solubility limited by viscosity

Table 4. 4. Solubility of Kraft lignin, cellulose and xylan (% w/w) in the reagents and PILs from aromatic amine bases (after heating/stirring at 90 °C for 24 h).

	lignin	cellulose	xylan
Py	> 50[a]	0.10 ± 0.00	0.02 ±0.02
Pyri	_[d]	_[d]	_[d]
Mim	> 50	0.24 ± 0.02	6.34 ± 0.17
Im	_[b]	_[b]	_[b]
mMim	_[b]	_[b]	_[b]
Pyr	5.03 ± 0.04	0.86 ± 0.05	0.88 ± 0.04
mPyr	2.29 ± 0.07	1.09 ± 0.06	1.24 ± 0.11
[Py][Ac]	> 50[b]	0.12 ± 0.03	0.82 ± 0.02
[Pyri][Ac]	> 50[b]	0.25 ± 0.20	0.99 ± 0.10
[Mim][Ac]	> 50[b]	0.20 ± 0.05	5.60 ± 0.77
[Im][Ac]	6.98 ± 0.20	0.09 ± 0.01	2.72 ± 1.40
[mMim][Ac	> 50[a]	0.80 ± 0.07	4.58 ± 0.7
[Pyr][Ac]	< 5[c]	< 5[c]	< 5[c]
[mPyr][Ac]	> 50[a]	1.21 ± 0.04	2.41 ± 0.06

[a] Solubility limited by viscosity [b] Solid at room Temperature [c]Quantitative results were not obtained [d]Reagent unavailable.

Table 4. 5. Solubility of Kraft lignin, cellulose and xylan (% w/w) in the reagents and PILs from oxygenated aliphatic amine bases (after heating/stirring at 90 °C for 24 h).

	lignin	cellulose	xylan
EtAmOH	7.49 ± 0.24	0.34 ± 0.05	0.40 ± 0.14
Eth	> 50[a]	0.53 ± 0.09	16.26 ± 0.23
1A2P	> 50[a]	0.38 ± 0.03	2.46 ± 0.22
3A1P	> 50[a]	0.33 ± 0.11	3.06 ± 0.35
MoxEt	15.58 ± 0.20	0.31 ± 0.05	2.81 ± 0.20
Morph	> 50[a]	0.27 ± 0.03	0.51 ± 0.01
mMorph	5.67 ± 0.05	0.36 ± 0.08	0.39 ± 0.02
[EtAmOH][Ac]	> 50[a]	0.21 ± 0.06	10.81 ± 0.97
[Eth][Ac]	> 50[a]	0.75 ± 0.06	11.54 ± 0.88
[1A2P][Ac]	> 50[a]	0.51 ± 0.07	8.97 ± 0.35
[3A1P][Ac]	> 50[a]	0.47 ± 0.05	9.74 ± 0.49
[MoxEt][Ac]	> 50[a]	1.04 ± 0.11	3.64 ± 0.14
[Morph][Ac]	> 50[a]	0.88 ± 0.05	10.38 ± 1.41
[mMorph][Ac]	> 50[a]	0.27 ± 0.02	1.27 ± 0.83

[a] Solubility limited by viscosity

Table 4. 6. Solubility of Kraft lignin, cellulose and xylan (% w/w) in the reagents and PILs from hybrid (oxygenated-cyclic-aliphatic) amine bases (after heating/stirring at 90 °C for 24 h).

	lignin	cellulose	xylan
[PipOH][Ac]	3.74 ± 0.14	0.54 ± 0.10	0.51 ±0.04
MorphOH	> 5%	0.60 ± 0.09	0.58 ± 0.03
PyMe	–[a]	–[a]	–[a]
[PipOH][Ac]	> 5%	0.56 ± 0.07	1.43 ± 0.14
[MorphOH][Ac]	> 5%	0.31 ± 0.03	0.51 ± 0.01
[PyMe][Ac]	> 50[b]	1.41 ± 0.59	2.42 ± 0.86

[a] Solid at room temperature

4.2.1. Solubility of Microcrystalline Cellulose in PILs

Most PILs dissolved less than 1% w/w of cellulose, with the exception of [mPyrr][Ac], [mPyr][Ac], mPyr and [PyMe][Ac], which dissolve about 1.5% w/w cellulose (Table 4. 2–4. 6). In general, this is a negligible amount of cellulose, which is important for the 'selective' extraction of lignin, resulting in uncontaminated separation streams during the actual biomass pretreatment. This low cellulose solubility is expected, as most PILs are known to dissolve a low amount of cellulose.[37–38] Naturally occurring cellulose is known to interact via extensive intra- and inter-molecular hydrogen bonding networks.[2] In order to disrupt this network and dissolve cellulose, a molecule that has available hydrogen bonding sites is essential. As this molecule interacts with the cellulose, the number of hydrogen bonds between the cellulose molecules is reduced–allowing for the partial dissolution of the cellulose. In the case of PILs, ILs that contain cations and anions that strongly interact with one another using hydrogen bonding, there is little to no interaction with the cellulose molecules–resulting in the low dissolution.

4.2.2. Solubility of Kraft Lignin and Organosolv Lignin in PILs

All PILs in this study are able to dissolve large amounts of Kraft lignin (Indulin AT) with the exception of the [PyMe][Ac] PIL. On the other hand, the reagents do not dissolve large amounts of lignin. Two AA reagents (Py and Mim), as well as OAA reagents (alkanolamines and morpholine), are also able to dissolve large amounts of Kraft lignin. This could be due to the aromaticity of those bases as they are closer to complete aromatic species, and the presence of electron lone pairs in the –OH groups on the OAA PILs.

However, it is important to note that Kraft lignin is a lignin extract that has been modified and does not exactly match native lignin. Small amounts of Organosolv lignin, a purer lignin extract,[39] were obtained and used for similar solubility tests. The PILs tested also dissolved large amounts of Organosolv lignin providing further confirmation that PILs are able to dissolve lignin. Lignin dissolution in the PILs occurs preferentially relative to the majority of the neutral reagents tested indicating that the presence of ionic species favors lignin dissolution.

4.2.3. Solubility of Xylan in PILs

With the hemicellulose (xylan) solubility known to depend on ionicity, interesting trends are observed. A low to medium xylan solubility was found for the NAA PILs. The xylan solubility decreased with an increase in the degree of alkylation especially in amines with longer chain lengths such as the [DiProp][Ac] and [DiBut][Ac] PILs (Table 4. 2). In comparison, the CAA PILs have the highest xylan solubility of the PILs tested. These PILs are consistently able to dissolve at least 15% w/w of xylan, which has proven to be necessary for enhancing lignin removal in biomass pretreatment (Chapter 3). In comparison to their reagents, these CAA PILs have enhanced xylan solubility. This trend was previously observed in the [Pyrr][Ac] PIL (Chapter 3) and is confirmed for the [Pip][Ac] and [Hex][Ac] PILs (Table 4. 3).

Although these CAA PILs have similar ΔpK_a values to their acyclic counterparts (Table 4. 1), their xylan solubility is much higher indicating that their ionicity is higher (contains a lower amount of reagents than ions) that the NAA PILs. This suggests that using

ΔpK_a values as predictors for ionicity, as most researchers have done, is possibly erroneous. This difference in ionicity observed is possibly due to the increased degrees of freedom in the NAA PIL molecules. Motion is unrestricted resulting in multiple confirmations being adopted in the PIL's cation structure. This prevents the PIL's cation from consistently orienting itself favorably with the anion. In contrast, the CAA PILs have cations with a more restricted orientation that has limited motion and indicating that they may have a fixed alignment with the anion that favors increased ionicity.

Steric hindrances in CAA PILs also likely play a role in preventing ionic interactions. When an alkyl chain was introduced to nitrogen on the ring structure, there was a large decrease in the observed xylan solubility indicating that secondary amine bases ionize better that tertiary amine bases. This could also be due to the fact that the addition of the alkyl chain length adds extra degrees of freedom resulting in unfavorable confirmations being adopted. Once again, the ΔpK_a approximations have proven to be impractical. The addition of the methyl group to the [mPyrr][Ac] PIL (as compared to the [Pyrr][Ac] PIL), for example, destabilizes the ring structure due to increased motion and steric hindrance. This orientation, in the [mPyrr][Ac] PIL is unfavorable for the formation of ionic species resulting in a lower ionicity. This also confirms that an increased degree of alkylation is not favorable for the formation of PILs with high ionicity.

AA PILs, in general, do not dissolve large amounts of xylan indicating that they form relatively low ionicity PILs. In this situation, the ΔpK_a values are decent approximations for the behavior of the PILs (Table 4. 4). This low ionicity is expected because the ionization of

an aromatic molecule to form a cation destabilizes the aromatic ring resulting in a higher energy state. Therefore, bases from aromatic amines are less likely to be ionized completely, hence the weak ionicity and resulting low xylan solubility. Pyrrole, for example, looses resonance stabilization if ionized.

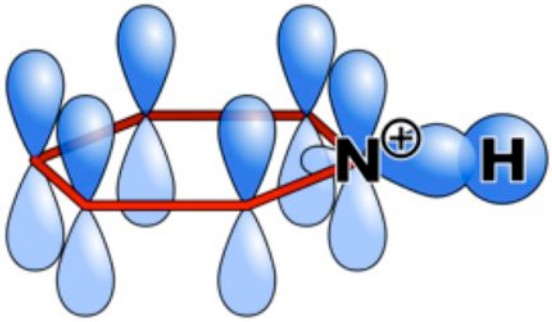

Figure 4. 2. Orbitals present in the pyridinium anion.

With pyridine, ionization is also unfavored, however, this is due to a different reason. Interestingly, the pyridinium ion (the conjugate acid) remains aromatic, because when the unshared electron lone-pair bonds to a proton, the C–H bond is in the trigonal plane which does not remove any electrons from the pi electron system. (Figure 4. 2) This places the unshared electron lone-pair in an sp^2 atomic orbital (AO), which is much lower in energy than the electron lone-pair of aliphatic amines (sp^3 AO).[30] Therefore, pyridine is less easily protonated than analagous aliphatic amines such as piperidine. The imidazolium-based PILs

are able to dissolve a larger amount of xylan than the other AA PILs. Using the previously described reasons, protonation of imidazole-like molecules is highly favorable since this results in aromatic cations with resonance stabilization. For these AA PIls, the addition of methyl groups increases the xylan solubility unlike the aliphatic PILs where the reverse is the case since such groups further stabilize the cations (Table 4. 4).

OAA PILs were considered due to the possibility of developing a PIL with a stronger hydrogen-bonding network with the PIL's cation. The resulting highly viscous PILs have medium to high xylan solubility of about 8–12% w/w xylan (Table 4. 5). These PILs are also observed to disperse cellulose to form stable cellulose suspensions (see below). Variation in the structure of the alkanolanime PIL had little to no effect on the xylan solubility. The structure of the PIL was varied to enact a reduction in viscosity and a possible increase in xylan solubility. Out of the OAA PILs, the simpler structure [Eth][Ac] resulted in a PIL with the highest xylan solubility, while the longer chain and branched base structure reduced the observed xylan solubility. The position of the oxygen was also significant for high xylan solubility. When the oxygen was terminal (C–OH group) vs. incorporated into the chain (C–O–C), this resulted in greater H-bonding. Hence, higher xylan solubility was observed. The cyclic OAA PIL [Morph][Ac] was also able to dissolve a large amount of xylan following the trend of CAA PILs. The solubility also greatly decreased upon the addition of a methyl group in [mMorph][Ac].

Noting the high xylan solubility of CAA and OAA PILs, hybrid PILs with both features were synthesized and tested for xylan solubility (Table 4. 6). These PILs had very

low xylan solubility. These hybrid PILs can be treated like those with an increased alkyl chain length, which have been shown to have low xylan solubility. The addition of the OH group had little to no effect and the hydrogen bonding network is reduced as the –OH groups rarely interact as they are obstructed by the ring structure. More work could be done to determine the optimal placement of the –OH group, if any, for the formation of hybrid PILs with enhanced xylan solubility.

4.3. Energy Minimization

A two dimensional structure was depicted by Chemdraw (*Cambridge Software*) and was converted to a three dimensional structure by Chem 3D (*Cambridge Software*) followed by a structural optimization (lowest energy) using MM2 (molecular mechanics 2). The MM2 parameters are based on information provided by Dr. Allinger with minor modifications by Dr. Ponder.[25-26, 41-43] The following color scheme is used to interpret the images generated from the model: red (oxygen), blue (nitrogen), dark grey (carbon) light grey (hydrogen), pink (electron lone-pairs), dashed lines (H–bonds). H–bonds with a less than ideal geometry are displayed with a blue tint. The intensity of the color increases as the bond becomes less ideal.

Interestingly the minimum energy structures that were observed for each PIL group also match the trend in ionicity established from the biopolymer solubility tests in the previous section. All the primary NAA PILs, with similar xylan solubility, form the same structure upon ionization. The H–bond is between two amine–Hs and one acetate–O creating a rhombic shape with one line of symmetry (Figure 4. 3). Of the secondary NAA PILs, [DiEt][Ac] also has a similar H–bond interaction and shape with the primary NAA PILs.

However, this rhombus has two lines of symmetry and the bond is between one amine–H and two acetate–Os (Figure 4. 4). This PIL also has similar xylan solubility with the primary NAA PILs. The longer chain secondary NAA PILs [DiProp][Ac] and [DiBut][Ac] both have similar structures, as well as similar xylan solubilities (Figures 4. 3–4. 4 and Table 4. 2). The H–bonds interaction has an asymmetric hexagonal shape creating bonds with less than ideal geometry, resulting in this orientation that produces low ionicity PILs.

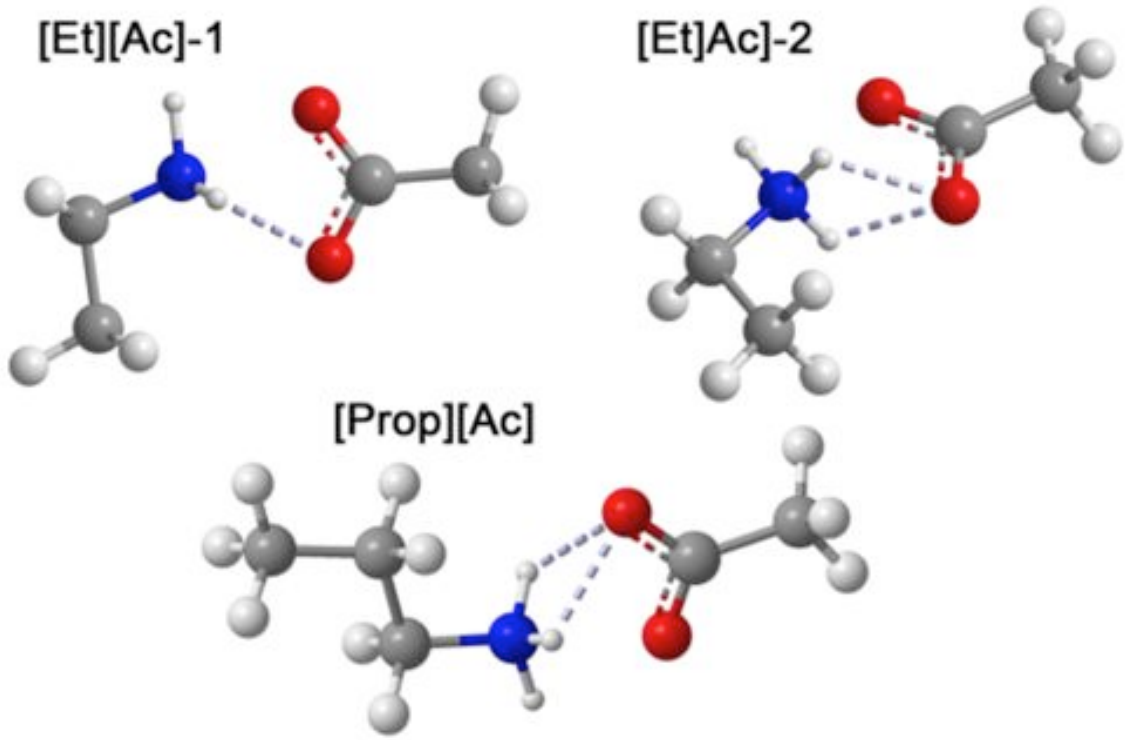

Figure 4. 3. Minimum energy structures of primary NAA PILs using one ionic couple.

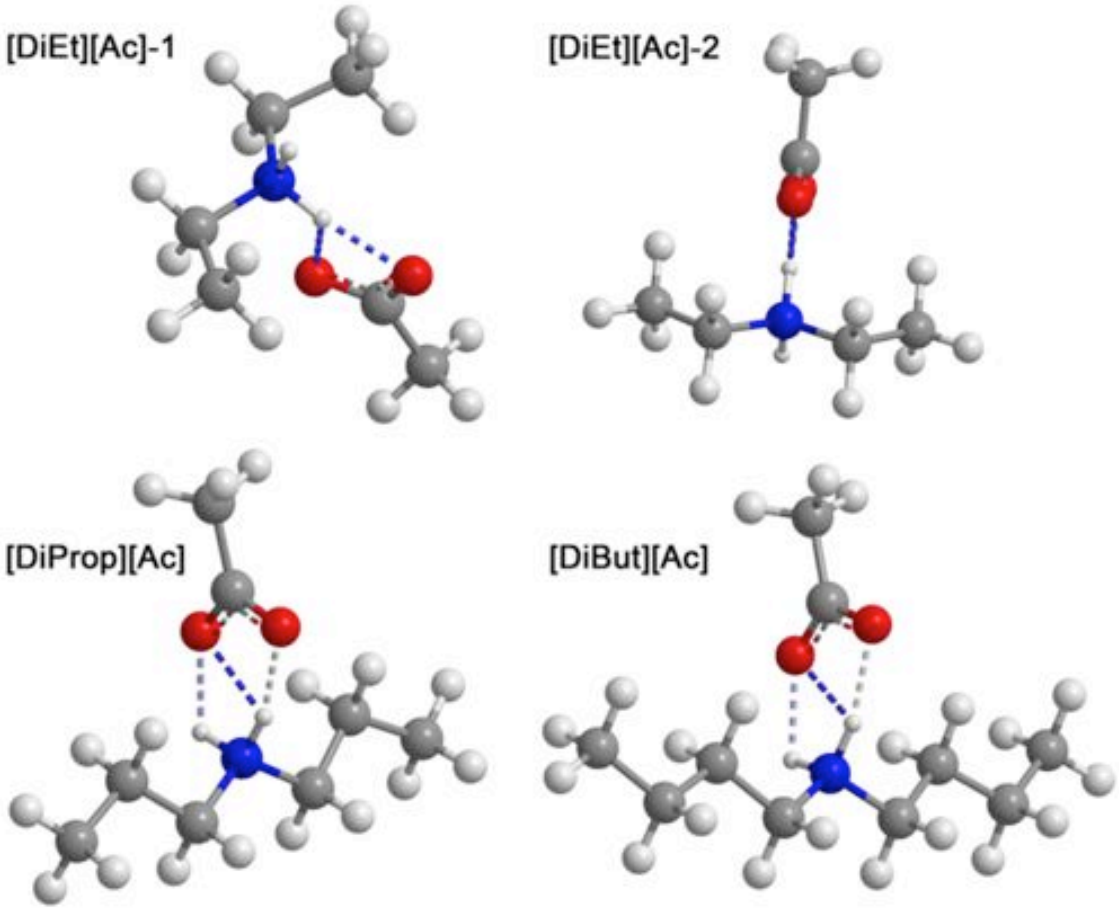

Figure 4. 4. Minimum energy structures of secondary NAA PILs using one ionic couple.

The CAA PILs, for example the secondary [Pyrr][Ac] PIL, creates a three–dimensional rhombus with one lines of symmetry (Figure 4. 5) and the bond is between two amine–Hs and two acetate–Os. This shape is unique to these CAA PILs thus giving better understanding for the high ionicity and xylan solubility observed in these PILs. This intricate structure has multiple H–bonds, which result in the effective ionic bond seeming stronger

(Figure 4. 5). Once again, the restricted ring structure allows the amine–Hs to be easily accessible, unlike with the NAA PILs. Tertiary CAA PILs such as [mPyrr][Ac] do not have this same interaction (Figure 4. 5). The methyl group reduces the amount of amine–Hs present resulting in the asymmetric rhombus observed. AA PILs have no direct H–bond between the PIL ions as the aromatic ring interacts more strongly with the anion than does the N–H proton (Figure 4. 6).

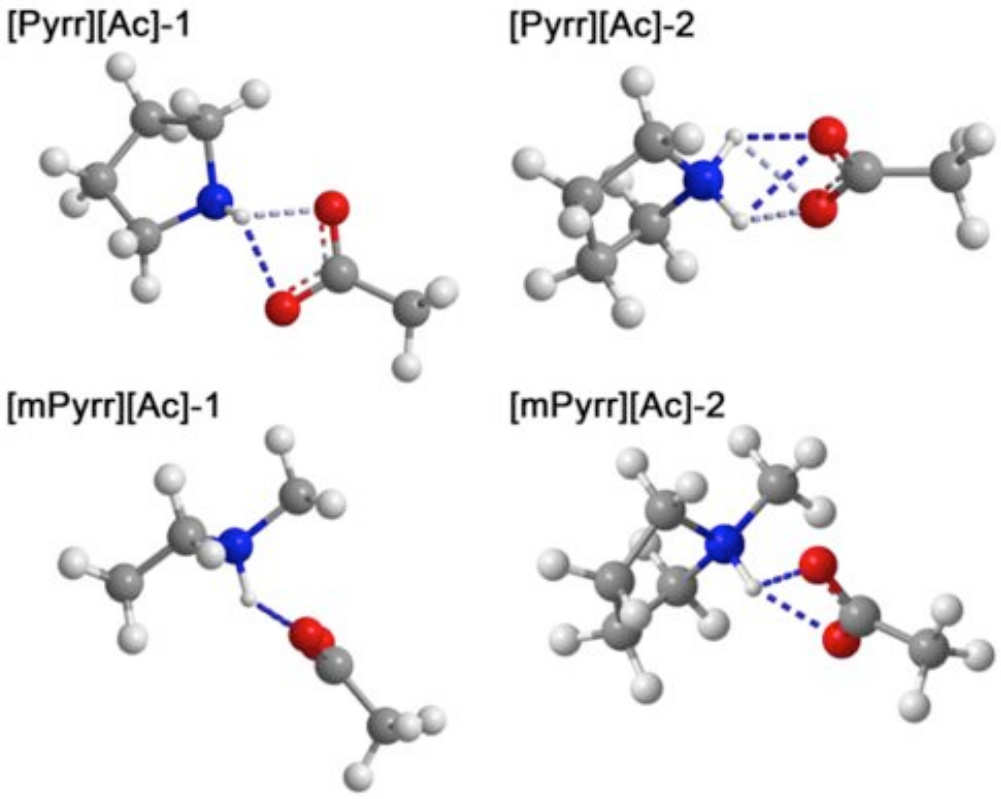

Figure 4. 5. Minimum energy structures of CAA PILs using one ionic couple.

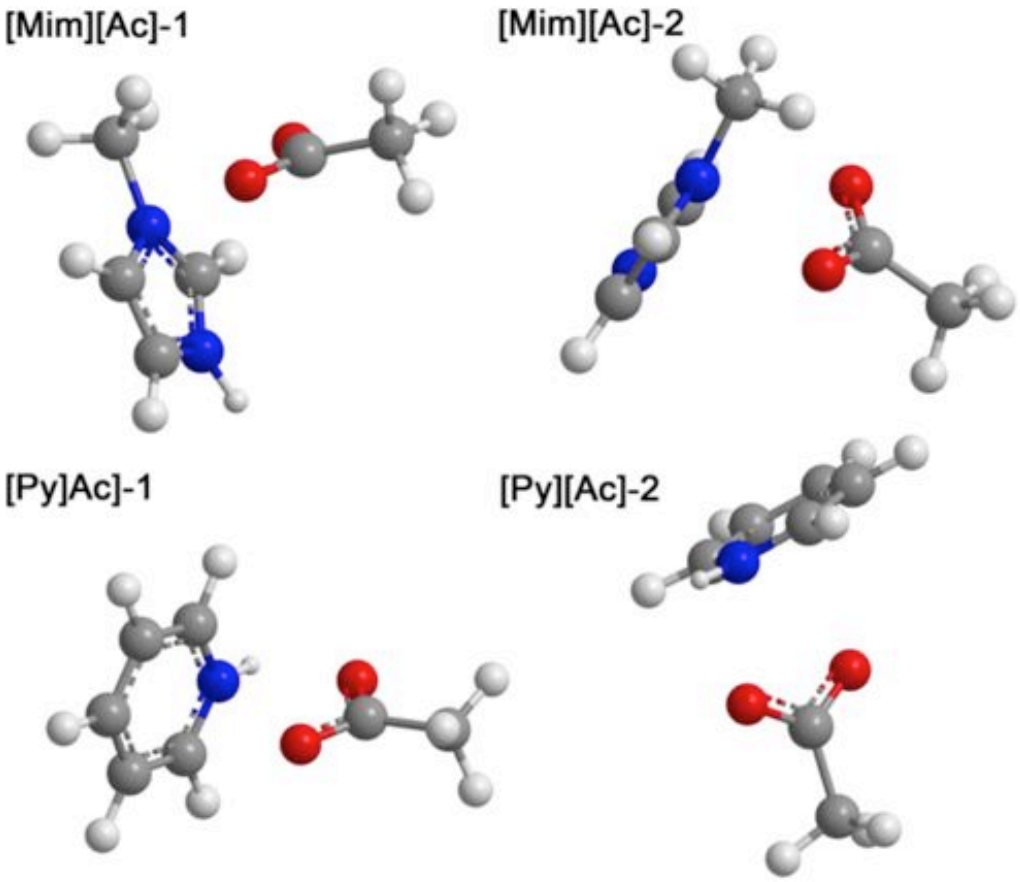

Figure 4. 6. Minimum energy structures of the AA PILs [Py][Ac] and [Mim][Ac] using one ionic couple.

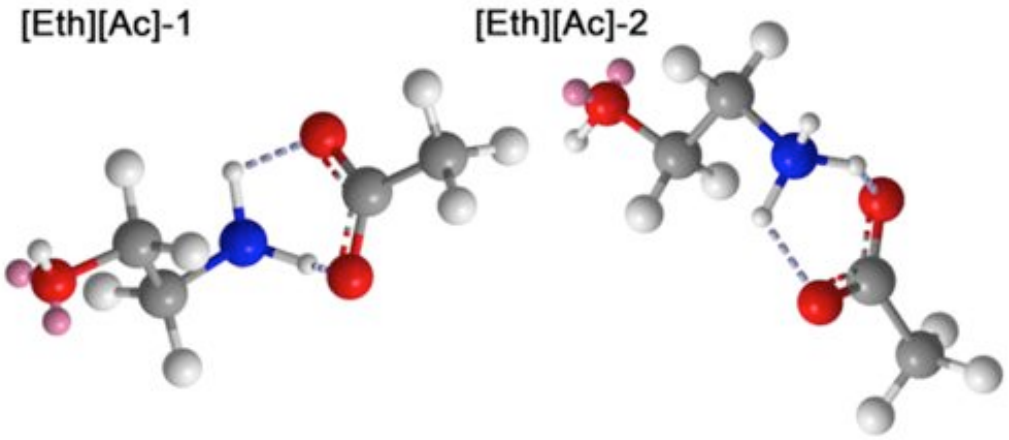

Figure 4. 7. Minimum energy structures of the OAC PIL [Eth][Ac] using one ionic couple.

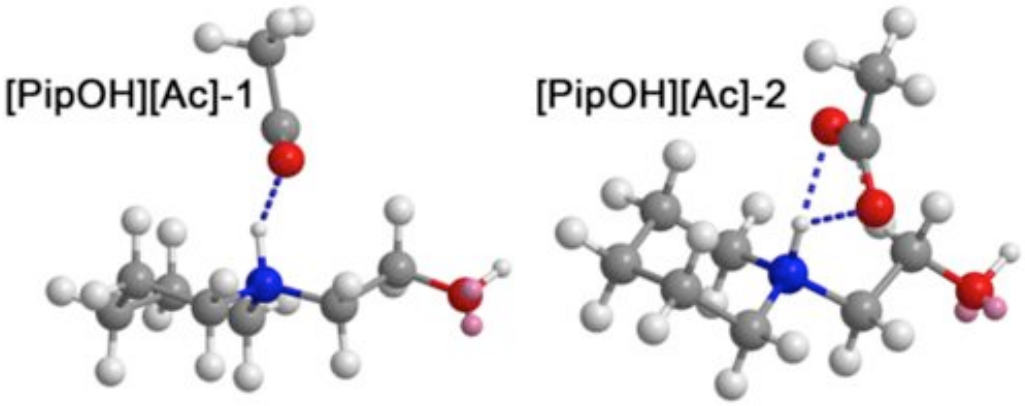

Figure 4. 8. Minimum energy structures of the hybrid PIL [PipOH][Ac] using one ionic couple.

The OAA PIL [Eth][Ac] also has an asymmetric hexagonal structure between the PIL ions (Figure 4. 6). In comparison to the analogous NAA PIL [Et][Ac], both Hs partake in the H–bond resulting an increase in the effective ionicity and xylan solubility. The hybrid PILs were not strong xylan solvents. They behave just like the tertiary [mPyrr][Ac] PIL (Figure 4. 5 and 4. 8), which explains why this PIL has such low xylan solubility. The position of the ethanol group will have to be modified to impact the ionicity of this PIL in order to produce a PIL with high ionicity and an improved H–bonding network.

4.4. Raman Spectroscopy

The complete Raman spectra for the PILs are listed in Appendix D. However, the peaks of interest for ionization are the N–H and O–H peak, which typically occur at about 3300 cm^{-1} and 3000 cm^{-1} respectively. In the [Pyrr][Ac] and [Pip][Ac] PILs, where ionicity is increased, the peaks for N–H previously seen in the reagents are lost. However, these PILs already have N–H groups, indicating that this effect is not due to the formation of additional N–H bonds, but is instead due to the ionization of the base (pyrrolidine) resulting in the diminished N–H peak (Figure 4. 9). The interactions between the PIL ions result in the peak being almost undetectable by Raman spectroscopy. This outcome is not observed in the [Prop][Ac] PIL–a similar secondary amine. No significant changes are observed in the Raman spectra of the other PILs ([Py][Ac] and [Mim][Ac]) indicating that there was little to no change upon formation of the PIL, as expected. The [Eth][Ac] PIL also did not loose its N–H peak indicating its xylan solubility is not due to a high ionicity, but also formation of an extensive H–bonding network (Figure 4. 9).

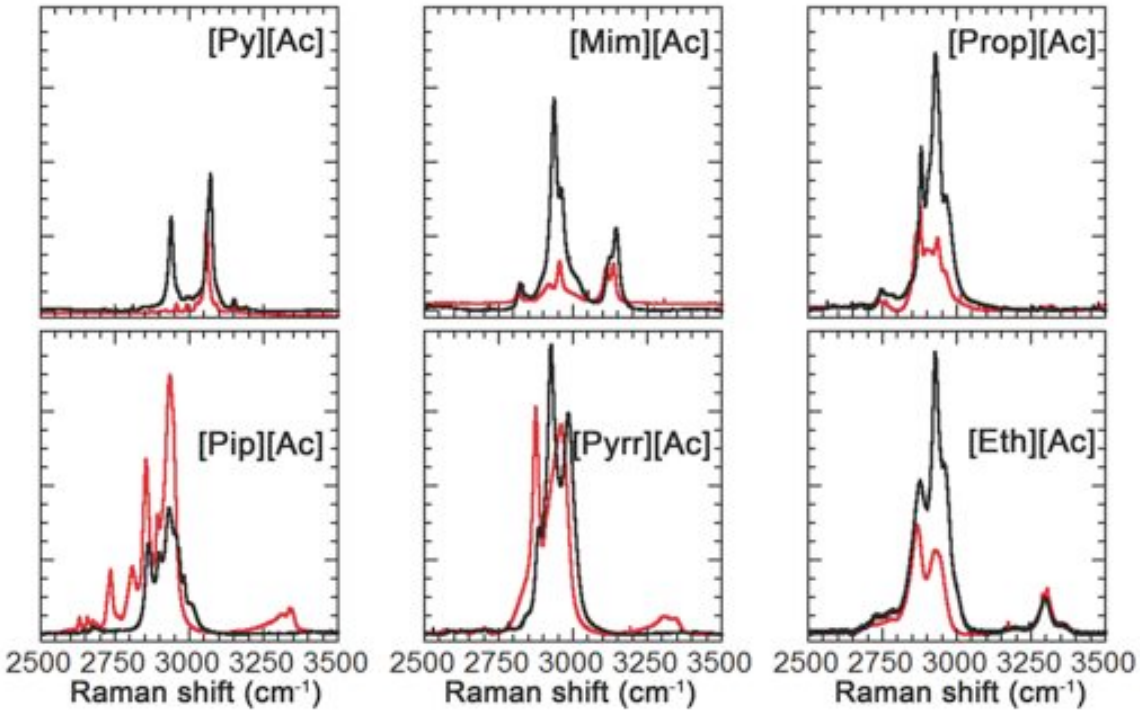

Figure 4. 9. Comparison of the Raman spectra (2500-3500 cm^{-1}) of PILs, as well as, their amine reagent (red) depicting the nature of the N-H peak in amines before and after protonation.

4.5. Cellulose Dispersion

Selecting one representative PIL from each section, the cellulose dissolution results can be observed better. After running the PIL/cellulose dissolution experiments for 24 h at 90 °C, the PILs did not dissolve any significant amounts of cellulose. (Table 4.X) However, the images show that the cellulose powders remain dispersed in solution in certain PILs, while they settled compactly to the bottom of the vial in others. Closer observations indicate that this trend follows the trends of the xylan solubility tests observed, thus, hinting that this

could be a result of changes in the ionicity. The alkanolanime PILs (such as [Eth][Ac]), however, disperse cellulose to a greater extent than the [Pyrr][Ac] PIL–which might prove to be important when processing actual biomass. The main difference between these two different classes of bases is the addition of absence of the ring structure and the presence of H–bonding groups (–OH). The absence of the ring structure accounts for the slight reduction in xylan solubility in these PILs, but the addition of the (–OH) makes up for it, as well as adds the new feature of being able to disperse the cellulose.

Cellulose dispersion might be important when it comes to processing actual fibers as it might an indicator of "cellulose swelling". This is when the cellulose is decrystallized by partially dissolving cellulose and precipitating it with the use of a non-solvent.[40] Disrupting the cellulose fibers is important for further down-stream processing via enzymatic hydrolysis as it increases the surface area available for enzyme binding.[40] These results, however, indicate that the ability to "swell" (or disperse) cellulose also contributes to lignin removal from actual biomass. The mass transfer limitation imposed by the crystalline cellulose in nature can be overcome by dispersing cellulose in solution thereby allowing PIL molecules to further penetrate this barrier in biomass fibers. Dispersing cellulose also ensures that PIL ions are constantly interacting with the biomass fibers resulting in an increased efficiency of the reaction, thereby, reducing some of the drawbacks of using a batch (one-pot) reactor.

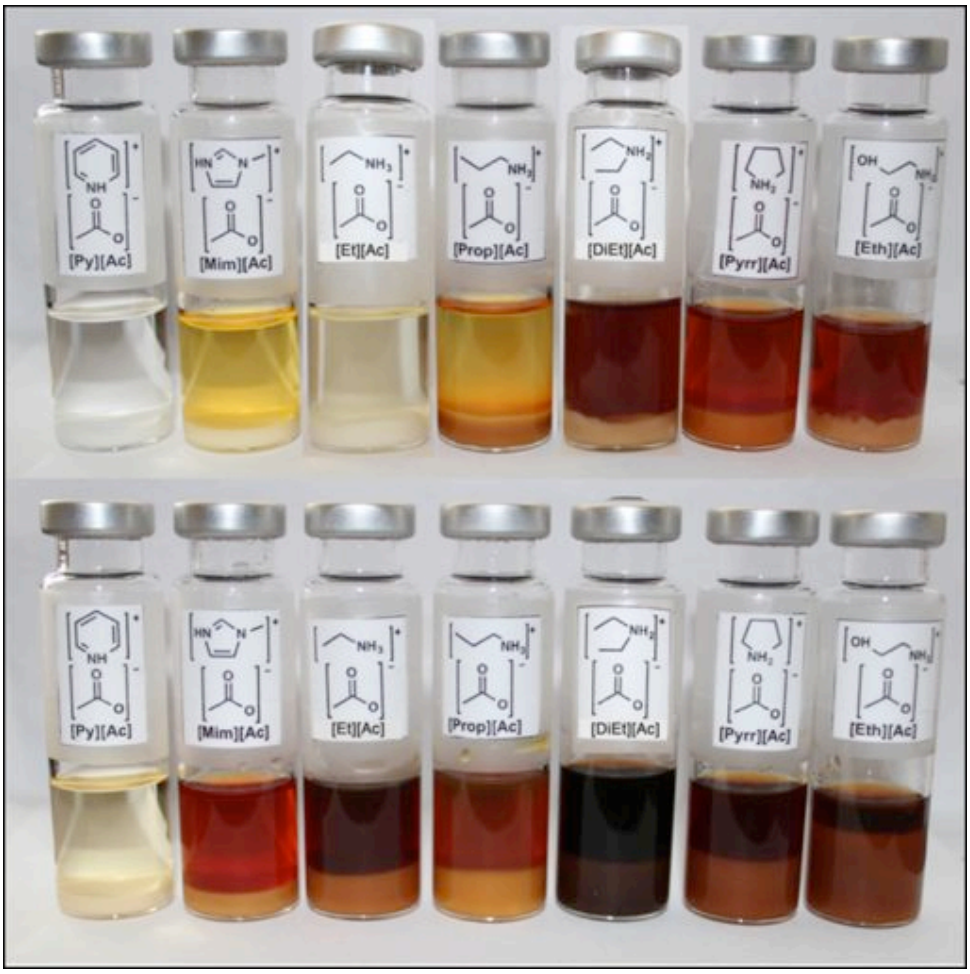

Figure 4. 10. Image showing the effect of different cation structures in the PIL on their ability to disperse cellulose after heating/stirring at 90 °C for 24 h).

4.6. Monomer Solubility Tests

Solubility tests with the [Eth][Ac], [Eth][Lac] and [Morph][Lac] PILs and glucose and xylose (monomers for cellulose and xylan respectively) indicate that PILs might be acting as acid catalysts to a low extent promoting the acid-catalyzed hydrolysis reactions. PILs are able to dissolve up to 15 % w/w of the sugars, however, solution turns slightly dark upon addition of the PILs, and after heating for at 90 ºC for 24 h, indicating the solubility of the sugars as well as some the production of some degradation products (Figure 4. 11).

Nevertheless, the acidity of PILs, however, is not strong enough for this to have a significant effect on the solubility of cellulose or xylan. In addition, the morphology of the biopolymers controls the reaction. Cellulose in nature is a tightly packed polymer with a crystalline matrix, which prevents the PILs from accessing the polysaccharides (hence the low solubility observed). Xylan, in contrast, is an amorphous, branched polysaccharide that has a lower degree of crystallinity[2] allowing for some of the PIL ions to interact with the xylan fibers. This gives an indication of the possible reaction that may occur during xylan dissolution. HPLC tests show that after the dissolution experiments were run, trace amounts of some other products were observed that are typical degradation products on acid treated samples. In general this effect is not significant as the amounts detected are minimal and this will occur at an even lower rate in the actual biopolymers.

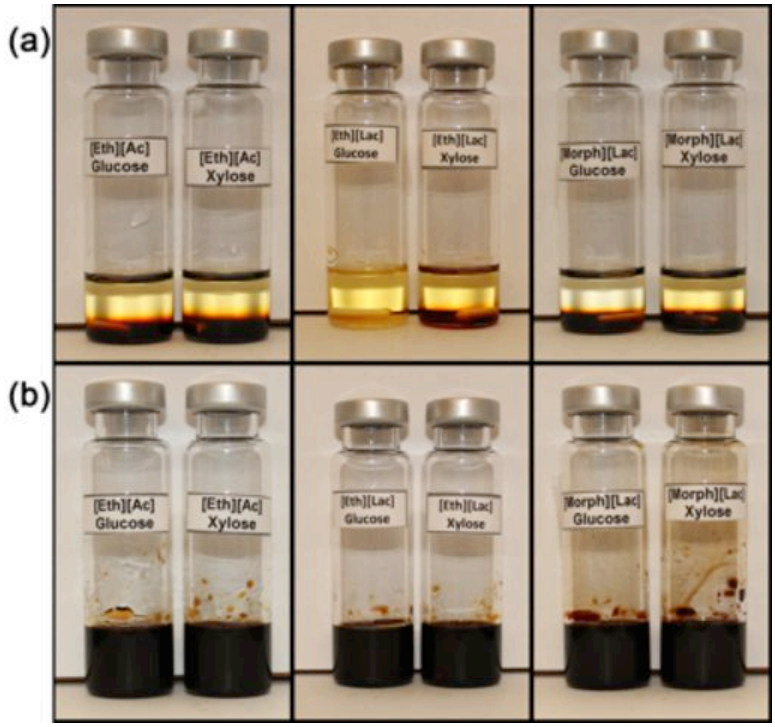

Figure 4. 11. Images depicting the solubility of 5% w/w sugars in the PILs: after stirring for (a) after stirring for 30 min at room temperature (25 °C) and (b) after stirring for 24 h at 90 °C (sample sizes were 5.0 g).

4.7. Conclusions

Combinations of experimental, analytical and theoretical techniques have been utilized to develop a better understanding regarding what specific features of PILs favor increased ionicity. Variations of the cation in acetate-based PILs show that cyclic amines have the highest ionicity resulting in the largest xylan solubility. Energy minimizations show that this is because of the favorable orientation that the cation adopts, which allow for a three dimensional H–bonding interaction between the PIL ions (Figure 4. 5). Any modification to

the structure creates additional steric hindrance, which reduce the effective ionicity. Raman spectra of these PILs also supplement this finding as the N–H peak is diminished upon formation of the PIL. This work also shows that the addition of strategically placed –OH groups also favor xylan solubility partially due to the increased ionicity of the PIL, but also due to the formation of an extensive H–bonding network with ideal geometry (Figure 4. 7) These PILs (alkanolanimes) are able to solvate the xylan polymer, as well as create a stable dispersion of the cellulose. This is beneficial for increasing the penetration of the ions into the fibers for enhanced lignin removal.

References:

1 Rogers, R. D.; Seddon, K. R. *Science* **2003**, *302*, 792–793.

2. Mäki-Arvelaa, P.; Anugwoma, I.; Virtanena, P.; Sjöholma, R.; Mikkola, J. P. *Ind. Crop. Prod.* **2010**, *32*, 175–201.

3. Greaves, T. L.; Weerawardena, A.; Fong, C.; Krodkiewska, I.; Drummond, C. J. *J. Phys. Chem. B* **2006**, 110, 22479– 22487George, A.; Tran, K.; Morgan, T. J.; Benke, P. I.; Berrueco, C.; Lorente, E.; Wu, B. C.; Keasling, J. D.; Simmons, B. A.; Holmes, B. M. *Green Chem.* **2011**, *13*, 3375–3385.

4. Brown, K. E.; Geng, X.; McDanel, W.; Henderson, W. *ECS Trans.* **2009**, *16*, 107–110.

5. Hou, X. D.; Smith, T. J.; Li, N.; Zong, M. H. *Biotechnol. Bioeng.* **2012**, *109*, 2484–2493

6. Liu, Q. P.; Hou, X. D.; Li, N.; Zong, M. H. *Green Chem.* **2012**, *14*, 304–307

7. Pinkert, A.; Dagmar, F.; Goeke, D. F.; Marsh, K. N; Pang, S. *Green Chem.* **2011**, *13*, 3124.

8. Welton, T. *Chem. Rev.* **1999**, *99*, 2071−2083.

9. Hallett, J. P.; Welton, T. *Chem. Rev.* **2011**, *111*, 3508−3576.

10. Yoshizawa, M.; Xu, W.; Angell, A. C. *J. Am. Chem. Soc.* **2003**, *125*, 15411–15419.

11. P. Z. Walden, *Physik Chem.*, **1906**, *55*, 207 and 246.

12. Angell, C. A.; Byrne, N.; Belieres, J.-P. *Acc. Chem. Res.* **2007**, *40*, 1228–1236.

13. Xu, W.; Angell, C. A. *Science* **2003**, *302*, 422–425.

14. Greaves, T. L.; Drummond, C. J. *Chem. Rev.* **2008**, 108, 206–237.

15. Nuthakki, B.; Greaves, T. L.; Krodkiewska, I.; Weerawardena, A.; Burgar, M. I.; Mulder, R. J.; Drummond, C. J. *Aust. J. Chem.* **2007**, *60*, 21.

16. Susan, M. A. B. H.; Yoo, M. Y.; Nakamoto, H.; Watanabe, M. *Chem. Lett.* **2003**, *32*, 836.

17. Matsuoka, H.; Nakamoto, H.; Susan, M. A. B. H.; Watanabe, M. *Electrochim. Acta* **2005**, *50*, 4015.

18. Noda, A.; Susan, M. A. B. H.; Kudo, K.; Mitsushima, S.; Hayamizu, K.; Watanabe, M. *J. Phys. Chem. B* **2003**, *107*, 4024.

19. Stoimenovski, J; Izgorodina, E. I.; MacFarlane, D. R. *Phys. Chem. Chem. Phys.* **2010**, 12, 10341–10347.

20. Meot-Ner, M. *Chem. Rev.* **2012**, *112*, PR22–PR103.

21. Kohler, F.; Atrops, H.; Kalall, H.; Liebermann, E.; Wilhelm, E.; Ratkovics, F.; Salamon, T. *J. Phys. Chem.* **1981**, *85*, 2520.

22. Kohler, F.; Gopal, R.; Go¨tze, G.; Atrops, H.; Demeriz, M. A.; Liebermann, E.; Wilhelm, E.; Ratkovics, F.; Palagyl, B. *J. Phys. Chem.* **1981**, *85*, 2524.

23. Kohler, F.; Liebermann, E.; Miksch, G.; Kainz, C. *J. Phys. Chem.* **1972**, *76*, 2764.

24. Kennedy, D. F.; Drummond, C. J. *J. Phys. Chem. B* **2009**, 113, 5690–5693

25. Burkert, U.; Allinger, N. L. *Molecular Mechanics* ACS Monograph 177, American Chemical Society, Washington, DC, 1982.

26. Schnur, D. M.; Grieshaber, M. V.; Bowen, J. P. *J. Comp. Chem.* **1991,** *12*, 844–849.

27. Bodo, E.; Mangialardo, S.; Ramondo, F.; Ceccacci, F.; Postorino, P. *J. Phys. Chem. B* **2012**, *116*, 13878–13888.

28. Berg, R. W.; Lopes, J. N. C.; Ferreira, R; Rebelo, L. P. N.; Seddon, K. R.; Tomaszowska, A. A. *J. Phys. Chem. A* **2010**, *114*, 10834–10841.

29. Kanzaki, R.; Doi, H.; Song, X.; Hara, S.; Ishiguro, S. I.; Umebayashi, Y. *J. Phys. Chem. B* **2012**, 1*16*, 14146–14152.

30. Brown, H. C.; McDaniel D. H.; Häflinger, O. *Determination of Organic Structures by Physical Methods*; Braude, E. A., Nachod, F. C., Eds.; Academic Press: New York, 1955.

31. H. K. Hall. *J. Am. Chem. Soc.*, **1957**, *79*, 5441–5444.

32. Walba, H.; Isensee, R. W. *J. Org. Chem.* **1961**, 26, 2789–2791.

33. Bruce, T. C.; Schmir, G. L. *J. Am. Chem. Soc.* **1958**, *80*, 148.

34. McComb, R. B.; Bowers, Jr. G. N.; *Clinical Chem.* 1972, 18.

35. Dwibedy, P.; Dey, G. R.; Kishore, Kamal. *Res. Chem. Intermed.* **1997**, 23, 801–817.

36. Hinman, R. L. *J. Org. Chem. 1958*, *23*, 1587.

37. Pinkert, A.; Marsh, K. N.; Pang S. *Ind. Eng. Chem. Res.* **2010**, *49*, 11809–11813

38. Achinivu E. C.; Howard R. M.; Li G.; Gracz H.; Henderson W. A. *Green Chem.* **2014**, *16*, 1114–1119.

39. Fox. C. M.S. Thesis, University of Idaho, Moscow, ID, May 2006.

40. Wang, H.; Gurau, G.; Rogers, R. D. *Chem. Soc. Rev.* **2012**, *41*, 1519–1537.

41. Goldstein, E.; Allinger, N. L. *Journal of Molecular Structur,* **1989**, *188*, 149–157.

42. Molecular Mechanics, Burkert, Ulrich and Allinger, Norman L., ACS Monograph 177, American Chemical Society, Washington, DC, 1982

43. Allinger, N. L. *Journal of the American Chemical Society* **1977**, *99*, 8127–8134.

CHAPTER 5: [Eth][Ac] as a model solvent for lignin removal from biomass

Abstract

This study demonstrates the extraction of lignin from biomass using oxygenated aliphatic ammonium acetate and lactate PILs. Predictions from the previous chapter outline this group of PILs as potential candidates for an enhanced lignin removal media. The addition of hydroxyl groups to a PIL's cation and anion results in an increase in the hydrogen bonding interactions, which modifies the observed PIL's properties. However, the position of the –OH group (linear or branched) can affect the observed PIL properties. Solubility tests, correlated with the lignin removal efficiency of the PILs, indicate that the PIL's ionicity regulates the lignin extraction to a greater extent than the H–bonding network–with the addition of the hydrogen bonds marginally supplementing this effect. For the [Eth][Ac] PIL, up to 84% of the lignin is extracted from cornstover and the PIL is recovered without undergoing the degrading side-reaction which form of amides. Therefore the selective addition of functional groups to the PIL's ion structure is beneficial for both enhancing the PIL's properties and lignin removal efficiency.

5.1. Introduction

PILs have been demonstrated in this work as effective solvents for lignin dissolution. Rigorous experimental and theoretical analyses in the previous chapters have determined two PIL groups that have favorable lignin removal characteristics. Lignin removal using the secondary cyclic aliphatic ammonium acetate [Pyrr][Ac] has been described extensively in Chapter 3. Oxygenated aliphatic ammonium PILs (OAA), however, have also been suggested

as PILs that will have a high lignin removal capability. OAA PILs are able to form extensive hydrogen bonding networks, which allow them to partially dissolve xylan and disperse cellulose. This feature could potentially increase the ability of these PILs to penetrate and disrupt the biomass fibers–resulting in an enhanced lignin removal.

Researchers, in the past, have investigated the impact of H–bonding on the PIL's physiochemical properties and agree that the presence of H–bonding donor and acceptor groups (formed on the ions via proton transfer) allows the PIL ions to form a multi-dimensional network that modifies the PIL's observed properties.[1–8] Therefore, it is beneficial to study this group of PILs as an increased H–bonding network could potentially improve the PILs' interaction with the polysaccharides and eventually enhance their lignin removal efficiency.

This study demonstrates the lignin extraction from cornstover using OAA PILs that were synthesized from the reagents noted in Figure 5. 1. Results from the previous chapters show that the addition of hydroxyl groups (–OH) to the PIL ions results in an increase in H–bonding. Therefore, lactic acid was considered as an acid source for the formation of PILs. The PIL [Eth][Ac] will also be highlighted as a model for the removal of large amounts of lignin from biomass. In addition, this PIL could be potentially fully recovered without the formation of side products. The [Eth][Ac] PIL is able to disperse cellulose and create a stable cellulose suspension, which allows the PIL to further diffuse into the biomass fibers for an improved lignin removal. This chapter will also consider the use of solvents/PIL mixtures in OAA PILs in order to reduce the observed viscosity for easy processing.

5.2. PIL Characterization

OAA PILs have been identified as PILs that arise from reagents with the opportunity for hydrogen bonding interactions. The addition of hydroxyl (–OH) groups to the PIL ions results in the formation of an extensive H–bonding network (Figure 5. 1 and 5.2), which modifies the observed properties of the PILs. The thermal stability of the OAA PILs follows the trend in ionicity established in the previous chapters. The lactate-based PILs have an increased thermal stability relative to their acetate counterparts (Figure 5. 3). Although individual H–bonds are weak and easily disrupted, in combination they are able to produce strong interactions that can regulate the properties of the resultant PIL.

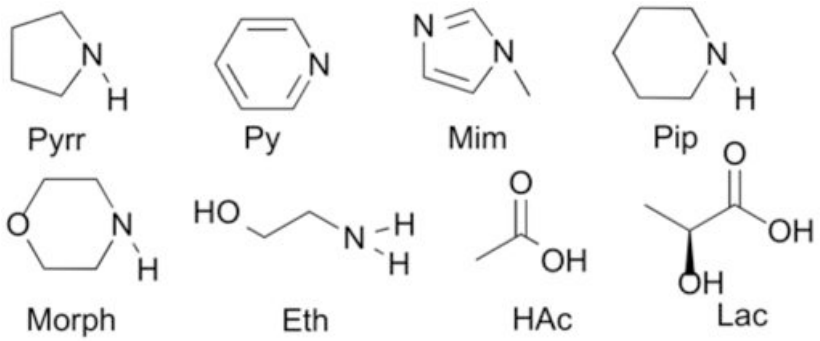

Figure 5. 1 Chemical structures of OAA PILs discussed in this chapter.

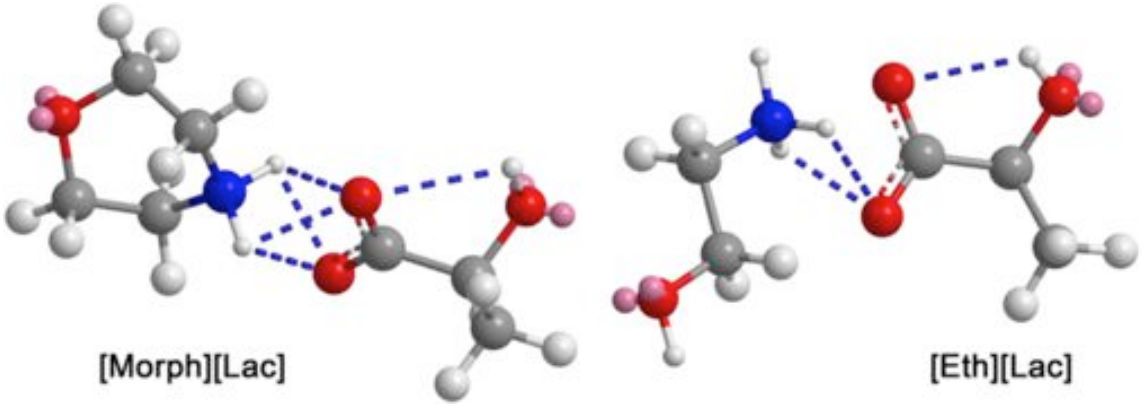

Figure 5. 2. Minimum energy structures of OAA lactate-based PILs using one ionic couple.

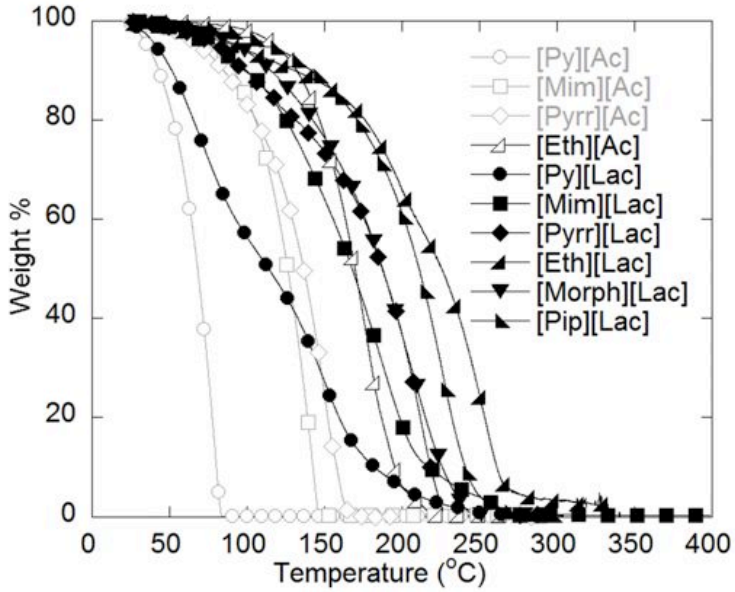

Figure 5. 3. Variable-temperature TGA heating traces (5 °C min^{-1}) of OAC PILs.

The Walden plot for these PILs also shows an increase in the observed ionicity of these PILs, but it has already been established (Chapter 4) that this is due to the H–bond interactions present in the PILs rather than the formation of ions (Figure 5. 4).

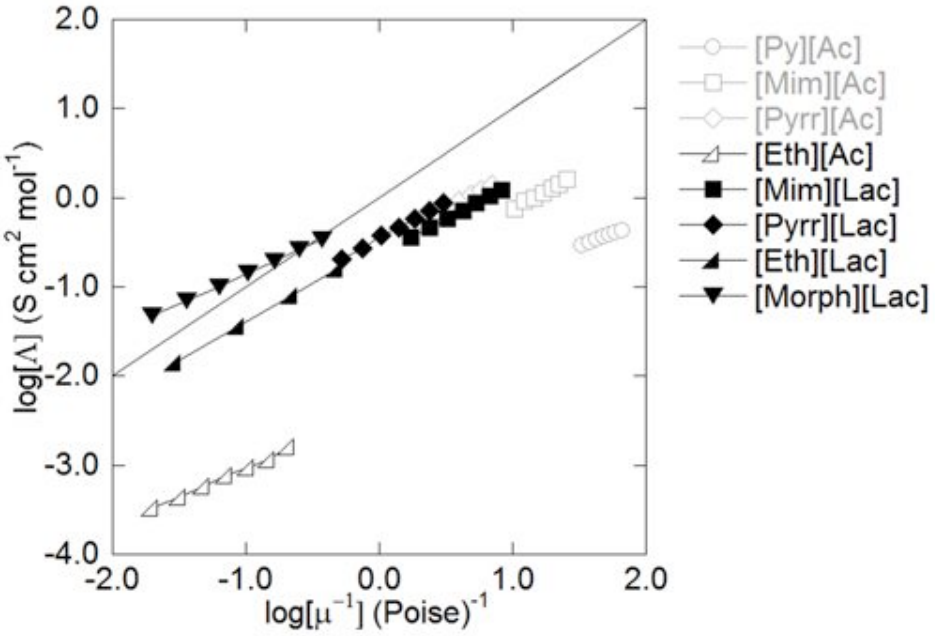

Figure 5. 4. Walden Plot as a measure of ionicity for PILs used in this study.

5.3. Solubility of Biopolymers in PILs

The solubility of commercially available biopolymers (Kraft lignin, xylan, and cellulose) was determined in the OAA PILs and their reagents (Figures 5.5–5.7) using already described procedures. The results confirm the previous findings that the addition of terminal –OH groups to the ions will increase the H–bonding interactions and result in an increase in the xylan solubility, as well as cellulose dispersion (Table 5. 1. and Figures 5.5–5.7). The solubility tests indicate that the ethanolamine and lactic acid reagents, as well as the lactate PILs, are also capable of dissolving large amounts of xylan–a prerequisite for enhancing lignin removal. This implies that these reagents and PILs should be able to extract large amounts of lignin from biomass, but the lactate PILs were found to have a low lignin extraction efficiency that follows the trend in ionicity of the PILs. (Figure 5. 4).

This information establishes that the formation of ions in the PIL is a major criterion for lignin extraction with PILs, although, this effect could be improved by the addition of H–bonding interactions. he lactate PILs have slightly lower lignin removal efficiency than the acetate PILs, with the exception of the [Mim][Lac] PIL, which only marginally increases. (Table 5. 1) The difference in the lignin removal between the different anions (lactate and acetate) for salts with the same cation is not significant indicating that the major contributing factor to the lignin removal efficiency is the PIL's ionicity; the addition of H–bonding groups increases the PILs interactions and the viscosity. These H–bonding groups could limit the solution properties of the PIL as the effect of mixing is reduced thereby minimizing the impact of the PIL's ions in the lactate-based PILs. The lignin extraction efficiency increased about 10% in the [Eth][Ac] PIL when compared with that of the [Pyrr][Ac] PIL. This might

seem like a relatively small improvement, however, when compared to the analogous ethylammonium acetate ([Et][Ac]), the addition of the –OH group to the PIL's cation significantly increases the PIL's ability to remove lignin from biomass (Table 5. 1).

The solubility tests also reveal that the OAA PILs are able to disperse the cellulose to a larger extent than their acetate counterparts. (Figure 5. 5) Since the OAA PILs can dissolve xylan comparably to the non-oxygenated PILs, the ability to disperse cellulose is the major difference in the properties of these PILs, which is a direct outcome of the H–bonding network observed for these PILs. Cellulose is know to interact via strong inter– and intra–molecular hydrogen bonding, (cite)[9–10] thus the addition –OH groups to the PIL ion structures results in PIL ions that are able to interact better with the cellulose hence the observed cellulose suspension (Figure 5. 5). As discussed in Chapter 4, cellulose dispersion should allow for further penetration of the biomass fibers, thereby allowing for improved lignin removal.

Table 5. 1. Solubility of Kraft lignin, cellulose and xylan (% w/w) in the OAA PILs and reagents mixtures (after heating/stirring at 90 °C for 24 h).

	lignin	cellulose	xylan	% lignin extracted
Eth	> 50[a]	0.53 ± 0.09	16.26 ± 0.23	
Mim	> 50[a]	0.24 ± 0.02	6.34 ± 0.17	
Morph	> 50[a]	0.27 ± 0.03	0.51 ± 0.01	
Pip	6.88 ± 0.04	0.37 ± 0.03	0.25 ± 0.08	
Pyrr	7.98 ± 0.10	0.63 ± 0.44	1.44 ± 0.07	
Py	> 50[b]	0.10 ± 0.00	0.02 ±0.02	
[Eth][Ac]	> 50[a]	0.75 ± 0.06	11.54 ± 0.88	84.0
[Eth][Lac]	> 50[a]	0.66 ± 0.06	10.23 ± 0.73	78.9
[Mim][Ac]	> 50[a]	0.20 ± 0.05	5.60 ± 0.77	30.0
[Mim][Lac]	> 50[a]	< 1[b]	> 15[a]	33.9
[Morph][Ac]	> 50[a]	0.88 ± 0.05	10.38 ± 1.41	–[c]
[Morph][Lac]	> 50[a]	1.95 ± 0.30	9.50 ± 0.37	62.8
[Pip][Ac]	> 50[a]	0.33 ± 0.03	> 15[a]	–[c]
[Pip][Lac]	> 50[a]	< 1[b]	> 15[a]	–[c]
[Pyrr][Ac]	> 50[a]	0.79 ± 0.04	> 15[a,]	76.6
[Pyrr][Lac]	> 50[a]	0.78 ± 0.08	10.37 ± 0.22	40.0
[Py][Ac]	> 50[a]	0.12 ± 0.03	0.82 ± 0.02	25.0
[Py][Lac]	> 50[a]	< 1[b]	10.17 ± 0.36	14.1

[a] Solubility limited by viscosity, [b] Not quantitatively determined, [c] Not determined

Figure 5. 5 Images depicting the solubility of 5% w/w microcrystalline cellulose in the reagents: (a) after stirring for 30 min at room temperature (25 °C) and (b) after stirring for 24 h at 90 °C (sample sizes were 10.0 g).

Figure 5. 6. Images depicting the solubility of 5% w/w xylan in the PILs: (a) after stirring for 30 min at room temperature (25 °C) and (b) after stirring for 24 h at 90 °C (sample sizes were 10.0 g).

Figure 5. 7. Images depicting the solubility of 5% w/w microcrystalline cellulose and xylan in the reagents: (top) after stirring for 30 min at room temperature (25 °C) and (bottom) after stirring for 24 h at 90 °C (sample sizes were 10.0 g).

5.4. Lignin Extractability From Biomass

The [Eth][Ac] PIL has already been identified as potentially being able to extract large amounts of lignin from biomass (Table 5. 1). The simple linear structure of the PIL's ions allows the ions to create tightly packed hydrogen bonds resulting in the enhanced physical and thermal properties observed. A compositional analysis on the [Eth][Ac] treated cornstover shows that that the extracted lignin accounts for approximately 84% of the lignin found in EF–CS (Table 5. 2). This improved efficiency is a direct result of the H–bonding

network established between the PIL's ions. This allows the [Eth][Ac] PIL to dissolve 12% w/w of xylan and also form a stable cellulose suspension (Table 5. 1 and Figure 5. 5). These features are responsible for the improved lignin extraction efficiency observed with this PIL.

Table 5. 2. Composition (% w/w) of EF-CS and PIL-CS after pretreatment (90 °C for 24 h).

	EF-CS	[Eth][Ac]-CS	[Eth][Lac]-CS
lignin	16.6	4.1	7.6
glucan	38.2	54.6	45.1
hemicelluloses	24.6	24.2	29.6

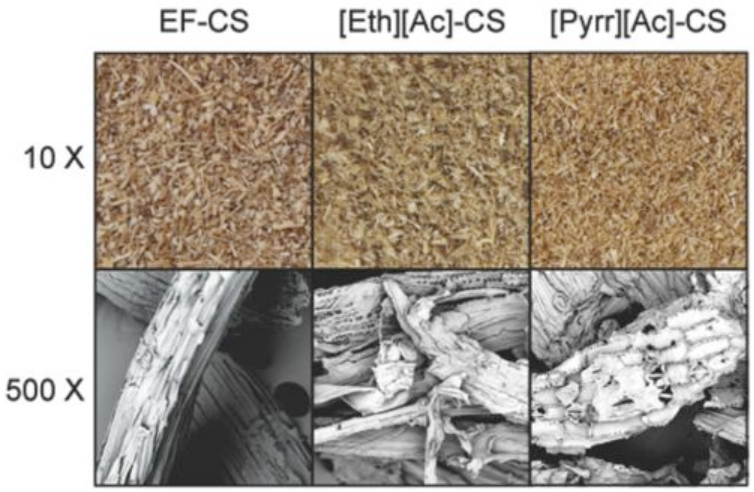

Figure 5. 8. Images depicting the effect of the PIL treatment on the CS fibers.

SEM analysis of the [Eth][Ac]–CS fibers before and after the PIL pretreatment confirmed that the increase in lignin removal does correspond with an increased disruption of the EF–CS fibers (Figure 5. 8). The intact EF–CS fibers are completely disrupted when compared to that of the [Pyrr][Ac]–CS fibers indicating that further penetration of the CS fibers has occurred by the [Eth][Ac] PIL as more lignin and hemicellulose are removed and the cellulose is partially disrupted. The [Eth][Ac]–CS fibers remain highly crystalline and have similar diffraction patterns to the original EF–CS fibers (Figure 5. 9). However, the relative intensities of the peaks are modified as the peak at 22º is reduced with respect to the smaller peak at about 16º. This results in a reduction in the crystallinity index with the solubilization of the hemicelluloses and lignin together likely the major reason for this change in cellulose crystallinity.[11–13]

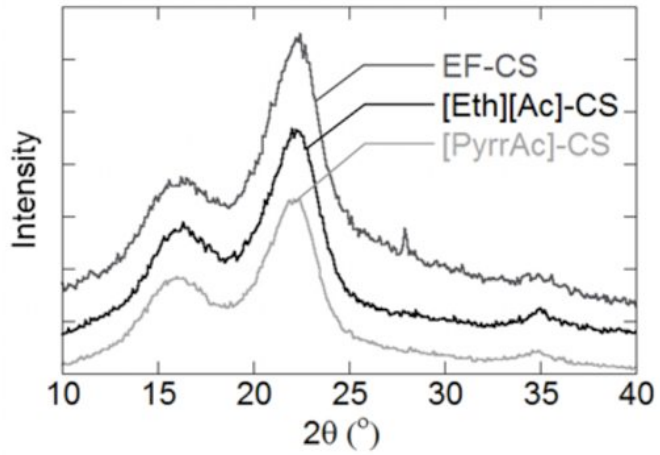

Figure 5. 9. XRD of CS recovered from PIL pretreatment.

5.5. Recyclability and Concerns About Purity Readdressed

The [Eth][Ac] PIL is also favorable for recovery via distillation as the formation of side products during the pretreatment process is mitigated. The dipole moment induced by the addition of the hydroxyl group decreases the reactivity of the amine group resulting in the mitigation of unwanted side products such as amides.[14] It is important to note that this PIL, like many others are prone to discoloring,[15–16] which is not always due to the presence of amides. Heating tests for the PIL at 90 °C for 24 h were used to track the formation of side products. There is a slight darkening of the color of the [Eth][Ac] PIL (Figure 5. 10c), which is supported by an increase in the intensity of the absorption spectra of the PIL after heating for 24 h (Figure 5. 10 a, b). Despite this slight discoloration, Figure 5. 11 shows that the PIL is fully recovered indicating that the amount of any side products is negligible as they are undetected via NMR analysis.

The [Eth][Ac] PIL was also recovered at a yield of 90% using the distillation setup at 150 ºC and 0.1 torr. This yield is less than the recovery desired for the PILs due to the increased thermal stability and high viscosity of the OAA PILs utilized. The H–bonding network established in the PIL contributes to these enhanced properties and results in PIL ions that are difficult to disrupt (i.e., form reagents). An isothermal TGA analysis of the PILs in this study shows that OAA PILs are more stable than non oxygenated PILs. (Figure 5. 12). When the temperature is held at 90 ºC, there is an initial mass loss in the PIL followed by stabilization–resulting in a slower degradation rate. Despite the higher temperature used for the distillation (150 ºC), residual amounts of the PIL remain with the extracted lignin. In

order to enhance the PIL recovery, a higher temperature could be utilized for the distillation; however, lignocellulosic biomass is temperature sensitive and prone to the formation of unwanted degradation products such as char or irreversible lignin condensation.

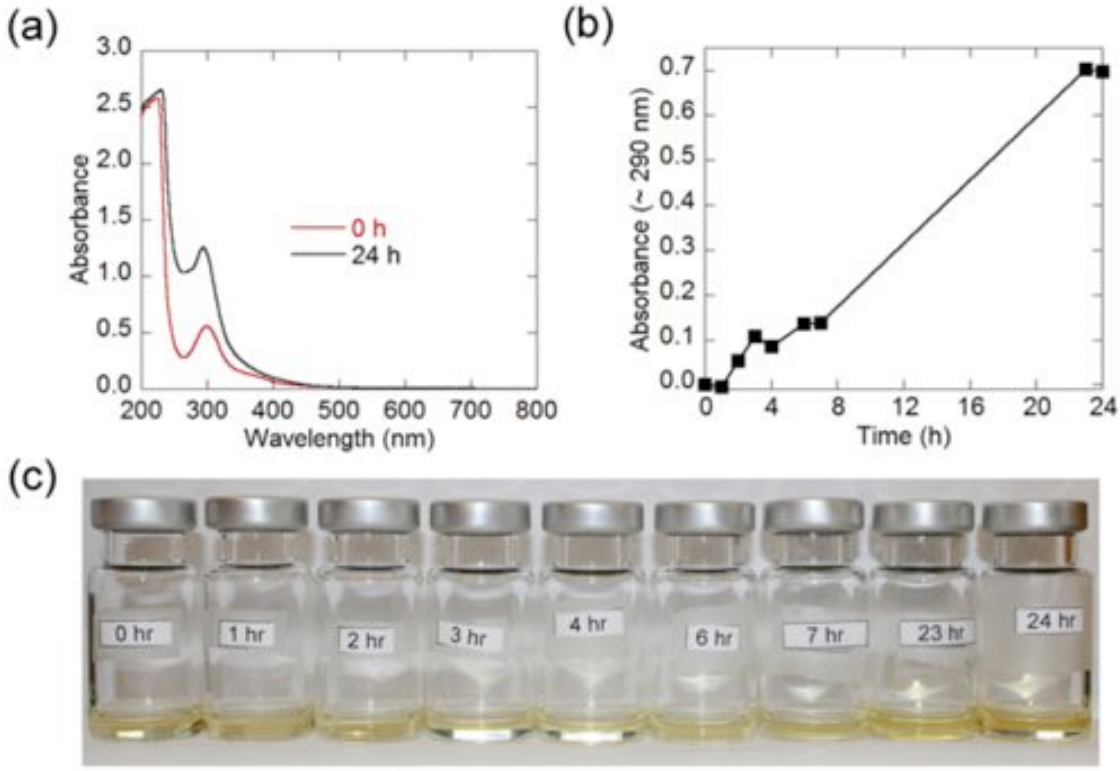

Figure 5. 10. Effect of heating on the [Eth][Ac] PIL showing (a) the absorption spectra of the PIL after heating for 24 h at 90 °C, (b) the time dependent rate of discoloration in the PIL and (c) images showing the effect of heating on the PIL's observed color.

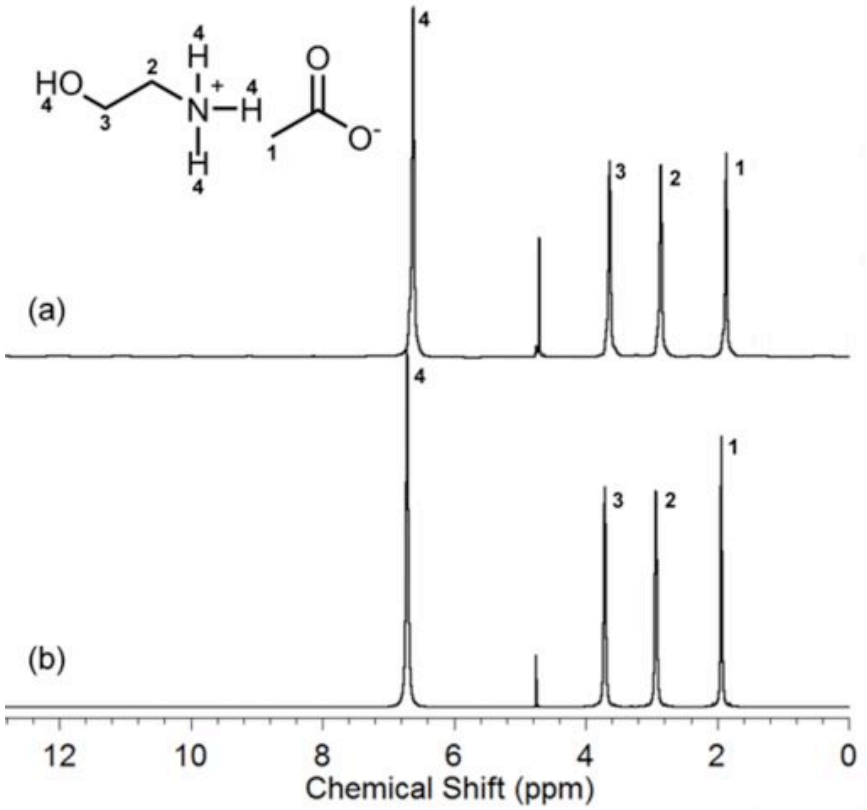

Figure 5. 11. ^{1}H-NMR spectra (δ_{solv} = 4.75 ppm) of PIL ([Eth][Ac]): (a) after synthesis and (b) after distillation from the CS-Lignin solution (Liquor 1).

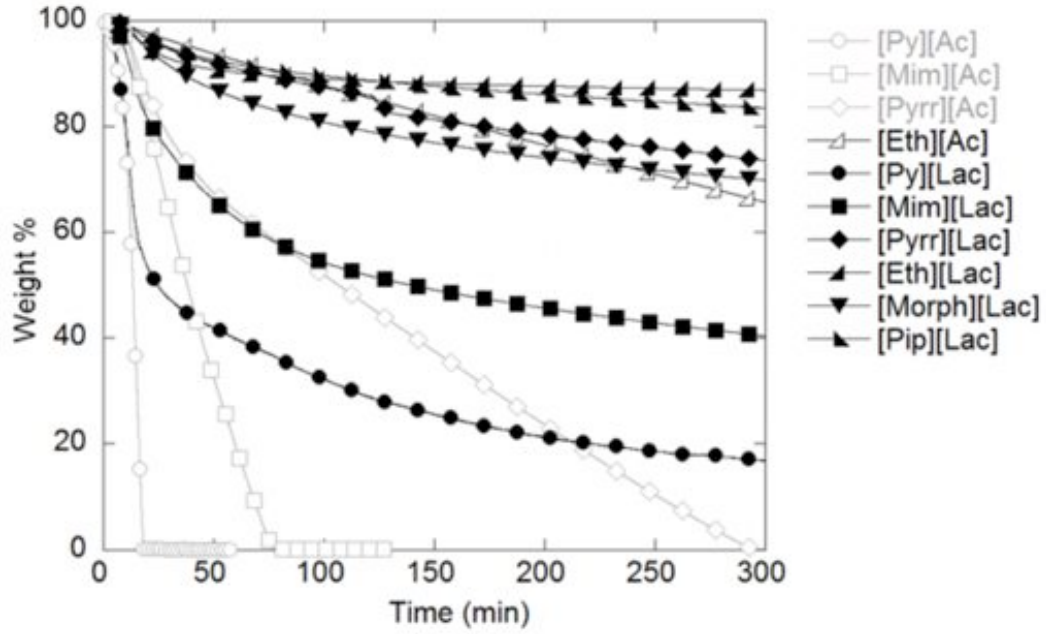

Figure 5. 12. Isothermal (90 °C) TGA heating traces (5 °C min^{-1}) of OAC PILs.

Dissolution experiments were performed using cellulose in order to observe any changes in the crystal structure and morphology of the polysaccharide after the PIL dissolution. Following the solubility experiment (90 °C for 24 h), the undissolved cellulose was recovered. The cellulose remains largely crystalline, but there is a small shoulder observed at about 20–23º comparable to that found for the [Pyrr][Ac]–cellulose, which could indicate the presence of a small amount of a different cellulose crystal structure (Figure 5. 13).[9] The physical appearance of the cellulose is also modified (Figure 5. 14). SEM analysis of the fibers indicates that the dispersion of the cellulose in the [Eth]Ac] PIL results in a

"sticky-looking" structure and the intact cellulose fibers have been completely disrupted (Figure 5. 14).

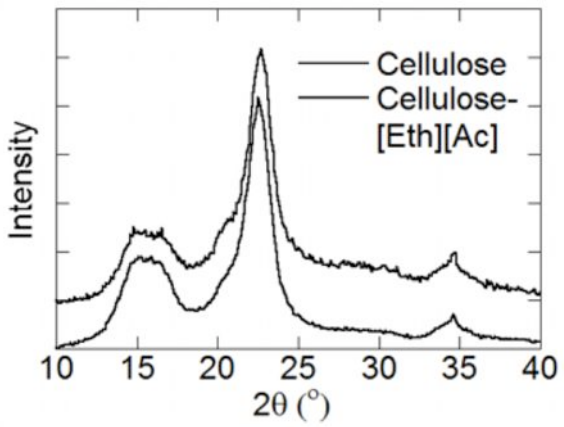

Figure 5. 13. XRD of cellulose recovered from PIL dissolution.

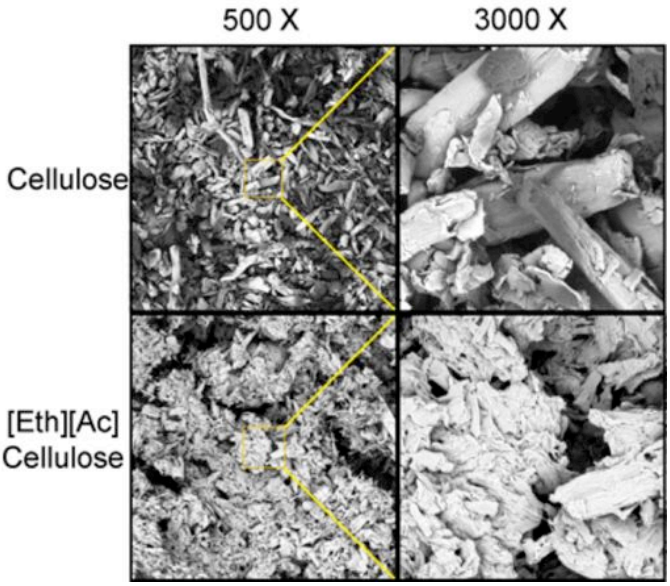

Figure 5. 14 Images of cellulose recovered from PIL dissolution (500X and 3000X).

5.6. Viscosity Reduction

The viscosity of the PIL used is very important from a practical point of view. The OAA PILs have high viscosities due to the H–bond interactions between the PIL ions. (Figure 5. 15) The lactate PILs are more viscous than the acetate PILs, however, the viscosity of the [Eth][Ac] PIL is slightly higher than that of the [Eth][Lac] PIL. (Figure 5. 15) A higher viscosity necessitates a higher dissolution temperature (to reduce the viscosity enabling stirring/mixing), which might induce the formation of unwanted side products from the PIL and/or the biomass biopolymers. The PIL properties are fixed by the ion structure, but the properties can be modified through the addition of solvents that will reduce the H–bonding interactions. This might also improve the recovery of the PILs via distillation. Both the solvent type and the amount of the solvent to be used needs to be optimized to determine the optimal conditions that will enhance the PIL properties without reducing the xylan solubility or cellulose dispersion. As part of the present work, the solvents acetone, ethanol, and DMSO were considered as candidates to reduce the viscosity of the [Eth][Ac] PIL. (Figure 5. 16)

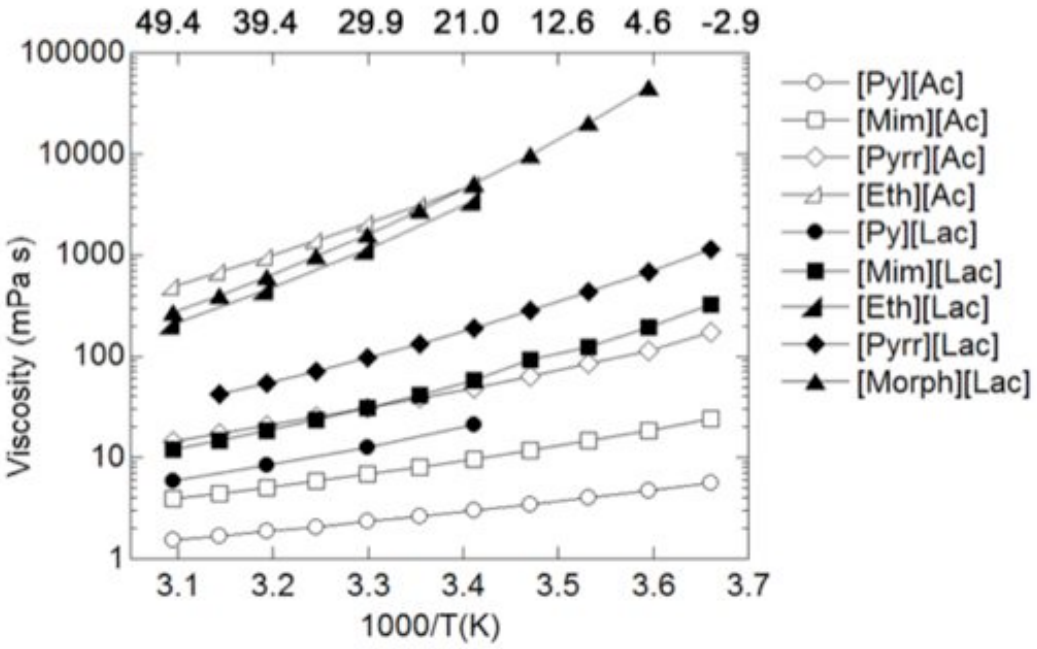

Figure 5. 15. Variable temperature viscosity OAC of PIL.

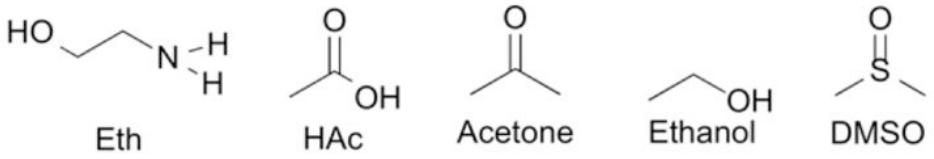

Figure 5. 16. Molecular solvents used to reduce the PIL's viscosity.

Acetone is insoluble in the [Eth][Ac] PIL resulting in a two-phase liquid, or an emulsion when agitated. (Figure E. 3) The viscous [Eth][Ac] PIL remains at the bottom while the undissolved acetone remains on top. (Figure E. 4) This prevents the utilization of this solvent for the reduction of viscosity since the solvent molecules are immiscible with the PIL's ions. The interaction of the mixture in the biopolymers is also diminished as the resulting mixture takes on the properties of acetone–see Appendix E. Such mixtures are able to dissolve less than 5% w/w of each biopolymer. Similar trends are observed with ethanol despite this solvent being soluble in the [Eth][Ac] PIL. The [Eth][Ac]/ethanol mixtures have low cellulose solubility and do not disperse cellulose like the original PIL. (Figure E. 4) The xylan solubility is also very low (< 5% w/w), but a xylan suspension is formed in the mixture with a mole ratio of 60:40 [Eth][Ac]/ethanol. (Figure E. 4) Although, these mixtures are able to disperse xylan and create a stable suspension, the xylan component is still insoluble in the PIL/solvent mixture. Significantly, the PIL/ethanol and PIL/acetone mixtures are also unable to dissolve Kraft lignin, as is the case for the pure solvents, which prevents the application of these solvents for lignin removal (Figures E. 4 and E. 5).

DMSO, however, is soluble in the PILs and has attractive properties for the dissolution of biopolymers. Pure DMSO can dissolve large amounts of Kraft lignin and xylan, while maintaining low cellulose solubility–all necessary requirements for selective lignin removal from biomass. However, the results from this study indicate that the presence of ions is beneficial for enhancing the lignin removal efficiency. The solubility tests also show that the [Eth][Ac]/DMSO properties are enhanced. The mixtures all have the high lignin solubility and increased xylan solubility that the PIL has. (Table 5. 3, Figure 5. 17) For

the cellulose solubility studies, the dispersion of cellulose is also unaffected and increases as the mole fraction of the PIL ions increases. The dispersed cellulose level starts to plateau at a 60:40 [Eth][Ac]/DMSO ratio. DMSO, therefore, is a potential candidate as a viscosity reducing co-solvent because the solvent/PIL mixtures have favorable interactions with the biopolymers for lignin removal applications. However, the viscosity of the PIL was not greatly reduced and DMSO could be toxic source of sulfur to biomass.[17] Some researchers have suggested that DMSO should be avoided, and instead propylene glycol or polyethylene glycol (PEG) could be used instead as viscosity reducing co-solvents.[17] Further tests will need to be conducted on those mixtures to detect the efficacy of such PIL/solvent mixtures for biomass component dissolution and to determine the optimal concentration for viscosity reduction, as well as enhanced solvent properties.

Table 5. 3. Qualitatively determined solubility of Kraft lignin, cellulose and xylan (% w/w) in the the DMSO/[Eth][Ac] mixtures (after heating/stirring at 90 °C for 24 h).

PIL=[Eth][Ac]	lignin	cellulose	xylan
100% DMSO	> 50[a]	1-5	< 20[a]
80% DMSO	> 50[a]	1-5	< 15[a]
60% DMSO	> 50[a]	1-5	< 15[a]
40% DMSO	> 50[a]	1-5	< 15[a]
20% DMSO	> 50[a]	1-5	< 15[a]
0% DMSO	> 50[a]	1-5	10-15

[a] Solubility limited by viscosity

Figure 5. 17. Images depicting the solubility of 5% w/w commercially available biomass components (Kraft lignin, microcrystalline cellulose and xylan) in the various concentrations of DMSO mixtures,: (a) after stirring for 30 min at room temperature (25 °C) and (b) after stirring for 24 h at 90 °C (sample sizes were 10.0 g).

5.7. Lignin Removal from Multiple Biomass Sources

Development of a robust and sustainable supply of biomass resources is necessary for the implementation of region-specific biorefineries. Lignocellulosic biomass is typically classified into forest and agricultural residues. Lignin extraction using the [Pyrr][Ac] and [Eth][Ac] PILs was demonstrated for the following feedstocks: cornstover, switch grass, pinewood, beechwood. These four groups encompass the main biomass categories that are usually considered for cellulosic ethanol processing: agricultural residues, herbaceous grasses and forest residues (softwoods and hardwoods)–respectively.[18–19]

Lignin removal from cornstover has been discussed in the previous chapters. Similarly, lignin was extracted from switch grass using PILs with the [Pyrr][Ac] PIL extracting up to 75% of the lignin found is switch grass (Figure 5. 18). The lignin removal efficiency for pinewood and beechwood, however, were surprisingly low. Researchers have previously experienced problems with softwoods like pine wood but have been successful with beechwood.[20] Softwoods comprise of guaiacyl-rich lignin, which is more condensed and typically requires more quantities of chemicals than hardwood lignin during the pulping and bleaching processes.[20–21]

SEM analysis of the PIL–treated fibers before and after the PIL treatment showed that the fibers did undergo a change in their morphology (Figure 5. 18). The [Pyrr][Ac]-PW fibers look significantly different than the original EF–PW fibers indicating that the fibers have been disrupted during the treatment process. Further analyses on the biomass fibers needs to be carried out to access any additional effects of the treatment other than the lignin removal that may be beneficial for biofuel processing. The crystallinity of the biomass PIL–treated biomass fibers matched that of the original biomass used (Figure 5. 19). Similar to the results previously obtained, the relative intensities of the peaks are modified, which results in a reduction in the biomass crystallinity index, as hemicelluloses and lignin are dissolved.[11–13]

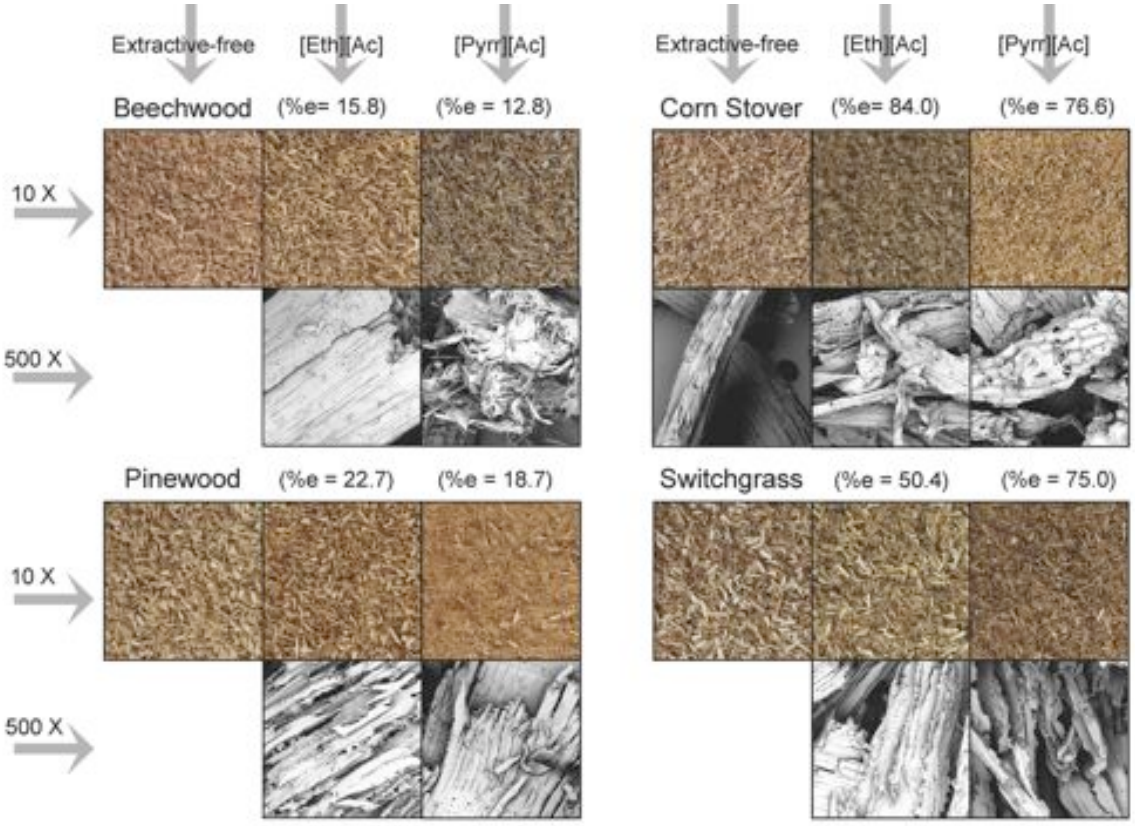

Figure 5. 18. Images depicting the biomass fibers before and after PIL treatment.

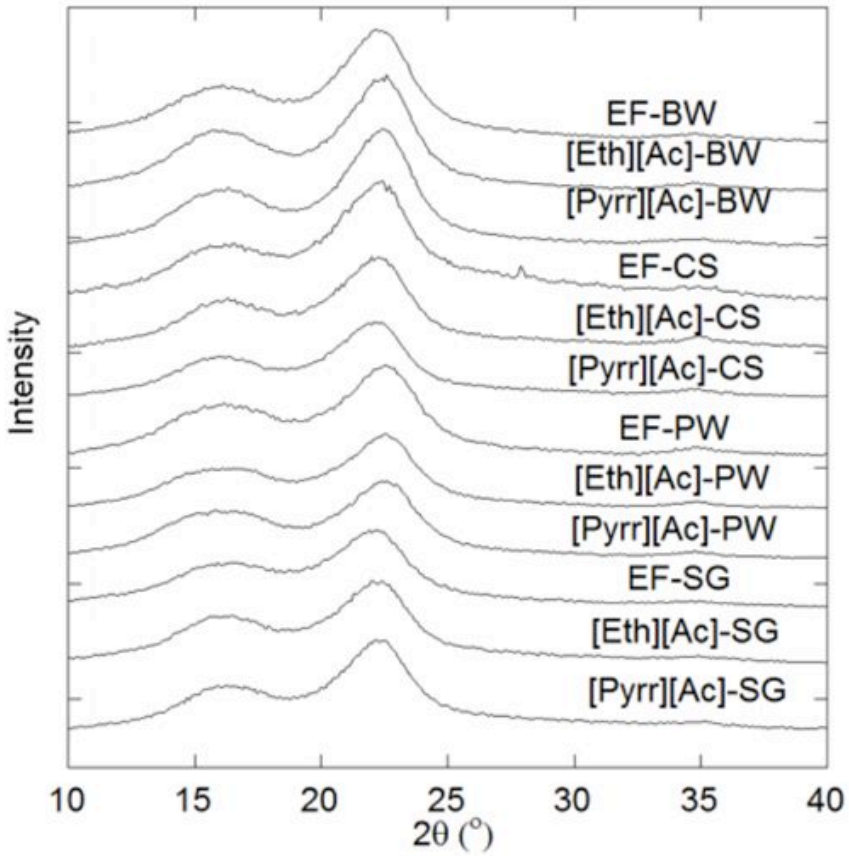

Figure 5. 19 XRD of the biomass fibers recovered from PIL pretreatment.

5.8. Conclusions

OAA-based PIL ions are able to interact strongly via H–bonding to create a strong network that improves the interactions of the PIL ions. This results in an increase in the PIL's ionicity, thermal stability and xylan solubility. These PILs, formed by the addition of –OH groups, have the potential to remove large amounts of lignin from biomass, but if the viscosity is too high, the solvent might not be suitable for use in practical applications. In

addition, this increase in viscosity could diminish the effect of the PIL's ions for lignin removal with the lactate PILs have a lower lignin removal capability than the acetate PILs, although their properties predict otherwise.

The [Eth][Ac] PIL, in particular, has a balance between ionicity and H–bonding that make it highly effective for lignin removal. In addition, the viscosity of the PIL can be modified using co-solvents. A careful selection of the solvent and the concentration is necessary, however, to formulate mixtures with the desired properties. The recovered biomass after the lignin extraction largely maintains its crystallinity, but with an overall reduction in the crystallinity index (due to the extraction of amorphous components). The [Eth][Ac] PIL is potentially fully recoverable by distillation without the formation of side products, which is beneficial for the recovery and reuse of the PILs. It has thus been demonstrated that careful modification of the PIL ions with H–bonding groups has the potential to improve the PIL's properties for an enhanced lignin removal and pure recovery. This will enable the formation of task-specific ILs for biomass processing. The lignin removal process was also effectively applied to switch grass, however woody materials (pinewood and beechwood) proved to be recalcitrant to the PIL treatment.

References:

1. Fumino, K.; Peppel, T.; Geppert-Rybczynska, M.; Zaitsau, D. H.; Lehmann, J. K.; Verevkin, S. P.; Köckerling, M.; Ludwig, R. *Phys. Chem. Chem. Phys.* **2011**, 13, 14064–14075.
2. Fumino, K.; Wulf, A.; Ludwig, R. *Angew. Chem., Int. Ed.* **2008**, 47, 8731–8734.
3. Miran, M. S.; Kinoshita, H.; Yasuda, T.; Susan, A. B. H.; Watanabe, M. *Chem. Commun.* **2011**, 12676–1279.
4. Fumino, K.; Wulf, A.; Ludwig, R. *Phys. Chem. Chem. Phys.* **2009**, 11, 8790– 8794.
5. Hayes, R.; Imberti, S.; Warr, G. G.; Atkin, R. *Angew. Chem., Int. Ed.* **2013**, 52, 4623–4627.
6. Fumino, K.; Wulf, A.; Ludwig, R. *Angew. Chem., Int. Ed.* **2009**, 48, 3184– 3186.
7. Dong, K.; Zhang, S. *Chem.—Eur. J.* **2012**, 18, 2748– 2761.
8. Katsyuba, S. A.; Vener, M. V.; Elena E. Zvereva, E. E.; Fei, Z.; Scopelliti, R.; Laurenczy, G.; Yan, N.; Paunescu, E.; Dyson, P. J. *J. Phys. Chem. B*, **2013**, *117*, 9094–9105.
9. Wang, H.; Gurau, G.; Rogers, R. D. *Chem. Soc. Rev.* **2012**, *41*, 1519–1537.
10. Mäki-Arvelaa, P.; Anugwoma, I.; Virtanena, P.; Sjöholma, R.; Mikkola, J. P. *Ind. Crop. Prod.* **2010**, *32*, 175–201.
11. Xiao, L.-P.; Sun, Z.-J.; Shi, Z.-J.; Xu, F.; Sun, R.-C. *BioResources*, **2011**, *6*, 1576–1598.
12. Lee, J. M.; Jameel, H.; Venditti, R. A *Bioresour. Technol.* **2010**, *101*, 5449–5458.

13. Inoue, H.; Yano, S.; Endo, T.; Sakaki, T.; Sawayama, S. *Biotechnol. Biofuels* **2008**, 1, 1–9.

14. Greaves, T. L.; Weerawardena, A.; Fong, C.; Krodkiewska, I.; Drummond, C. J. J. *Phys. Chem. B* **2006**, *110*, 22479–22487.

15. Weidig, C. F. Discoloration inhibitor for aromatic amines. U.S. Patent 4,861,914, August 29, 1989.

16. Gugumus, F. Photooxidation of Polymers and Its Inhibition. In *Oxidation Inhibition in Organic Materials*; Pospíšil, J., Klemchuk, P. P., Eds.; CRC Press: Boca Raton, 1989-1990; Vol. 2, pp 144–146.

17. Willauer, H. D.; Huddleston, J. G.; Li, M.; Rogers, R. D. *J. Chromatogr.B* **2000,** *743*, 127–135.

18. Simmons, B. A.; Loque, D.; Blanch, H. W. *Genome Biology* **2008**, *9*, 242.

19. Vogel, K. P. *J. Soil and Water Conserv.* **1996**, *51*, 137–139.

20. Santos, R. B.; Hart, P. W.; Jameel, H.; Chang, H.-m. *BioResources* 2013, *8*, 1456–1477.

21. Sarkanen, K. V.; Ludwig, C. H. *Lignins: Occurrence, Formation, Structure and Reactions*; John Wiley and Sons, New York, 1971.

CHAPTER 6: Lignin Characterization Commentary

Abstract

The Kraft lignin recovered after dissolution in the PILs and the lignin extracted form cornstover have been characterized using elemental, molecular weight distribution and FT-IR analyses. For the more ionic [Pyrr][Ac], there is an increase in the fragmentation of lignin resulting in lignin with a smaller average molecular weight and a more uniform polydispersity. Energy minimization calculations show that the [Py][Ac] PIL and its pyridine reagent are able to dissolve lignin via the staking of the π electrons in the aromatic rings. The PIL ions have been show to be incorporated within the lignin extracted, which confirms that it is the PIL ions direct interaction with the lignin that is responsible for the lignin dissolution.

6. 1. Introduction

This chapter provides a brief commentary on some techniques that have been used to elucidate the structure of the extracted lignin from lignocellulosic biomass, as well as give further insight into the interactions between the PIL ions and lignin that support high lignin solubility. The previous chapters demonstrate clearly that the components of the cation and anion in the PILs can be easily fine-tuned to adjust their physicochemical properties, which affect their implementation for the extraction and recovery of lignin from biomass. However, the mechanism for lignin dissolution and regeneration in the PILs is not fully understood.

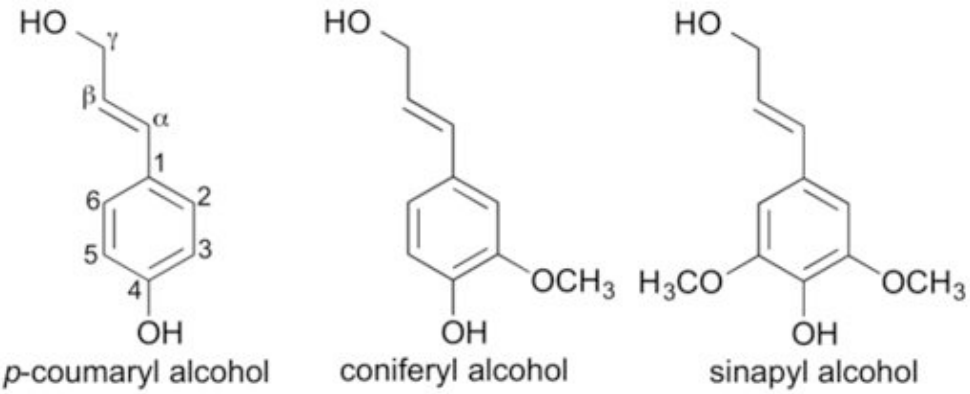

Figure 6. 1. The basic units of lignin; *p*-coumaryl (hydroxyphenyl), coniferyl (guaiacyl), and sinapyl (syringyl) alcohol.

Lignins from different plant sources are usually classified according to the abundance of their basic phenylpropane units: guaiacyl (G), syringyl (S), and 4-hydroxyphenyl (H).[1–8] (Figure 6. 1) The characteristics of the lignin obtained depend on both the source of the lignin and intensity of the delignification process.[1–8] Elemental, molecular weight distribution, and FT-IR analyses, as well as energy minimization calculations, have been used to analyze the extracted lignin in order to determine the mechanism behind the lignin dissolution and extraction from biomass. The effect of the solvent used to regenerate the lignin was also considered.

6. 2. Elemental Analysis

Table 6. 1 shows the elemental analysis, C_{900} formula, and degree of unsaturation (DOU) of Kraft lignin, PIL-treated Kraft lignin and lignin extracted from cornstover using PILs. The degree of unsaturation is calculated with the formula below:

$$Ring + \pi Bonds\ (DOU) = C - \frac{H}{2} - \frac{X}{2} + \frac{N}{2} + 1$$

where C = number of carbons, H = number of hydrogens, X = number of halogens and N = number of nitrogens; oxygen and other divalent atoms do not contribute to the degree of unsaturation. The molecular masses for C, H, and N used are 12.0107, 1.00794, and 14.0067 g mol^{-1}, respectively.

Table 6. 1. Elemental analysis and C_{900} empirical formula of the lignins.

PIL	C (%)	H (%)	N (%)	C_{900} formula	Degree of unsaturation
Kraft lignin	62.2	6.1	0.9	$C_{900}H_{1046}N_{11}$	383
[Py][Ac]-K. lignin	63.7	5.8	1.4	$C_{900}H_{969}N_{16}$	425
[Mim][Ac]-K. lignin	63.5	6.0	3.7	$C_{900}H_{1016}N_{45}$	416
[Pyrr][Ac]-K. lignin	64.5	7.2	4.0	$C_{900}H_{1203}N_{48}$	324
[Py][Ac]-CS lignin	51.6	7.0	6.9	$C_{900}H_{1452}N_{104}$	227
[Mim][Ac]-CS lignin	48.9	7.3	18.7	$C_{900}H_{1603}N_{295}$	247
[Pyrr][Ac]-CS lignin	52.1	10.3	10.1	$C_{900}H_{2121}N_{149}$	-85
EF-CS	43.0	5.7	0.9	$C_{900}H_{1428}N_{16}$	195

The results indicate that the [Py][Ac]– and [Mim][Ac]–Kraft lignins have a much higher DOU than the original Kraft lignin. This is not due to the formation of additional double bonds during the dissolution experiments as other researchers have found,[1] but is more likely due to the incorporation of the PIL ions into the lignin. These two PILs arise from aromatic base reagents, which could contribute to the observed DOU of the recovered

lignin. This finding is supported by the slight increase in the N amount as the main source of nitrogen to the system is from the PIL's cation. The Kraft lignin recovered from the [Pyrr][Ac] PIL on the other hand has a much lower DOU despite the increase of the N amount. This cyclic aliphatic PIL does not contribute much to the observed unsaturation and could also be possibly partially depolymerizing the lignin resulting in smaller lignin segments with a lower amount of double bonds in the lignin backbone.

For the lignin extracted from cornstover, different trends are observed. The overall DOU is much lower than that for the Kraft lignin samples, but higher than that for EF–CS. The N amount also increased again indicating that the PIL cations are incorporated into the lignin. Typically, if the DOU is negative, such as with the [Pyrr][Ac]–CS lignin, it is necessary to add degrees of unsaturation, i.e., remove Hs without changing the molecular weight. Replacing CH_4 with O could do this. This has the effect of adding one degree of unsaturation. The lignin extracted from cornstover could be connected to some carbohydrates via lignin–carbohydrate–linkages, which add Os to the empirical formula, thereby increasing the theoretical O amount. C_2H_4 could also be replaced with N_2. This also has the effect of adding one degree of unsaturation. The [Pyrr]Ac] PIL has been shown to have the ability to dissolve xylan–the secondary carbohydrate molecule found in cornstover which suggests that the extracted lignins might be directly connected the carbohydrates (xylan).

6. 3. Molecular Weight Distribution

Changes in the average molecular weight of the lignin provide insight into the mechanism for lignin fragmentation during the PIL treatment processes. Lignin samples were

acetylated and dissolved in THF and analyzed using a GPC.[2] The observed average molecular weights for the PIL-recovered lignins are lower than the original Kraft lignin indicating that the PIL dissolution process results in smaller fragments of lignin being produced (Table 6. 2). The fragmentation, however, is not uniform in the [Py][Ac] and [Mim][Ac] PILs as the polydispersity of the observed lignins is increased. The more ionic [Pyrr][Ac] PIL fragments the Kraft lignin into smaller segments and the process results in lignin with a more uniform structure. This effect is increased with the CS-extracted lignin for which there is better control over the starting material since Kraft lignin is a lignin extract with an already modified chemical structure. The molecular weights of the lignin recovered from [Pyrr][Ac] extraction are smaller than for any of the Kraft lignin samples and the polydispersity of the recovered lignins is also much lower than for any of the Kraft lignin samples indicating that the regenerated lignin had a more homogenous composition (Table 6. 2).

Table 6. 2. Weight-average (M_w) and number-average (M_n) molecular weights (g mol^{-1}) and polydispersity (M_w / M_n) of the Kraft lignin recovered from PIL dissolution and the lignin extracted from CS using the [Pyrr][Ac] PIL.

PIL	M_n	M_w	M_w / M_n
K. Lignin (Indulin AT)	1600	6500	4.06
[Py][Ac]-K. lignin	830	4,983	6.00
[Mim][Ac]-K. lignin	646	3,919	6.06
[Pyrr][Ac]-K. lignin	528	1,797	3.40
[Pyrr][Ac]-CS lignin	330	900	2.73

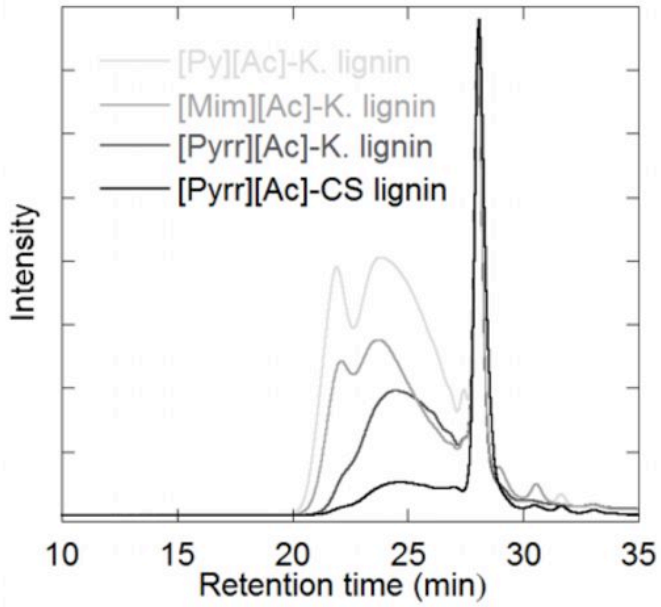

Figure 6. 2. Size exclusion chromatograph of acetylated Kraft lignin recovered from PIL dissolution and CS lignin from the [Pyrr][Ac] PIL.

This finding is supported by the SEC chromatographs from which the molecular weights were calculated. Figure 6. 2 shows that in the [Pyrr][Ac] lignin, with lower polydispersity, there is a reduction of the broad peak at t < 27 min for larger-sized lignin, while the intensity of the peak at ~28 min for smaller sized lignin is heightened. This confirms that the [Pyrr][Ac]-PIL is more suitable for uniform lignin fragmentation. It is important to also note that for the [Pyrr][Ac]-CS lignin, the acetylated lignin samples are not completely dissolved in THF as this lignin is closer to native lignin and is not easily dissolved in the typical solvents for Kraft lignin. This has also been observed in other IL-extracted lignins.[2] However, the conclusions described in the previous paragraph remain valid as the data from the [Pyrr][Ac]-Kraft lignin supports the trend observed.

6. 4. Lignin FT-IR Analyses

FT-IR analysis was used to characterize the absorption bands for representative functional groups in the lignin (Figure 6. 3). Table 6. 3 lists the peaks observed, as well as their assignments using previously assigned biomass samples.[3–8] Corn stover, being a grass species, has the three types of lignin components present (guaiacyl and syringyl lignin, and *p*-hydroxyphenyl).[7] Guaiacyl and syringyl peaks are typically easier to characterize and have s significant absorbance peaks that enable the clear conclusions derived from the FT-IR spectra. Kraft lignin is extracted form pinewood, a softwood lignin, which mainly consists of guaiacyl units.[6] The characteristic peaks for syringyl absorption at 1325 cm^{-1}, as well as the C–H out of plane in position 2 and 6 (syringyl units) at 825 cm^{-1}, are not present in the Kraft lignin samples. The peak at 875 cm^{-1} for C–H out-of-plane vibrations in position 2, 5, and 6

of the guaiacyl units is only observed in the Kraft lignin samples and the peak unique to guaiacyl due to the C–O stretching of the guaiacyl unit, found at 1250 cm^{-1}, is much higher in Kraft lignin than that of cornstover lignin due to the higher ratio of guaiacyl to syringyl units in softwood lignin.

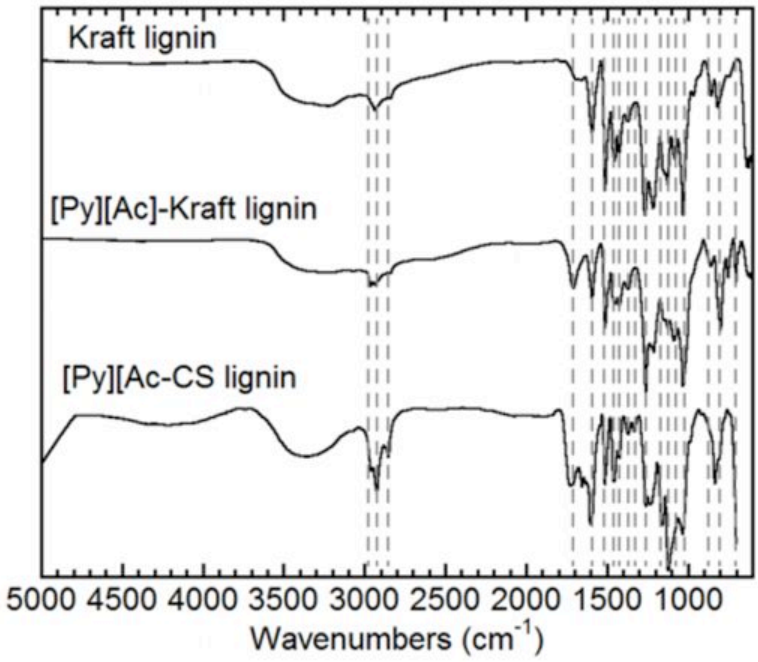

Figure 6. 3. FT-IR spectra for Kraft lignin recovered from PIL dissolution and the lignin extracted from CS using the [Pyrr][Ac] PIL.

By comparing the two Kraft lignin samples, the effect of the PIL dissolution can be observed. [Py][Ac] is a PIL that arises from the aromatic base pyridine which has a strong peak at 1600 cm^{-1} for aromatic skeleton vibrations, which gives rise to the increase in the intensity of the peak at 1600 cm^{-1} in the [Py][Ac]-treated samples (Figure 6. 4). This confirms the conclusions from the elemental analysis as small amounts of the PIL remain with the lignin samples after recovery by distillation. The maximum PIL recovery (from Chapter 3) was 98% observed with the use of [Py][Ac] PIL. There is also a similar increase in the peak observed for the anion, which should have a characteristic peak for the C=O stretching of the carbonyl groups at ~1700 cm^{-1} (Figure 6. 3–6. 4). This effect is greater for the anion and indicates that the anions, accompanied by the cations, are interacting directly with the lignin.

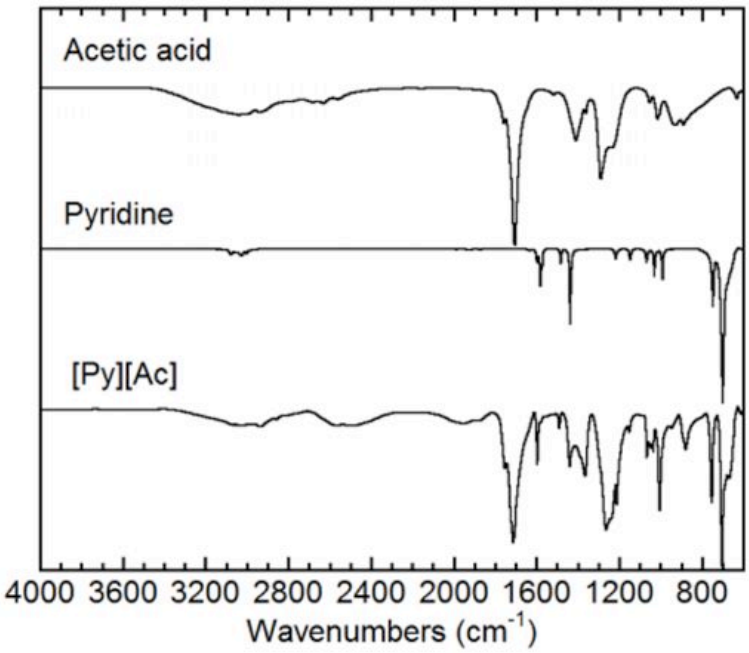

Figure 6. 4. FT-IR spectra for the [Py][Ac] PIL and the reagents used to synthesize it (pyridine and acetic acid).

Table 6. 3. Absorption peak assignment in FT-IR spectra of Kraft lignin recovered from PIL dissolution and the lignin extracted from CS using the [Py][Ac] PIL.[3–8]

Approximate band (cm^{-1})	Assignment
3350-3400	O–H stretching in hydroxyl groups
2975, 2925	C–H stretching in methyl and methylene groups, C–H stretching aromatic methoxyl groups
2850	$–CH_2–$ symmetry stretching in methyl and methylene groups
1700-1725	C=O stretching in unconjugated ketone, carbonyl, and ester groups
1650[a]	C=O stretching in conjugated ketone p-subst. Aryl ketones
1600[b]	Aromatic skeleton vibrations plus C=O stretching; S > G
1500-1525	Stretching of aromatic skeleton; G > S aromatic skeletal vibrations
1450	C–H deformations (asymmetry in methyl group – $CH_3–$ and $–CH_2–$) $O–CH_3$ in-plane deformations.
1375	Aliphatic C–H stretching in methyl and phenol OH (C–O of syringyl ring)
1325[a]	S unit plus G unit condensed (G unit bound via position 5)
1250	C–O stretching of guaiacyl unit
1225	C–C plus C–O plus C=O stretching
1125[a]	Typical of S unit; also secondary alcohol and C=O stretch
1050-1025[c]	C–O of primary alcohol, C–O–C ether stretch, guaiacyl C–H
875[c]	C–H out of-plane vibrations in position 2, 5 and 6 of the guaiacyl units
825[a]	C–H out of plane in position 2 and 6 (syringyl units)

Peaks highlighted are significant to [a] CS-lignin, [b] [Py][Ac]-treated lignins, [c] Kraft lignin

6. 5. Energy Minimization

The components of lignin are connected with several linkages, such as β-O-4, 5-5, β-5, 4-O-5, β-1, dibenzodioxocin, and β-β linkages (Figure 1. 5). The β-O-4 linkage is dominant, consisting of more than 50% of the linkage between the monolignol structures of lignin.[9] Therefore, 1-(4-methoxyphenyl)-2-methoxyethanol (LigM) (β-O-4 linkage) is chosen as a model of lignin to investigate the interactions between lignin and the PIL ions at the molecular level.[9] Energy minimization calculations were carried out with the LigM structure and the LigM-LigM dimer to identify the corresponding interactions found in the lignin monomers, which were then compared to that of the PIL-LigM structures (Figure 6. 5–6. 7).

The resulting structures show intra and inter molecular H-bonding between the terminal –OH groups in the LigM molecules (Figure 6. 5). The LigM-LigM 2 structure with H-bonding had the lowest energy state. The simulations also show that in this configuration, LigM molecules are able to stack for π−π interactions between the benzene rings, although, asymmetrically. For the [Py][Ac] PIL, the aromatic cation is also able to have π−π interactions with the benzene rings of LigM. This orientation also depicts the PIL ions hydrogen bonding, as the N from the amine cation interacts with the O from the anion−an orientation that the PIL ions do not have without the LigM structure (Figure 6. 6) The pyridine base is also able to have π−π interactions with the benzene rings of LigM explaining the high Kraft lignin solubility observed in this reagent. (Figure 6. 6)

The pyrrolidine base, of the other hand, interacts with the –OH groups in the LigM molecules and has no interactions with the benzene rings. This reagent has a low Kraft lignin

solubility indicating that the π–π interactions between aromatic groups are important for lignin dissolution in the AA PILs. The PILs of interest, however, are the [Pyrr][Ac] and [Eth][Ac] PILs which have been shown to extract large amounts of lignin from biomass. This has been attributed to the high ionicity of the PILs and the H-bonding network established in these PILs. The simulations, however, do not provide much information about the interactions between these PIL ions and the LigM molecule (Figure 6. 7). The minimal energy state is the same for the ions and molecules when they are apart. The only difference observed is with the [Eth][Ac] PIL, which takes on a different orientation than that which has been shown to be dominant in the [Et][Ac] PIL. This indicates that the terminal –OH groups in the [Eth][Ac] PIL is interacting with the LigM molecule–although this is not shown. More extensive simulations with multiple ions for the PILs and a three-dimensional lignin model will be beneficial for delineating the mechanism behind lignin dissolution in these PILs.[9–10]

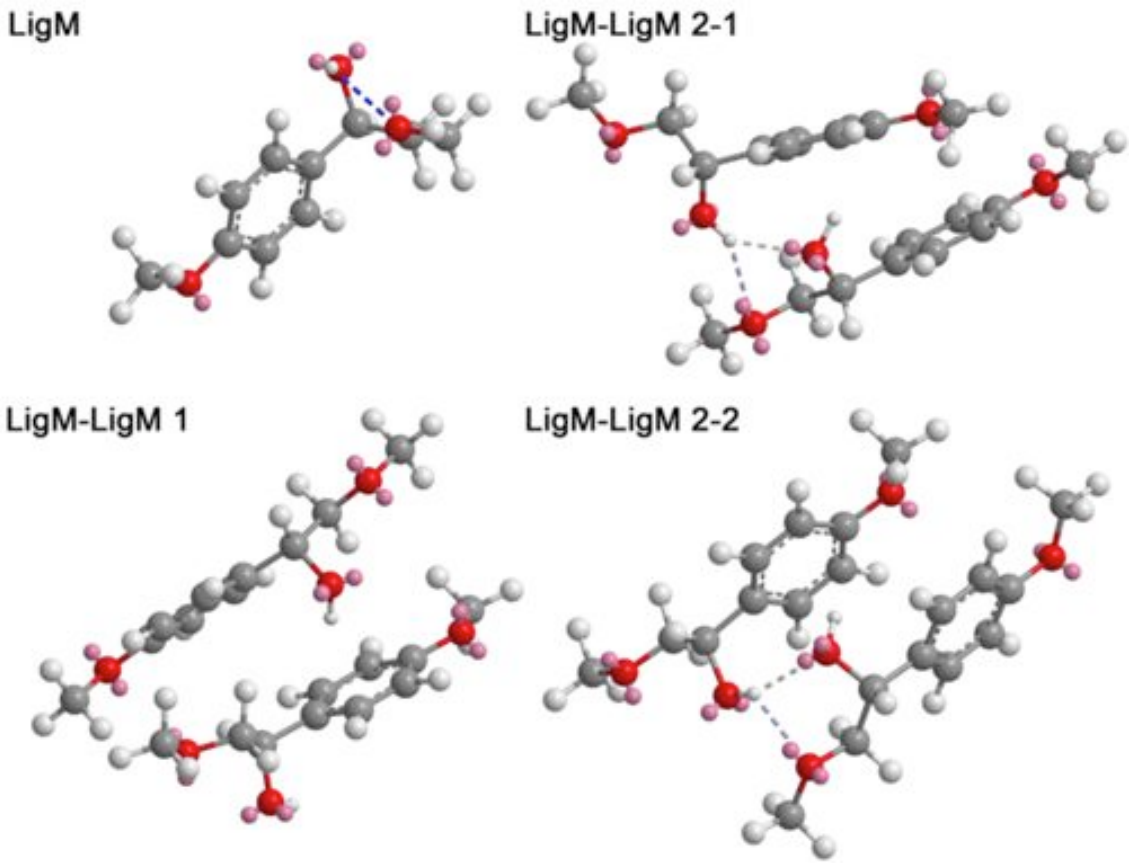

Figure 6. 5. Energy minimization of the lignin model compound (LigM), LigM-LigM.

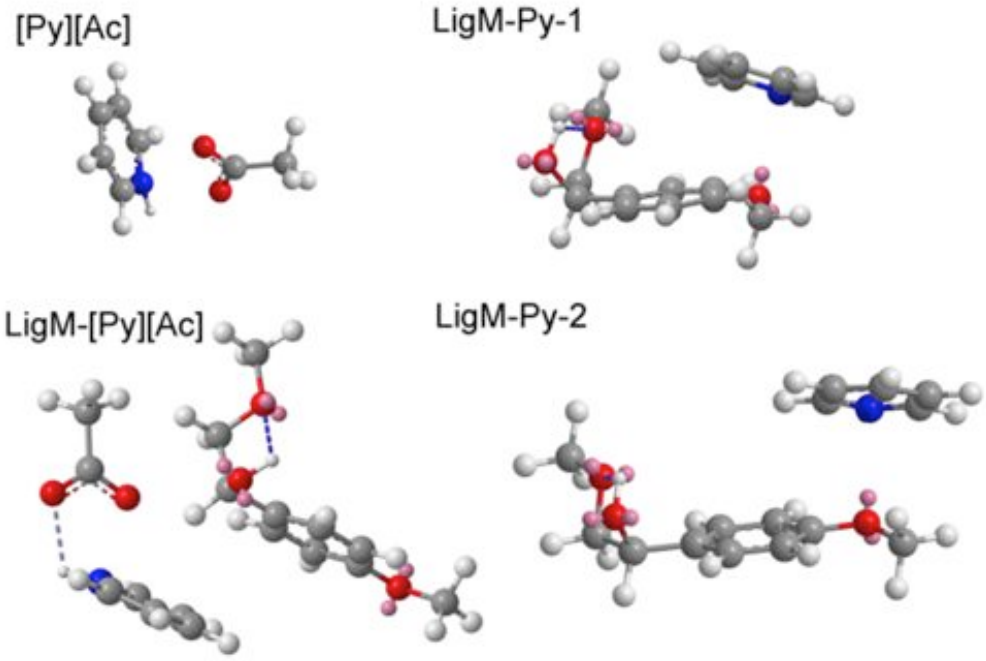

Figure 6. 6. Energy minimization for LigM-PIL for the [Py][Ac] PIL, LigM-[Py][Ac], and LigM-Py.

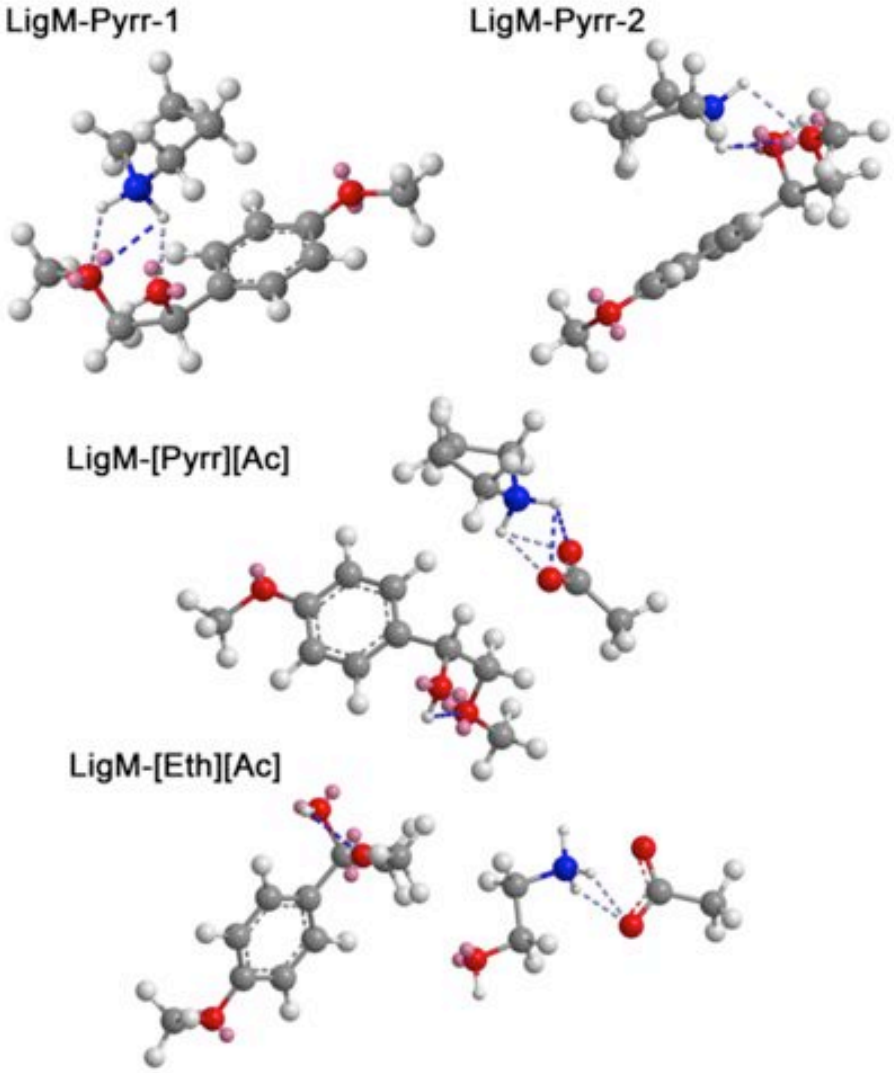

Figure 6. 7. Energy minimization for LigM-PIL for the [Pyrr][Ac] and [Eth][Ac] PILs and LigM-Pyrr.

6. 6. Effect of the Solvent Type on Lignin Regeneration

Following the lignin extraction step, the lignin solids are typically washed/precipitated in water and separated from the solution. The type of solvent used to precipitate the solids out of solution typically governs to some extent the resulting solid particles' size and morphology which could be important for lignin applications. The solvent used has to be insoluble in lignin, but most molecular solvents are only able to dissolve small amounts of Kraft lignin indicating their suitability for recovering lignin.

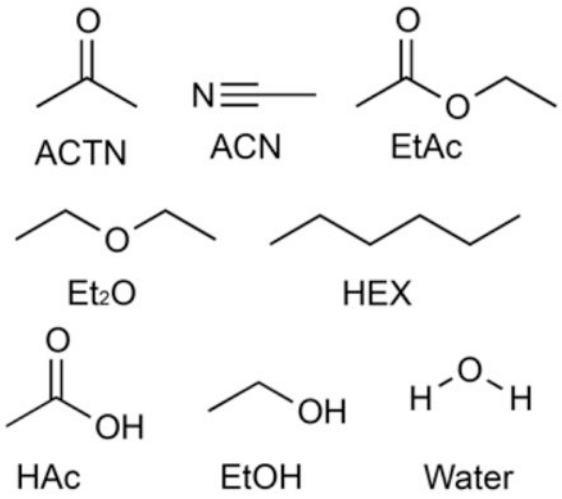

Figure 6. 8. Solvents used for lignin dissolution and regeneration study.

The solubility of lignin in ACTN, ACN, EtAc, Et_2O, HEX, HAc, EtOH and water (Figure 6. 8) was determined gravimetrically using the procedure previously described. The solubility was also confirmed using UV/Vis analysis by re-dissolving the recovered lignin residue in 0.1 M NaOH and using a Kraft lignin calibration curve to determine the amount of lignin present (Figure 6. 9). The calculated solubility is reproducible with an error of less than 5% and closely matches the solubility expected by observing color changes in the solvent used (Figures 6. 9). Polar protic solvents dissolve the highest amount of lignin, however, this amount is relatively small when compared to that of the PILs. The solubility for water, for example, is ~18 g/L which is about 0.018% w/w (using the units in previous chapters, $\rho_{water} \sim 1$ g ml^{-1}).

The solids recovered from the solvent-lignin dissolution experiments all have different physical appearances, as the lignin assembles into clusters while being recovered (Figure 6. 10). The lignin, however, remain chemically unchanged. Figure 6. 11 shows the FT-IR analysis of the Kraft lignin solid recovered after solvent dissolution. The absorption spectra acquired are largely identical for all the solvents used. However, there is a peak around 1700 cm^{-1} that is intensified in the acetone-lignin and acetic acid-lignin samples. This peak is due to the C=O carbonyl functional group found in both solvents mentioned. Residual amounts of the solvent might be remaining within the lignin, which give rise to this peak observed. The Kraft lignin recovered after water dissolution has relatively fine particles, which might be ideal for the application of recovering homogenous lignin solids (6. 10). This could positively affect the polydispersity of the lignin as well. Figure 6. 12 shows a comparison between the lignin recovered from EF-CS using the [Pyrr][Ac] PIL and the

resulting lignin solids after a water wash. The result, as expected, indicates that more uniform lignin solids are being recovered, but they are greater in size than for the water-Kraft lignin samples.

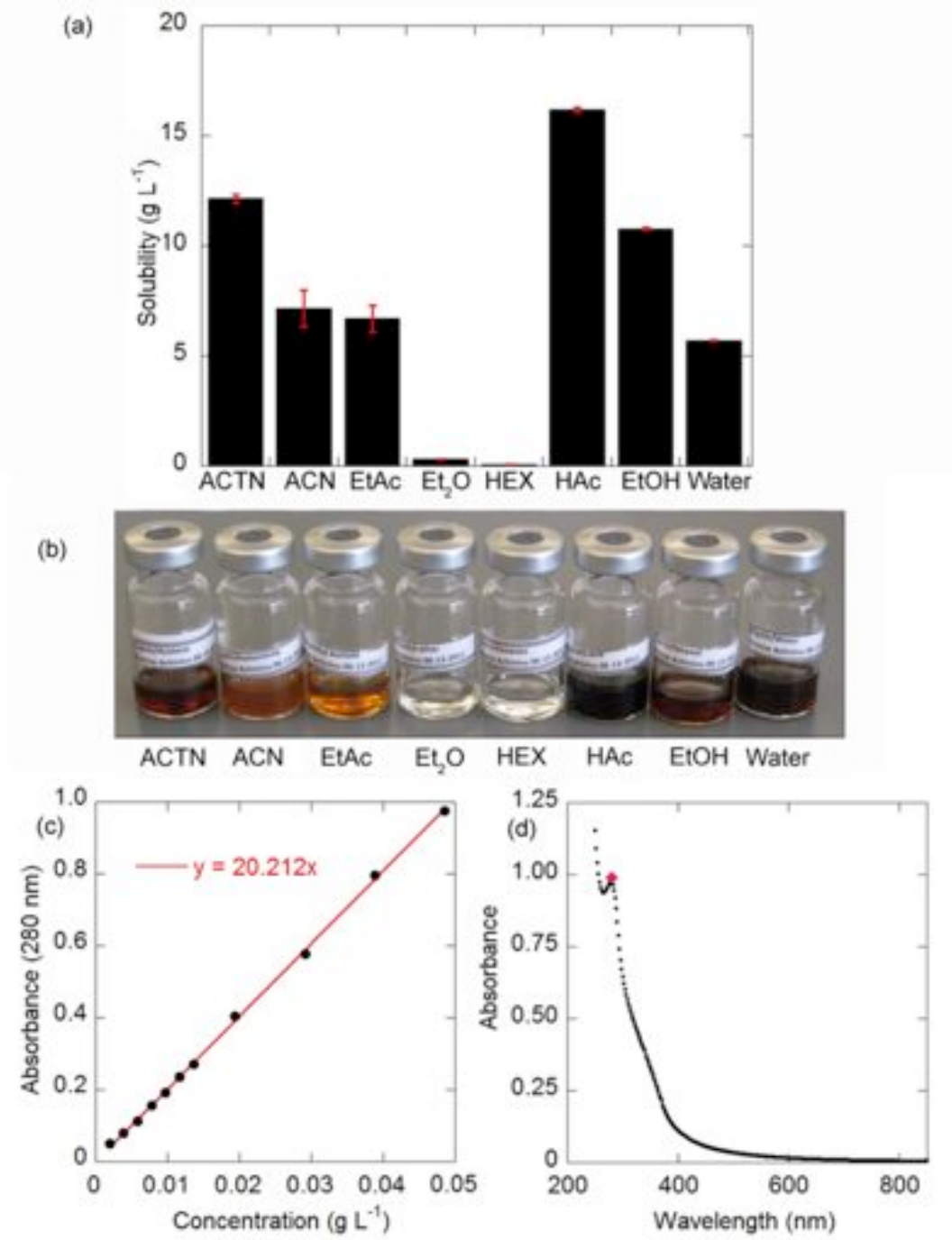

Figure 6. 9. (a) The solubility of lignin in some common solvents after (b) stirring for 24 h at 90 °C, recovering the supernatant, solvent evaporation, and re-dissolution in 0.1M NaOH as determined by: (c) the Kraft lignin calibration curve at (d) the wavelength of maximum absorbance.

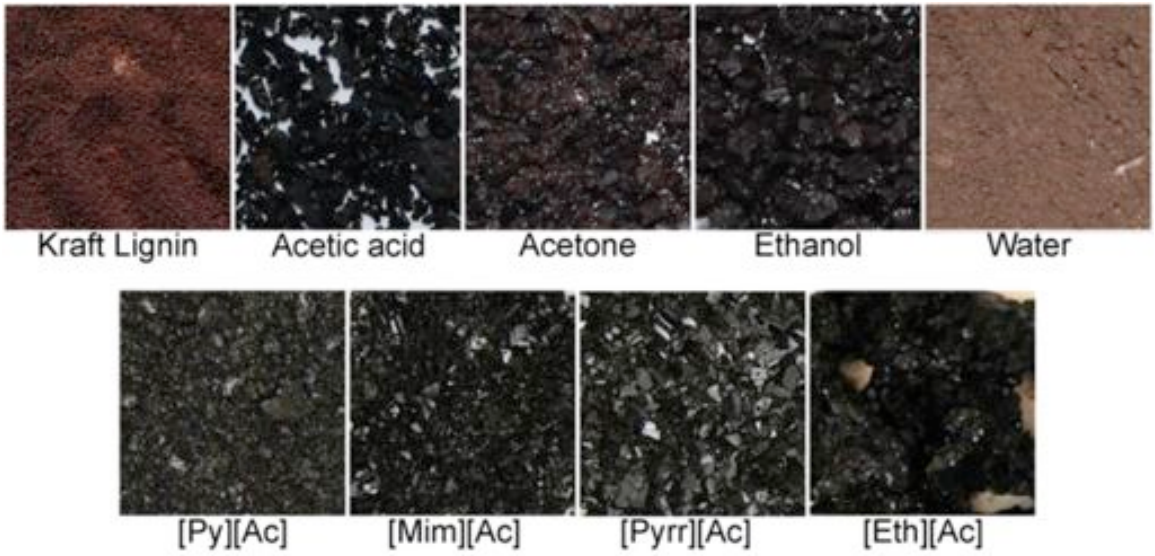

Figure 6. 10. Images (10X) of lignin recovered from solvent and PIL dissolution after heating at 90 °C and 24 h.

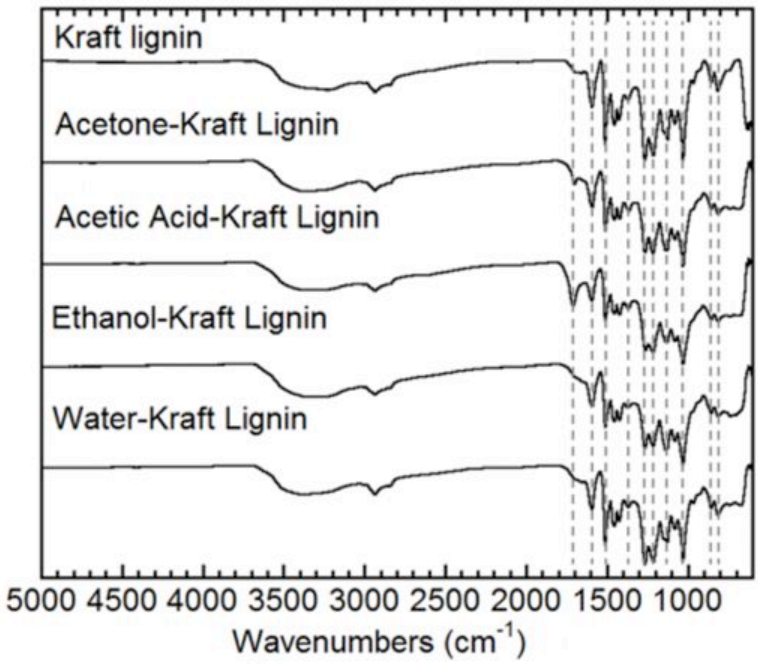

Figure 6. 11. FTIR spectra of lignin regenerated from solvent dissolution after heating at 90 °C and 24 h.

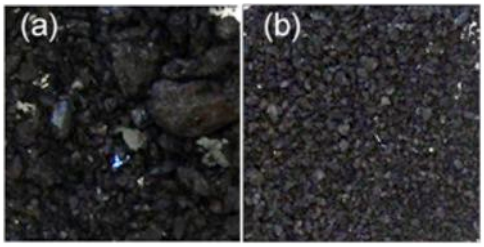

Figure 6. 12. Images (10X) of lignin showing the lignin extracted from CS using the [Pyrr][Ac] PILs: (a) the solids recovered after the PIL removal, and (b) solids after passing the solids form (a) through a water wash step.

6. 7. Conclusions

The information in this chapter provides deeper insight into the characteristics of the lignin after its interacting with the PIL ions. FT-IR analysis confirms the peak observed for lignin from cornstover and gives an understanding into the mechanism for lignin dissolution using PILs. The results show that the cation interacts directly with the lignin molecules, while also interacting with the anion. Both interactions, working together, distinguish the ionic solvent (PIL) that is able to dissolve large amounts of lignin. The lignin extracted using PILs is smaller in size indicating that the lignin is fragmented during the dissolution process. The [Pyrr][Ac] PIL, which has a greater ionicity, favors the fragmentation of lignin and results in more homogenous particles. Finally, solvents can be used to wash lignin after dissolution, which controls the morphology of the resulting fibers.

References:

1. Wen, J.-L.; Yuan, T.-Q.; Sun, S.-L.; Xu F.; Sun, R.-C. *Green Chem.* **2014**, *16*, 181–190.
2. Sathitsuksanoh, N.; Holtman, K. M.; Yelle, D. J.; Morgan, T.; Stavila, V.; Pelton, J.; Blanch, H.; Simmons, B. A.; George, A. *Green Chem.* **2014**, *16*, 1236–1247.
3. Yan, T.; Xu, Y.; Yu, C. *Journal of Applied Polymer Science*, **2009**, *114*, 1896–1901.
4. Mansouri, N.-E. E.; Yuan, Q.; Huang, F. *BioResources* **2011**, *6*, 2647–2662.
5. Fox, S. C.; McDonald, A. G. *BioResources* **2010**, *5*, 990–1009.
6. Kline, L. M.; Hayes, D. G.; Womac, A. R.; Labbé, N. *BioResources* **2010**, *5*, 1366–1383.
7. Kim, T. H.; Kim, J. S.; Sunwoo, C.; Lee, Y. Y. *Bioresource Technology* **2003**, *90*, 39–47.
8. Yang, X.; Zeng, Y.; Zhang, X. *BioResources* **2010**, *5*, 488–498.
9. Ji, W.; Ding, Z.; Liu, J.; Song, Q.; Xia, X.; Gao, H.; Wang, H.; Gu, W. *Energy Fuels* **2012**, *26*, 6393−6403.
10. Janesko, B. G. *Phys. Chem. Chem. Phys.* **2011**, *13*, 11393–11401.

CONCLUSIONS

The results reported demonstrate that PILs are able to extract large amounts of lignin from biomass. The dissolution, to some extent, of one or more of the polysaccharides, however, is necessary to enable PIL penetration of the biomass fibers and full access to the lignin. Partial dissolution of xylan, the major hemicellulose component in CS, disrupts the fibers enough to attain a very high amount of lignin extraction, which may be directly proportional to the salt ionicity. Systematic variations to the structure of ions confirms the trend in ionicity within the PILs, and reveals a secondary interactions between the PIL ions (hydrogen bonding) that is beneficial for creating PILs with high ionicity and lignin extraction efficiency.

PILs from cyclic amine ([Pyrr][Ac]) and PILs with hydroxyl groups ([Eth][Ac]) are two main PIL types that are able to extract large amounts of lignin from biomass. The cyclic ring fixes the amine base in an orientation that is favourable for interacting with the anion, thereby increasing the ionicity. The addition of hydroxyl groups to the backbone of the PIL ions is beneficial for modifying the PIL's properties. However, it is necessary to carefully select the position of the –OH substituent in order to prevent an increase in viscosity and to maximize the lignin extraction efficiency of he PIL.

Pure PILs can be recovered at yields approaching 100% using relatively mild distillation conditions (with a partial vacuum). For full PIL recovery, however, a careful selection of the anions/cations used to synthesize the PIL is necessary to avoid PILs that are susceptible to the formation of amide by-products due to thermal degradation. Increasing the

number of substituents on the amine group minimizes this reaction. This slight increase in steric hindrance on the cation could reduce the reactivity of the reagents and select for the lower energy state –the PIL.

The functionality/composition of the lignin extracted by the PILs appears to be largely retained. Future work recommended for this project will be to focus on identifying applications for the PIL–treated biomass (cellulose-rich pulp) and the extracted lignin. This will aid in further tailoring the PIL for specific properties, and this will direct the necessary characterisations for the biomaterials. Therefore, the use of potentially inexpensive PILs to selectively extract lignin from lignocellulosic biomass with high extraction efficiency and low waste generation is a quite promising means for the total utilization of lignocellulosic biomass—a necessary requirement for the implementation of a biofuel/biorefinery-based economy.

APPENDICES

APPENDIX A: PIL Synthesis

Figure A. 1. Apparatus utilized for the PIL Synthesis (Note: water bath is not included in picture).

APPENDIX B: Distillation Apparatus Used

Figure B. 1. Short path distillation apparatus Wilmad LG-6315

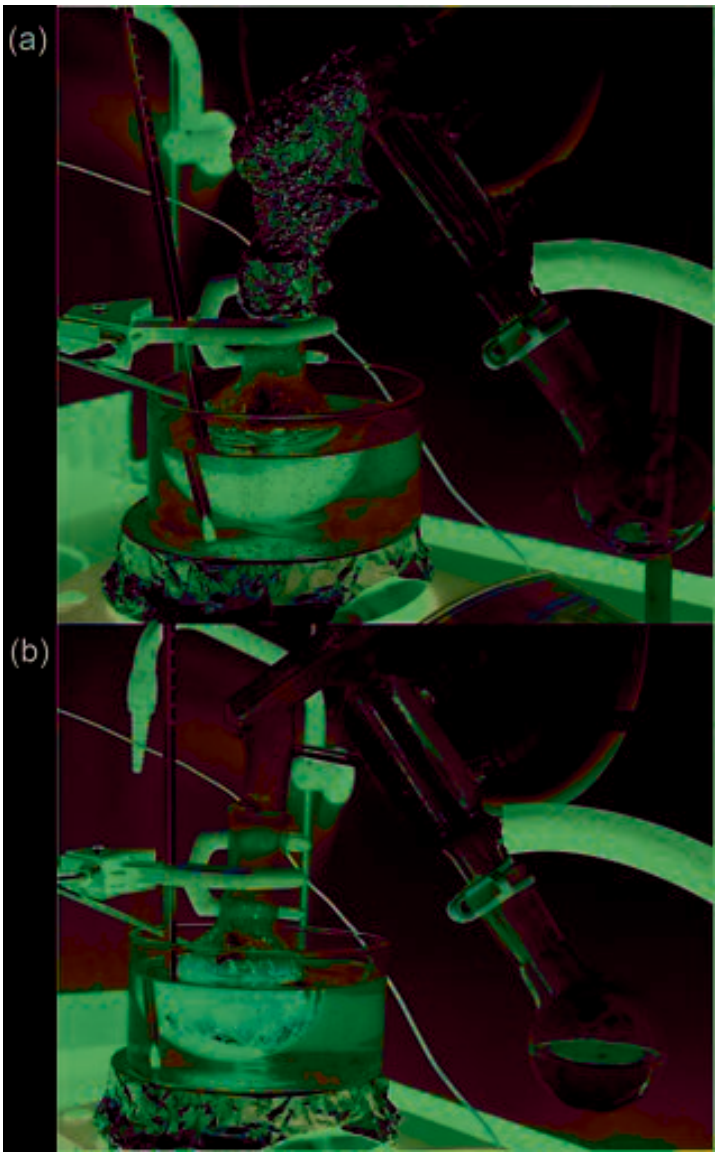

Figure B. 2. Distillation set up used to separate PILs from lignin showing: (a) initial set up and (b) after complete collection of distillate.

APPENDIX C: Supplementary Information-Chapter 3

C. 1. PIL Characterization

As previously noted, PILs are easily synthesized by the transfer of a proton from an acid to a base. The method to synthesize the pure PILs did not use water or other solvents as a reaction medium in order to minimize the PIL's water contamination and the heating required to remove the water/solvents after the PIL synthesis. The water content of the PILs did not exceed 0.50% w/w (Table C. 1). The purity of the PILs was also determined via NMR analysis (Figurs X-XX) The integrated areas for each PIL component were used to confirm the mole ratio of the acid (anion) to base (cation) (Table X). No side products were detected. Additional characterization of the PILs was also conducted to examine their thermal phase behavior (DSC) (Figure X). All of the PILs used in this study are liquid at room temperature. Peaks observed after 50 °C in the DSC heating traces are not melting peaks, but instead originate from thermal decomposition due to the low thermal stability of the PILs (see TGA data).

Table C. 1. Water content of PILs and acid-to-base ratio of the resulting PILs (as synthesized) determined from NMR analysis

PIL synthesized	water content (wt%, ppm)	mole ratio (acid:base)
[Py][Ac]	0.29, 2910	0.51:0.49
[Mim][Ac]	0.07, 7	0.50:0.50
[Pyrr][Ac]	0.32, 3156	0.50:0.50

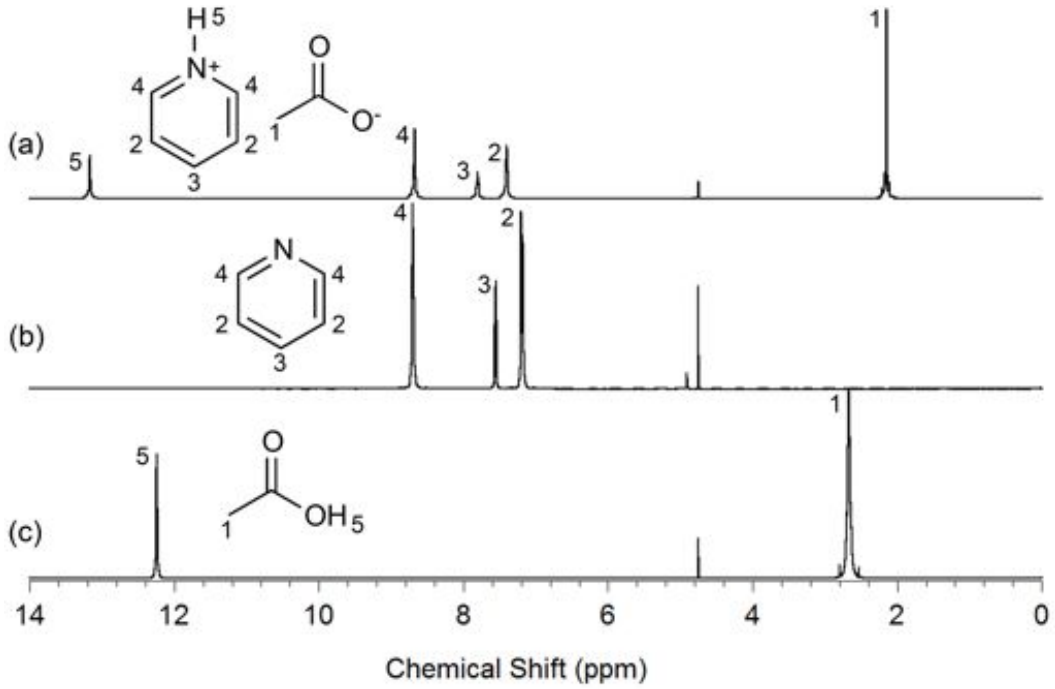

Figure C. 1. ^{1}H-NMR spectra (δ_{solv} = 4.75 ppm) of: (a) [Py][Ac], (b) pyridine (Py) and (c) acetic acid (HAc).

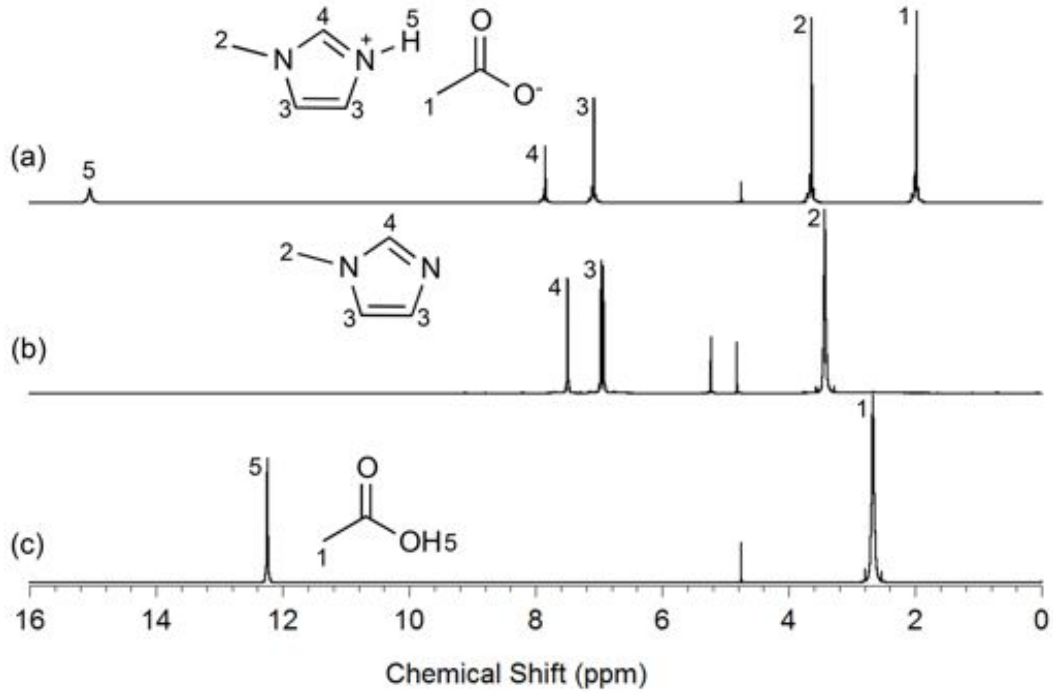

Figure C. 2. ^{1}H-NMR spectra (δ_{solv} = 4.75 ppm) of: (a) [Mim][Ac], (b) 1-methylimidazole (Mim) and (c) acetic acid (HAc).

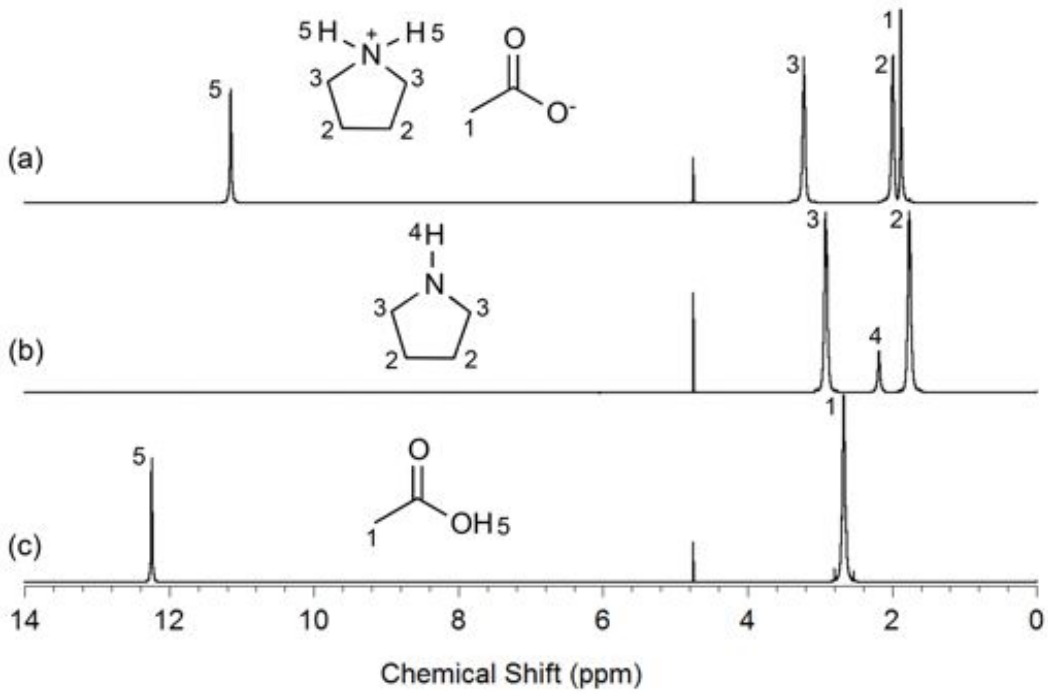

Figure C. 3. ^{1}H-NMR spectra (δ_{solv} = 4.75 ppm) of: (a) [Pyrr][Ac], (b) pyrrolidine (Pyrr) and (c) acetic acid (HAc).

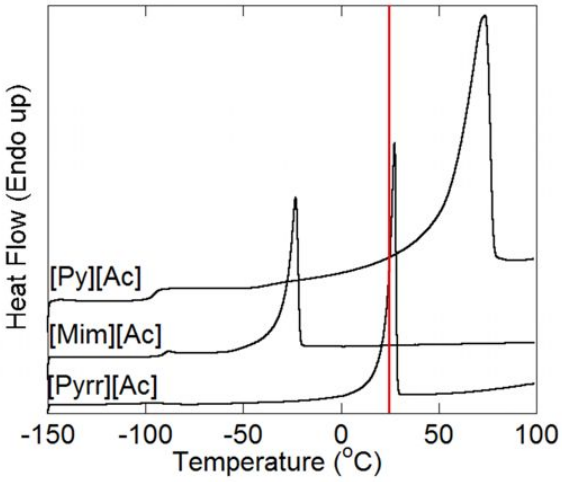

Figure C. 4. DSC heating traces of the PILs used for this study. The large peak for [Py][Ac] originates from the volatilization of the reagents rather than melting of the salt. The red line indicates ambient temperature.

C. 2 PIL Recyclability Tests-Kraft Lignin

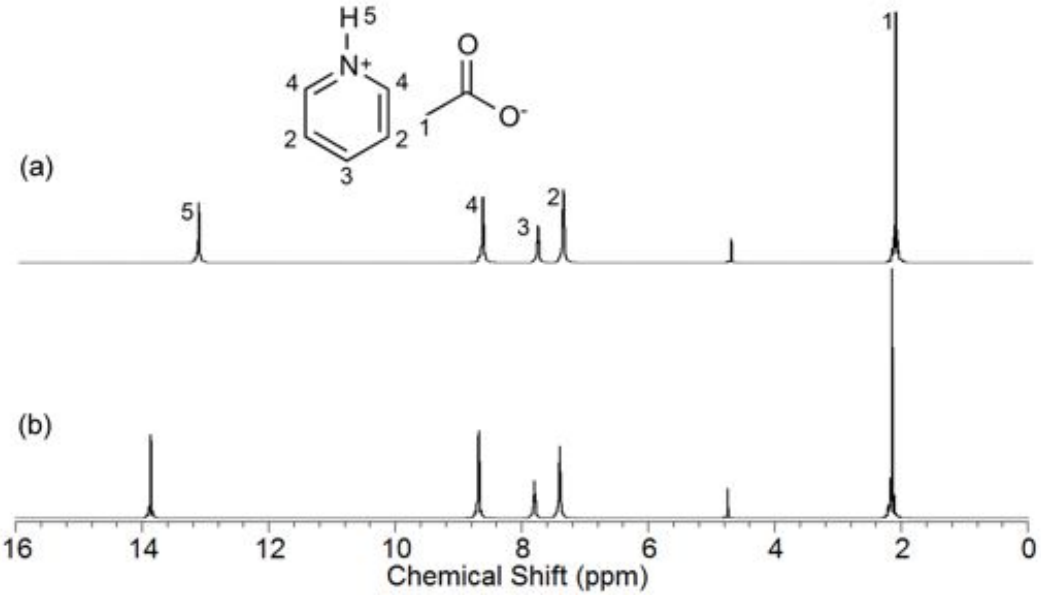

Figure C. 5. ^{1}H-NMR spectra (δ_{solv} = 4.75 ppm) of PIL ([Py][Ac]): (a) after synthesis and (b) after distillation from Kraft lignin/PIL solution.

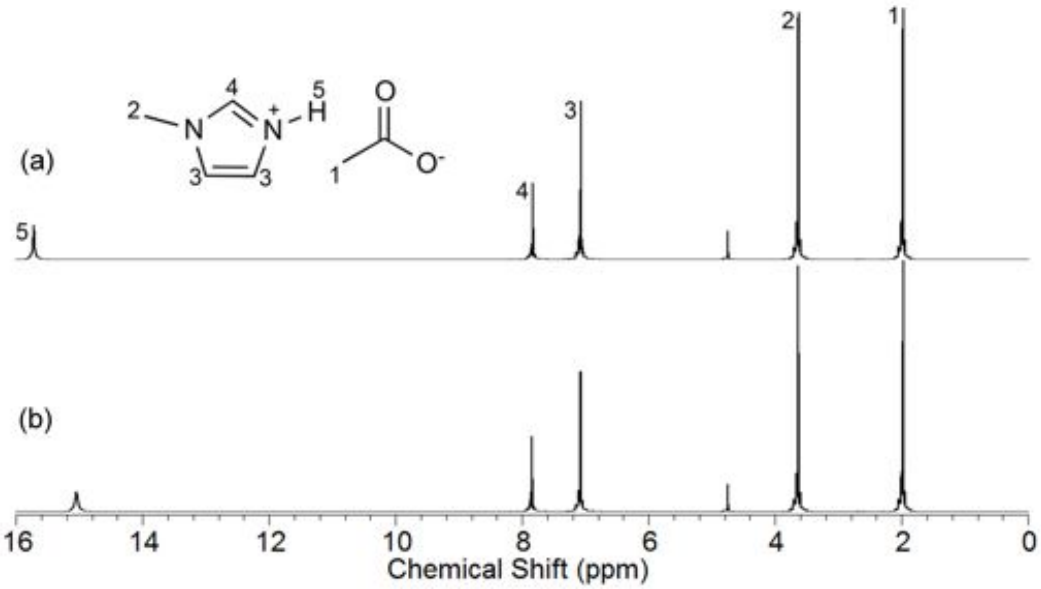

Figure C. 6. ^{1}H-NMR spectra (δ_{solv} = 4.75 ppm) of PIL ([Mim][Ac]): (a) after synthesis and (b) after distillation from Kraft lignin/PIL solution.

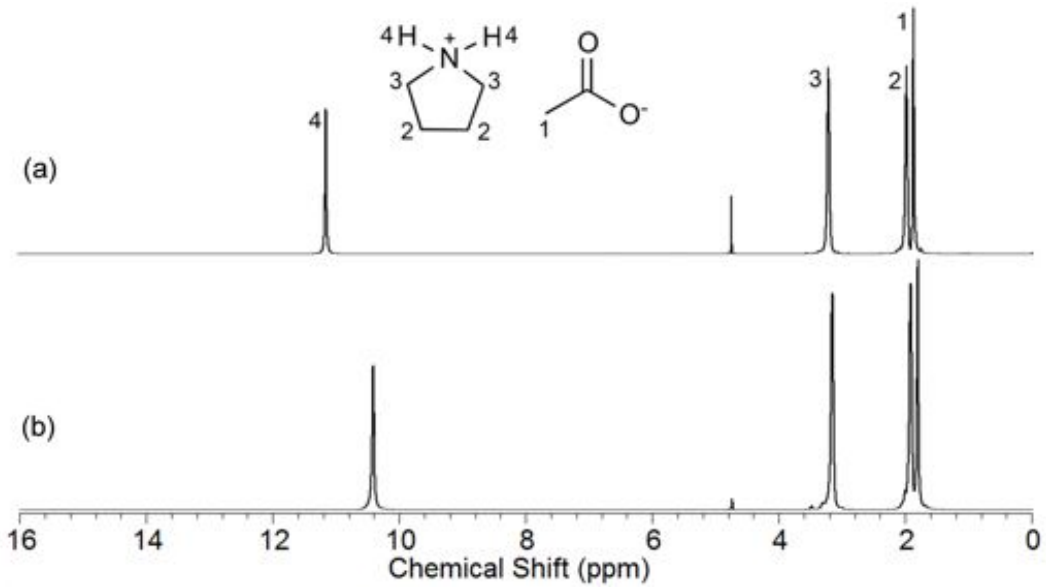

Figure C. 7. ^{1}H-NMR spectra (δ_{solv} = 4.75 ppm) of PIL ([Pyrr][Ac]): (a) after synthesis and (b) after distillation from Kraft lignin/PIL solution.

C.3. PIL Recyclability Tests-Cornstover Lignin

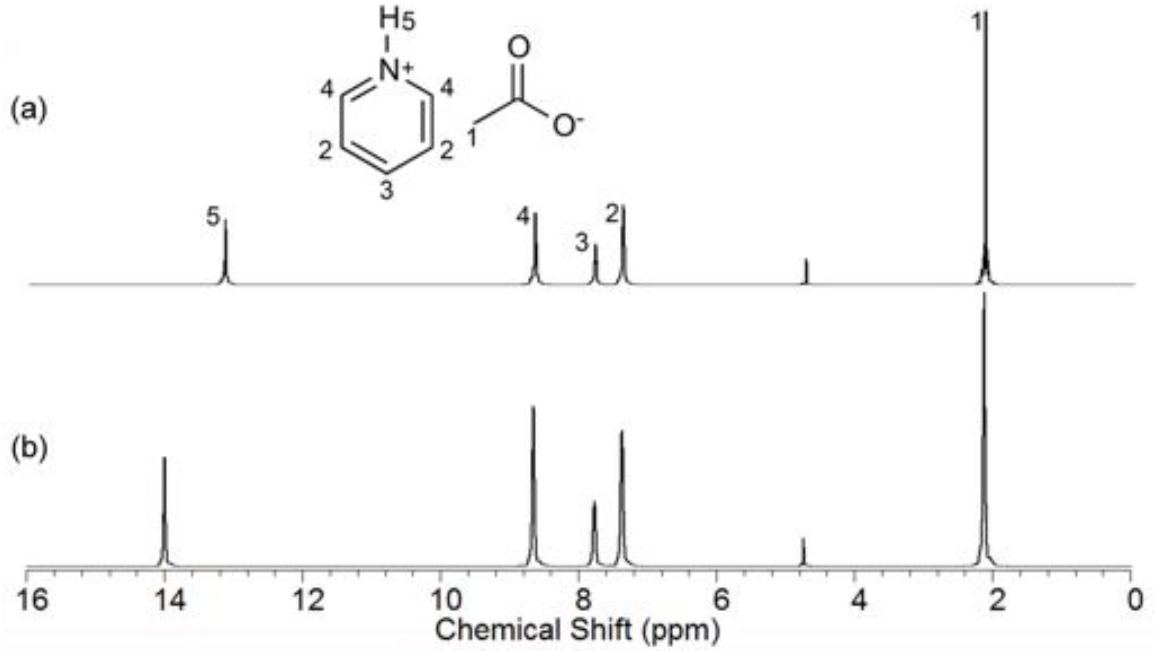

Figure C. 8. ^{1}H-NMR spectra (δ_{solv} = 4.75 ppm) of PIL ([Py][Ac]): (a) after synthesis and (b) after distillation from CS lignin/PIL solution (Liquor 1).

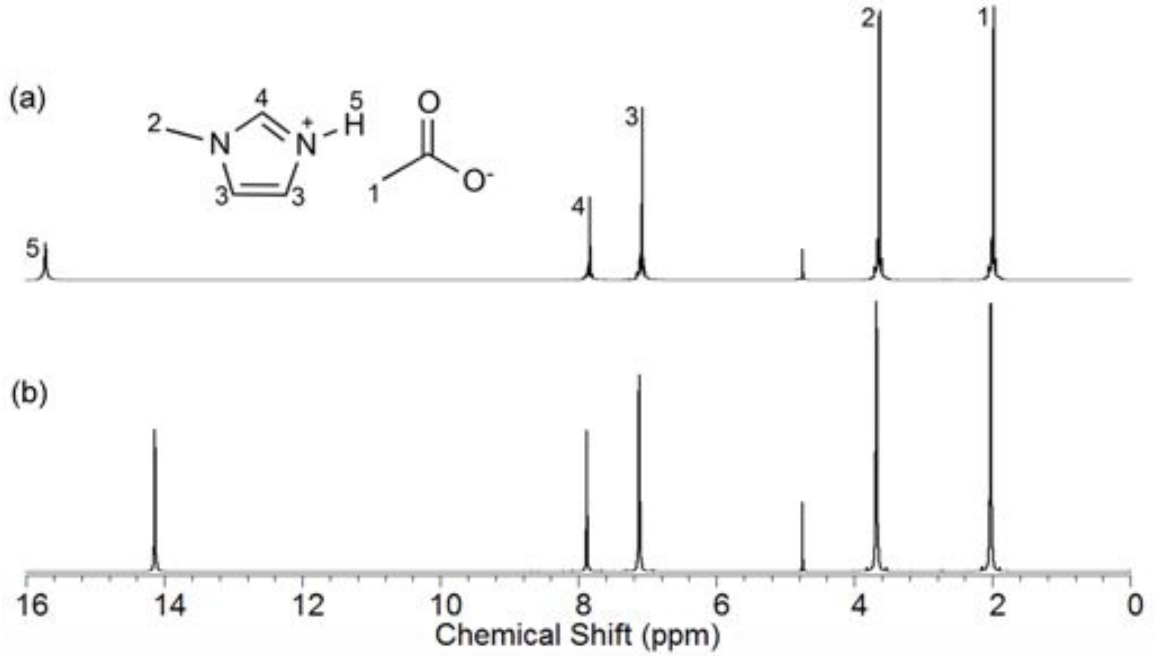

Figure C. 9. ^{1}H-NMR spectra (δ_{solv} = 4.75 ppm) of PIL ([Mim][Ac]): (a) after synthesis and (b) after distillation from CS lignin/PIL solution (Liquor 1).

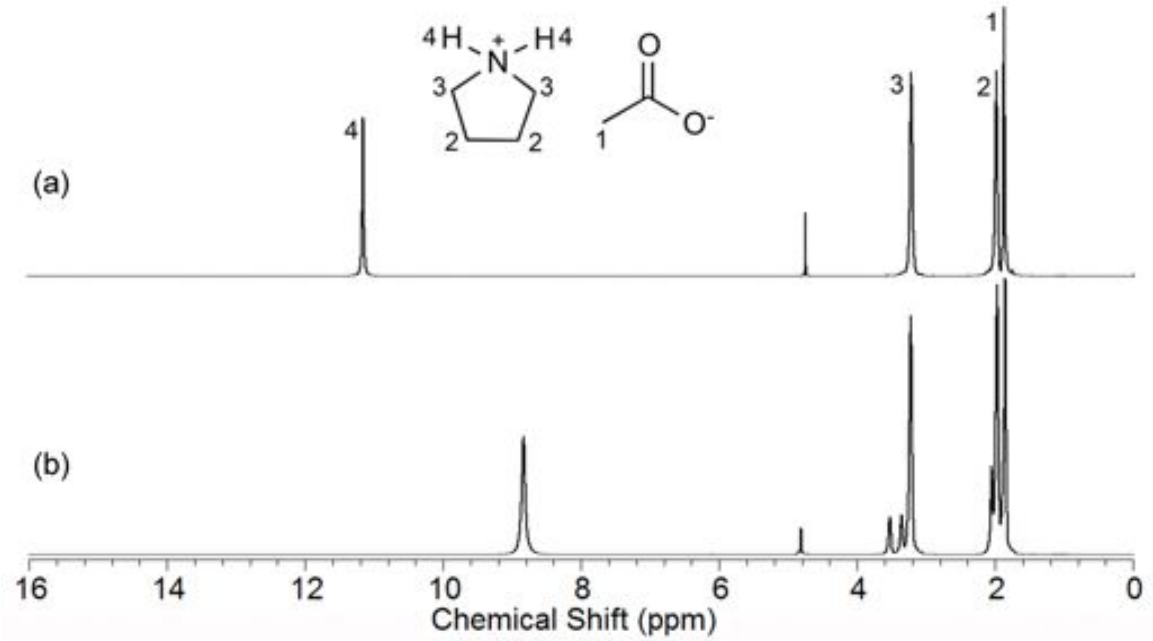

Figure C. 10. ^{1}H-NMR spectra (δ_{solv} = 4.75 ppm) of PIL ([Pyrr][Ac]): (a) after synthesis and (b) after distillation from CS lignin/PIL solution (Liquor 1).

APPENDIX D: Supplementary Information-Chapter 4

D. 1. PIL Characterization

As previously noted, the water content of the PILs typically did not exceed 0.50% w/w (Table D. X).

Table D. 1. Water content of PILs (as synthesized).

PIL synthesized	water content (wt%, ppm)	PIL synthesized	water content (wt%, ppm)
[Et][Ac]	–[a]	[Im][Ac]	–[a]
[Prop][Ac]	0.32, 3187	[mMim][Ac	0.15, 1450
[But][Ac]	0.19,1901	[Pyr][Ac]	0.21, 2132
[DiEt][Ac]	0. 28, 2343	[mPyr][Ac]	0.13, 1768
[DiProp][Ac]	0.91, 9098	[EtAmOH][Ac]	0.35, 3503
[DiBut][Ac]	0. 28, 2798	[Eth][Ac]	0.07, 698
[Pyrr][Ac]	0.32, 3156	[1A2P][Ac]	0.12, 1242
[Pip][Ac]	–[a]	[3A1P][Ac]	0.07, 719
[Hex][Ac]	2. 14, 21385	[MoxEt][Ac]	0.61, 6093
[mPyrr][Ac]	0.18, 1755	[Morph][Ac]	–[a]
[mPip][Ac]	2.17, 21731	[mMorph][Ac]	0.14, 1444
[Py][Ac]	0.29, 2910	[PyMe][Ac]	0.52, 5151
[Pyri][Ac]	0.16, 1572	[PipOH][Ac]	0.13, 1252
[Mim][Ac]	0.07, 7	[MorphOH][Ac]	0.06, 591

[a] Solid at ambient temperature

Additional characterization of the PILs was also conducted to examine their thermal phase behavior (DSC) (Figure X).

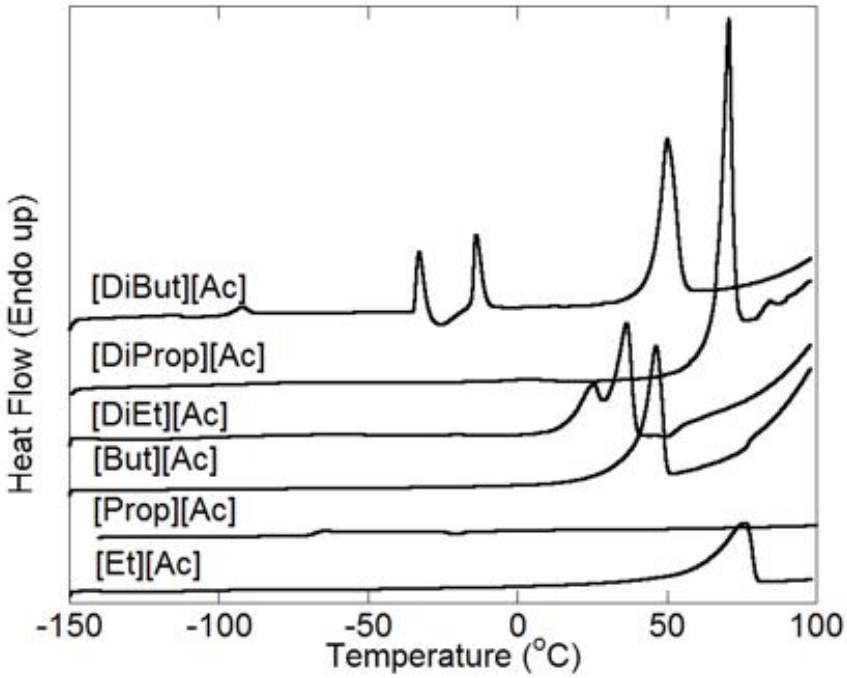

Figure D. 1. DSC heating traces of the NAA PILs used for this study.

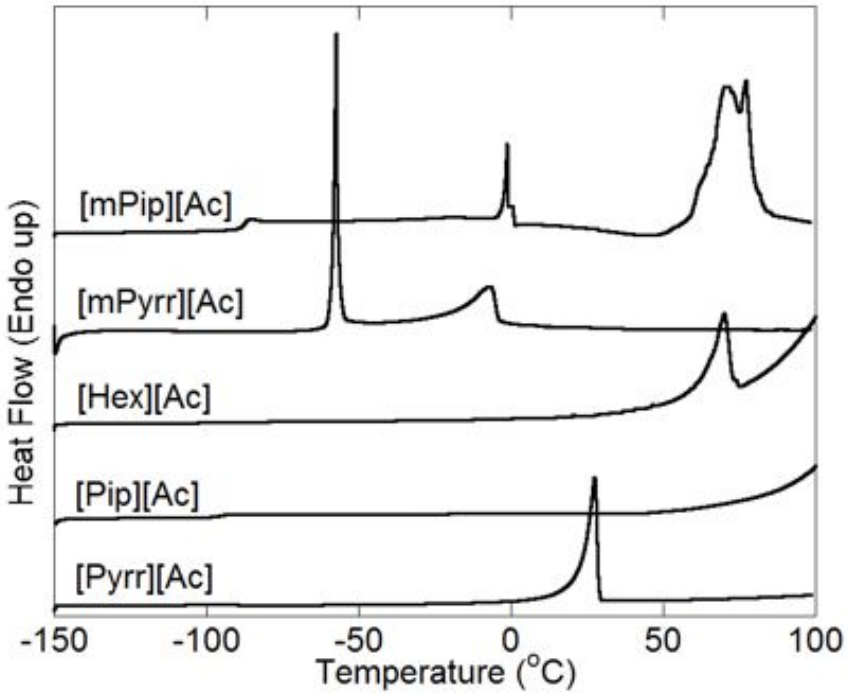

Figure D. 2. DSC heating traces of the CAA PILs used for this study.

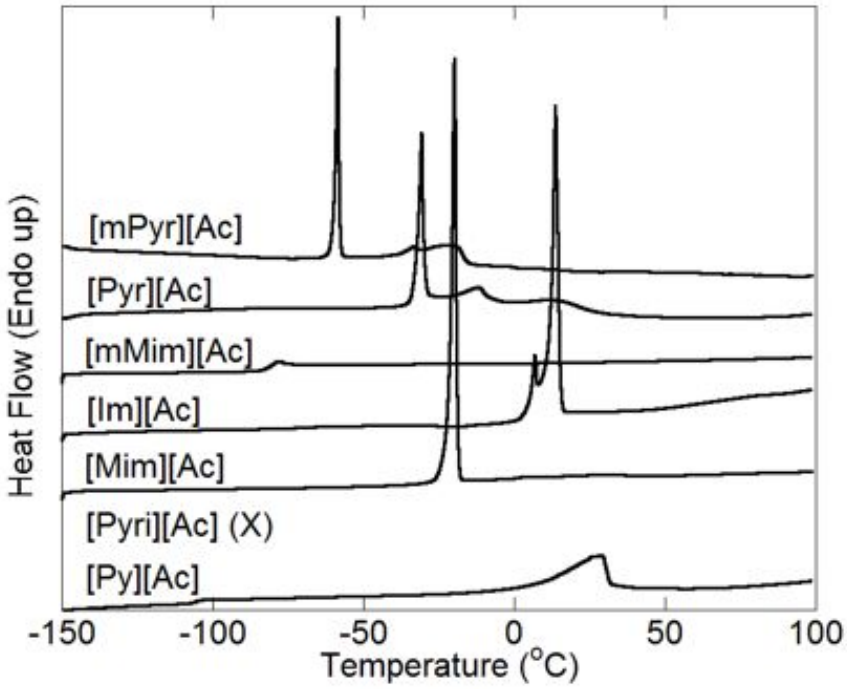

Figure D. 3. DSC heating traces of the AA PILs used for this study.

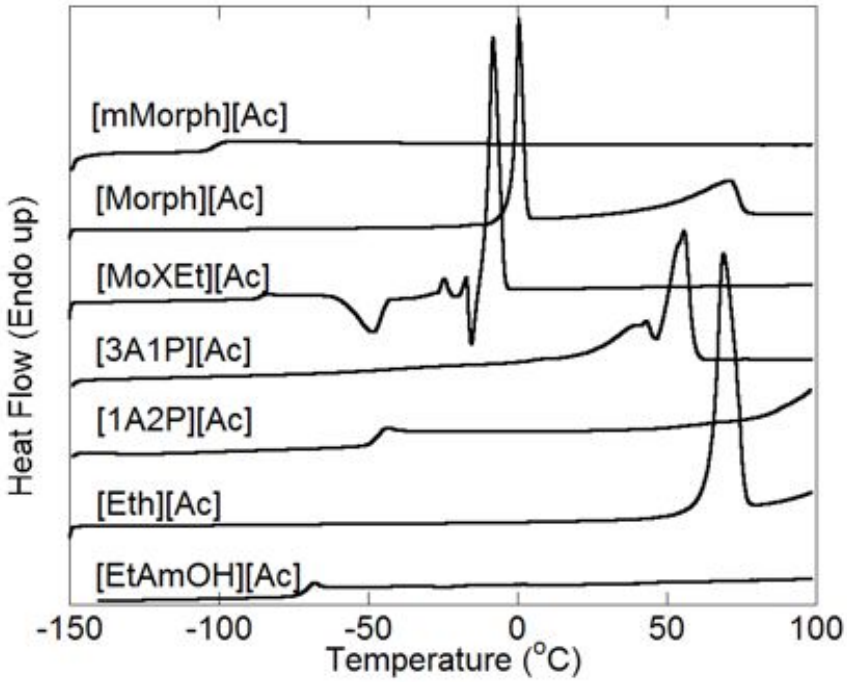

Figure D. 4. DSC heating traces of the OAA PILs used for this study.

D. 2 Biopolymer Solubility Tests

The following figures are images depicting the solubility of 5% w/w commercially available biomass components (Kraft lignin, microcrystalline cellulose and xylan) in the PILs and reagents tested. The top depicts the solubility after stirring for 30 min at room temperature (25 °C) and the bottom shows after stirring for 24 h at 90 °C. Sample sizes were typically 10 g, but smaller vials contain 7.5 g.

Figure D. 5. Solubility tests for biopolymers in the reagents for primary NAA PILs.

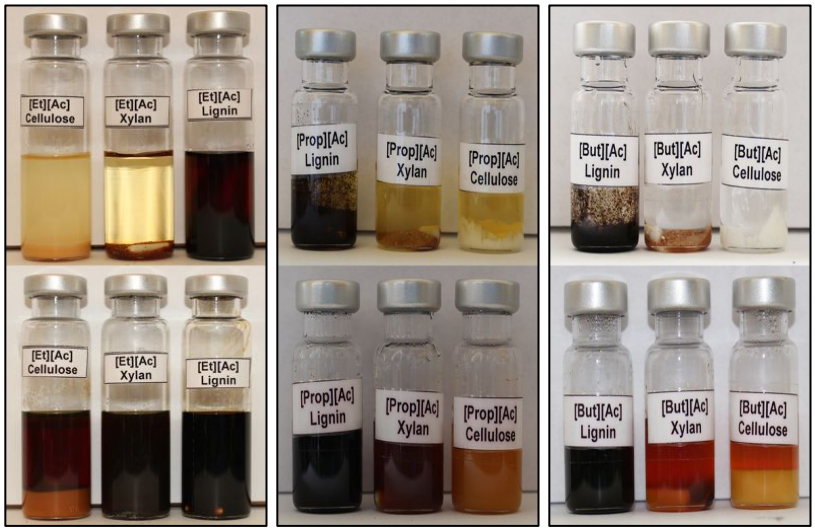

Figure D. 6. Solubility tests for biopolymers in primary NAA PILs.

Figure D. 7. Solubility tests for biopolymers in the reagents for secondary NAA PILs.

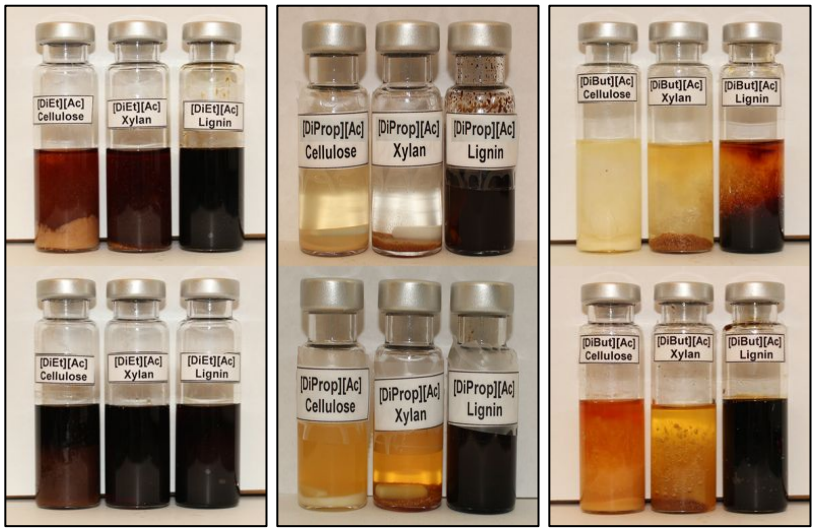

Figure D. 8. Solubility tests for biopolymers in secondary NAA PILs.

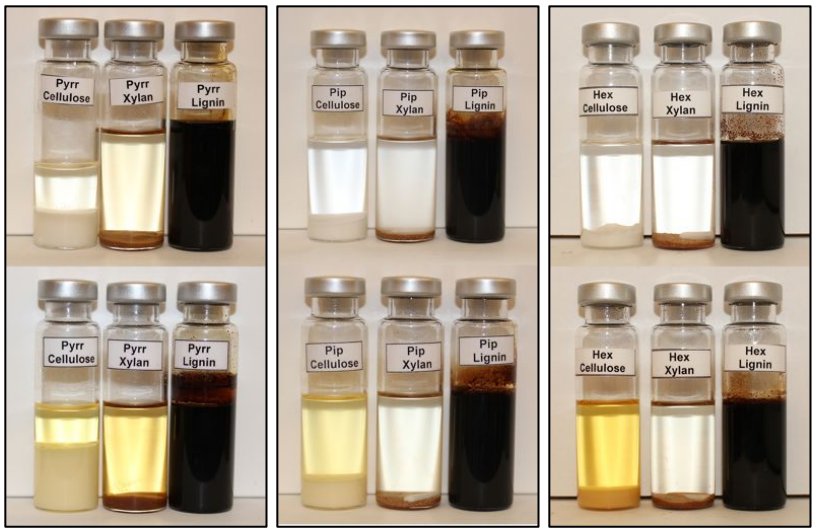

Figure D. 9. Solubility tests for biopolymers in the reagents for secondary CAA PILs.

Figure D. 10. Solubility tests for biopolymers in the reagents for tertiary CAA PILs.

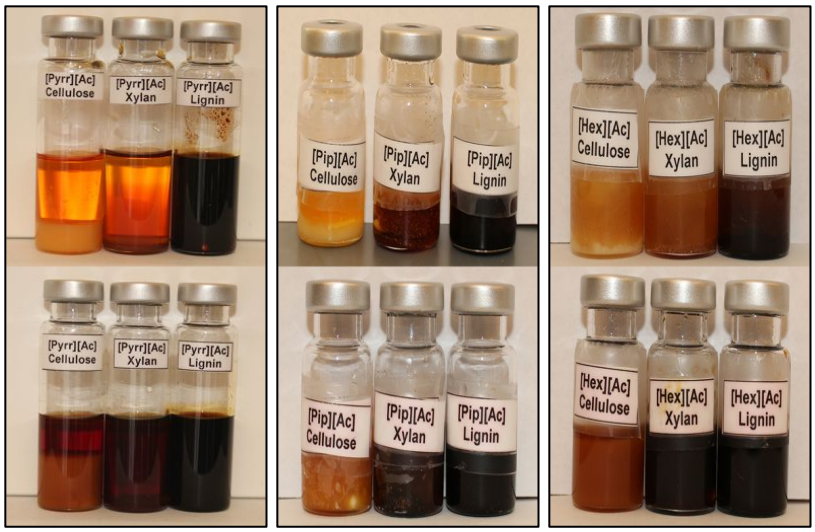

Figure D. 11. Solubility tests for biopolymers in secondary CAA PILs.

Figure D. 12. Solubility tests for biopolymers in tertiary CAA PILs.

Figure D. 13. Solubility tests for biopolymers in the reagents for the AA PILs.

Figure D. 14. Solubility tests for biopolymers in AA PILs.

Figure D. 15. Solubility tests for biopolymers in the reagents for the OAA PILs.

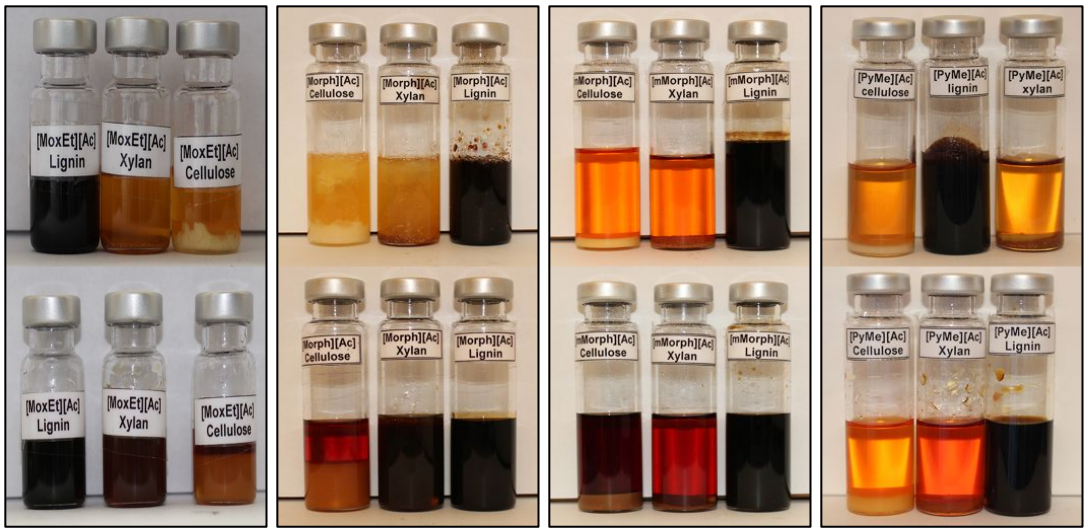

Figure D. 16. Solubility tests for biopolymers in the OAA PILs.

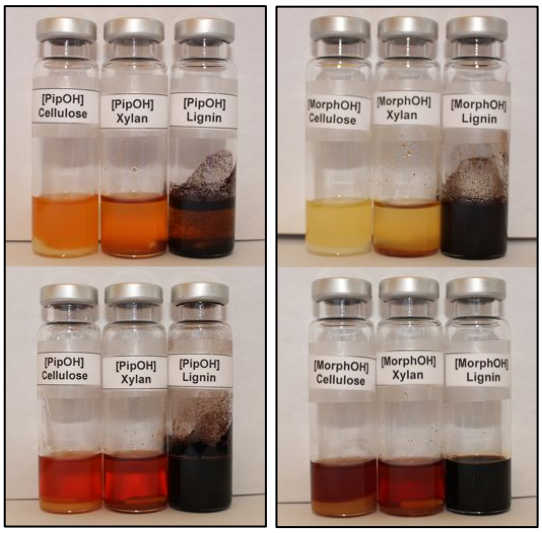

Figure D. 17. Solubility tests for biopolymers in the reagents for the hybrid PILs.

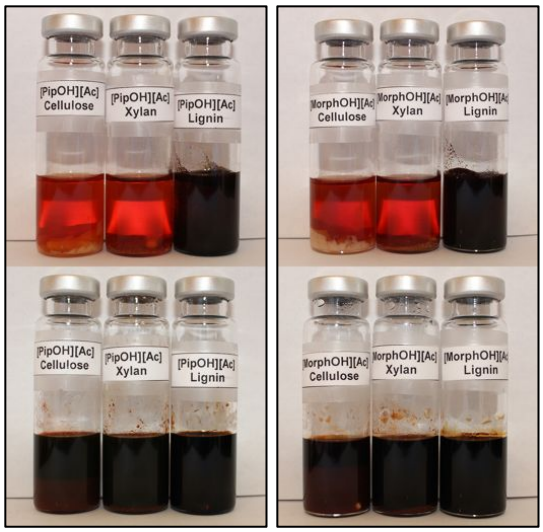

Figure D. 18. Solubility tests for biopolymers in hybrid PILs

D. 3. Energy Minimizations

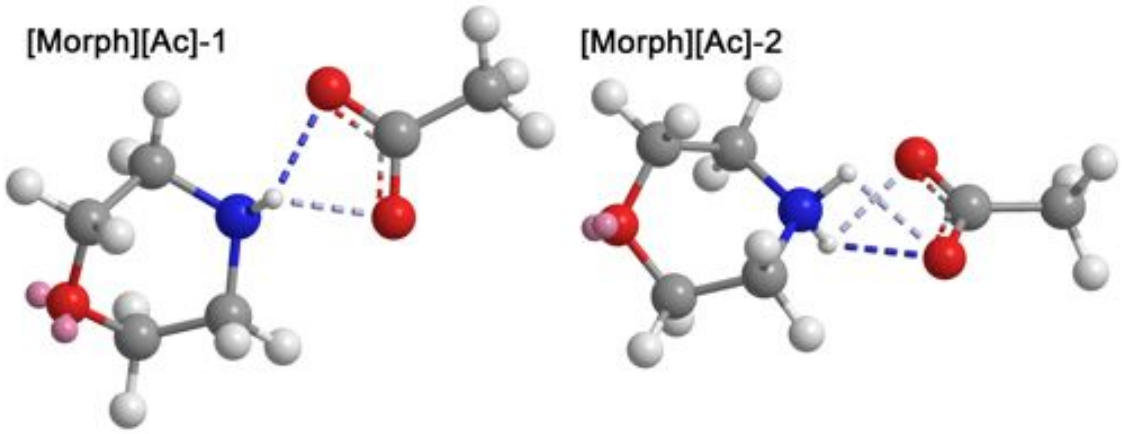

Figure D. 19. Minimum energy structures of the hybrid PIL [Morph][Ac] using one ionic couple.

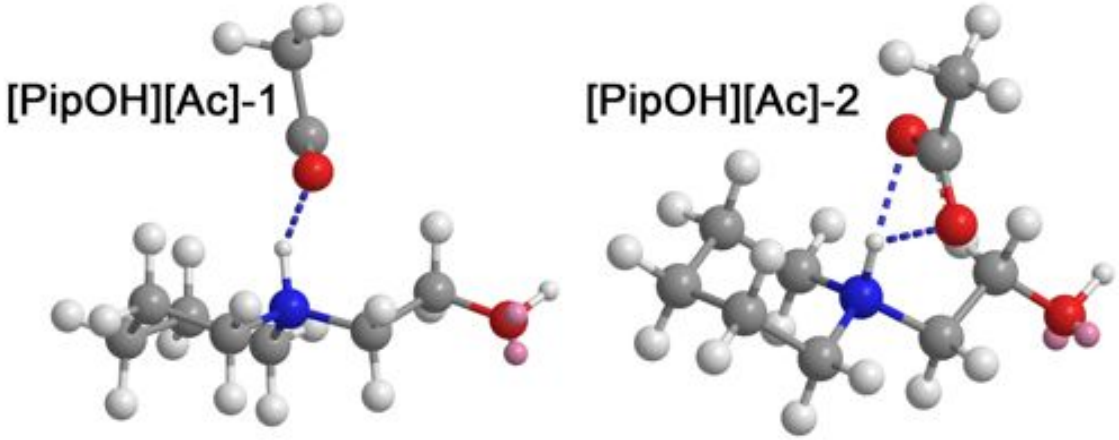

Figure D. 20 Minimum energy structures of the hybrid PIL [PipOH][Ac] using one ionic couple.

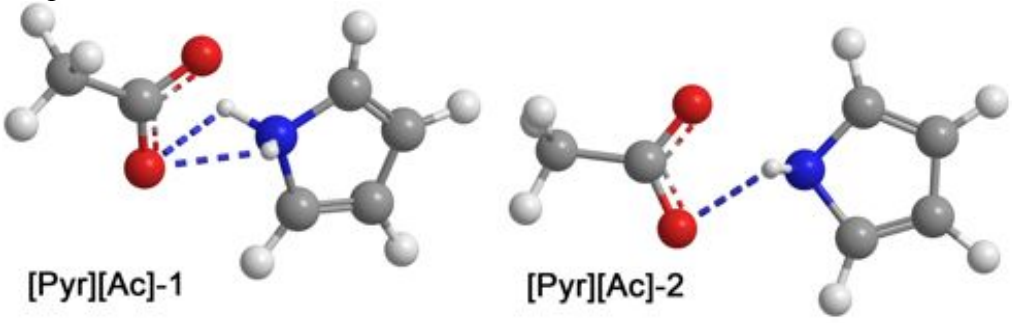

Figure D. 21. Minimum energy structures of the hybrid PIL [Pyr][Ac] using one ionic couple.

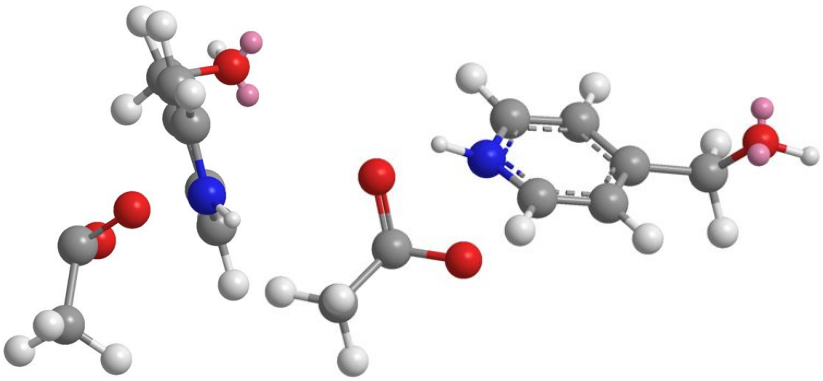

Figure D. 22. Minimum energy structures of the hybrid PIL [PyMe][Ac] using one ionic couple.

D. 4 Raman Spectroscopy

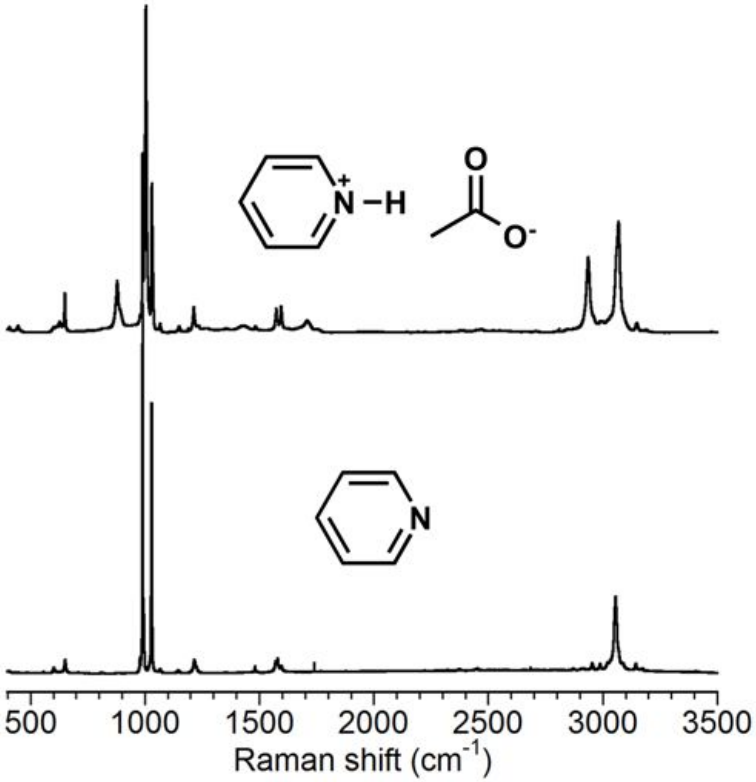

Figure D. 23. Raman Spectra (400 cm^{-1} to 3500^{-1}) for the [Py][AC] PIL.

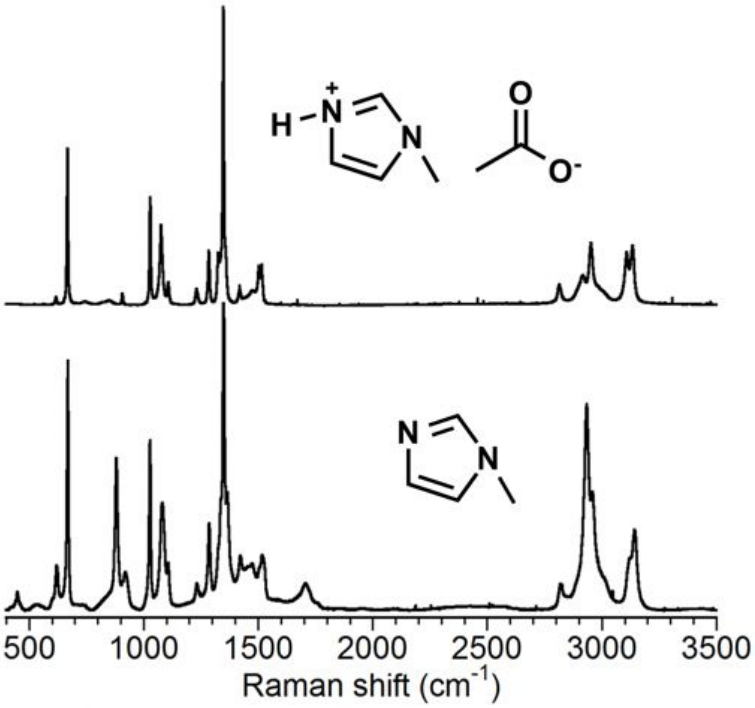

Figure D. 24. Raman Spectra (400 cm^{-1} to 3500^{-1}) for the [Mim][AC] PIL.

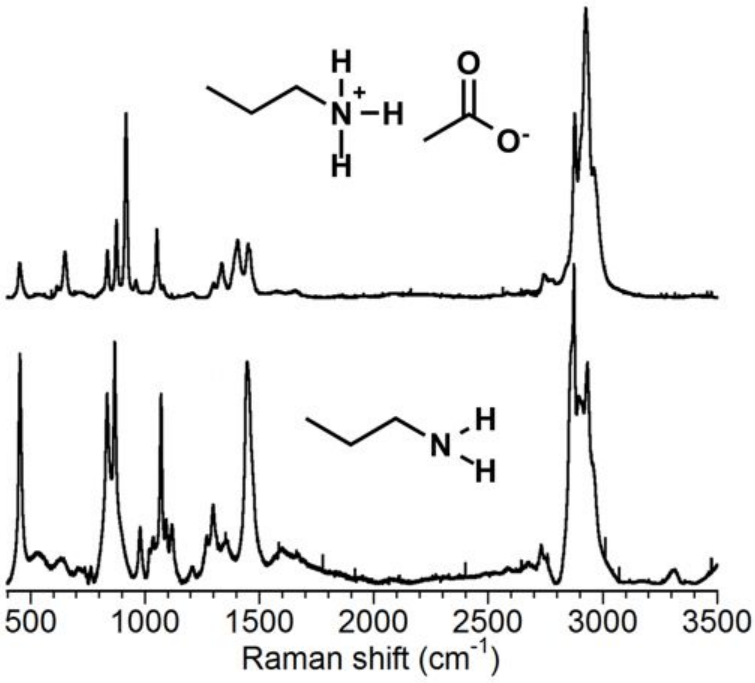

Figure D. 25. Raman Spectra (400 cm^{-1} to 3500^{-1}) for the [Prop][AC] PIL.

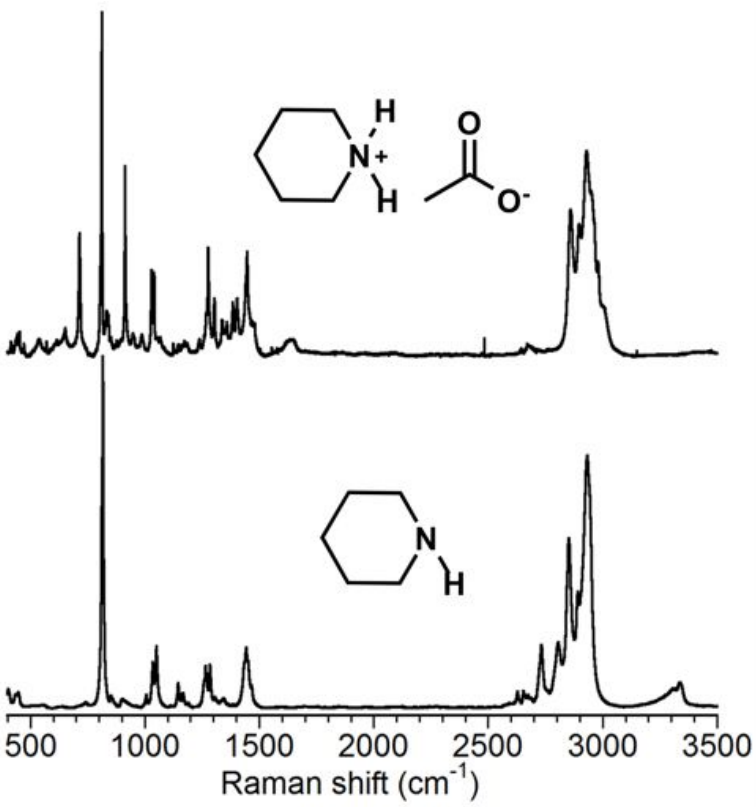

Figure D. 26. Raman Spectra (400 cm^{-1} to 3500^{-1}) for the [Pip][AC] PIL.

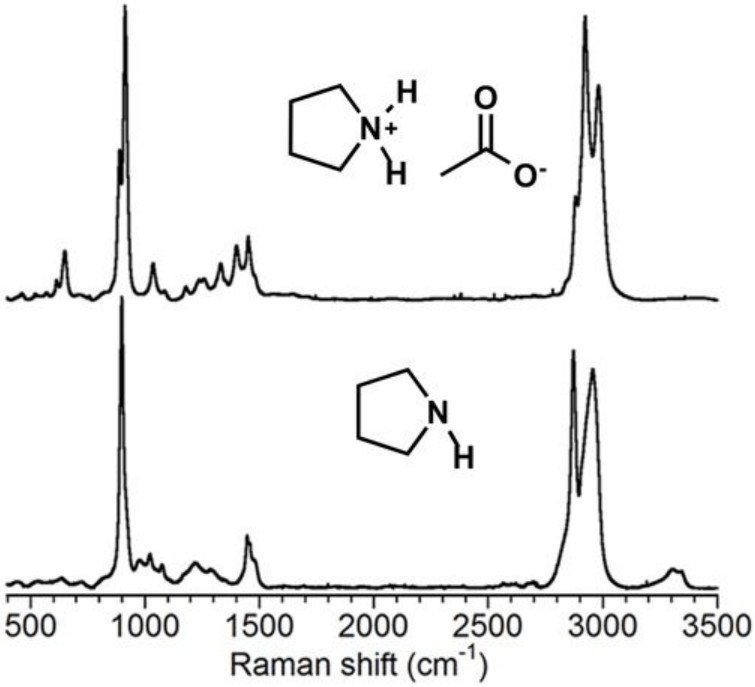

Figure D. 27. Raman Spectra (400 cm^{-1} to 3500^{-1}) for the [Pyrr][AC] PIL.

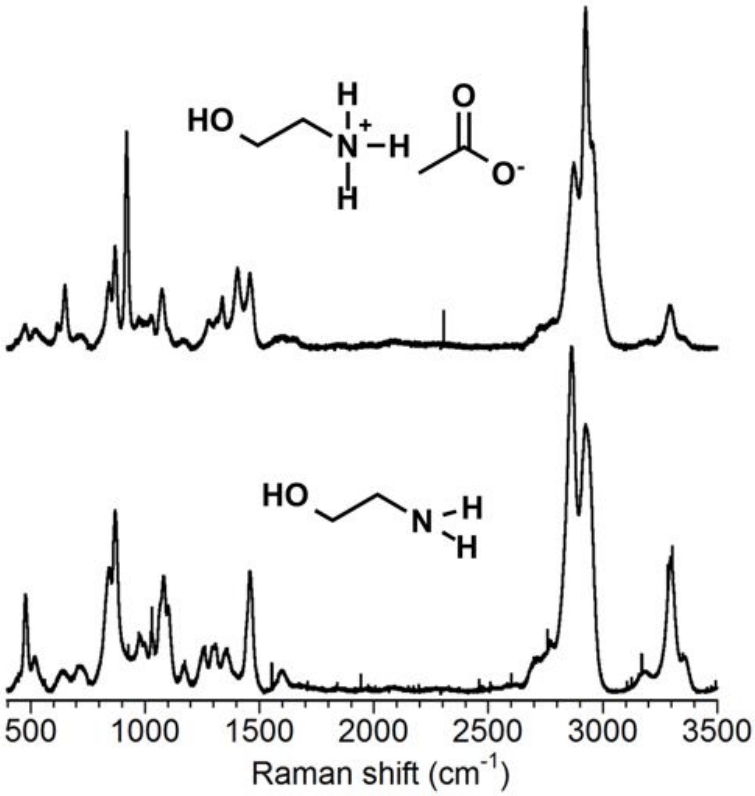

Figure D. 28. Raman Spectra (400 cm^{-1} to 3500^{-1}) for the [Py][AC] PIL.

APPENDIX E: Supplementary Information-Chapter 5

E. 1. PIL Characterization

Additional characterization of the PILs was also conducted to examine their thermal phase behavior (DSC) (Figure X).

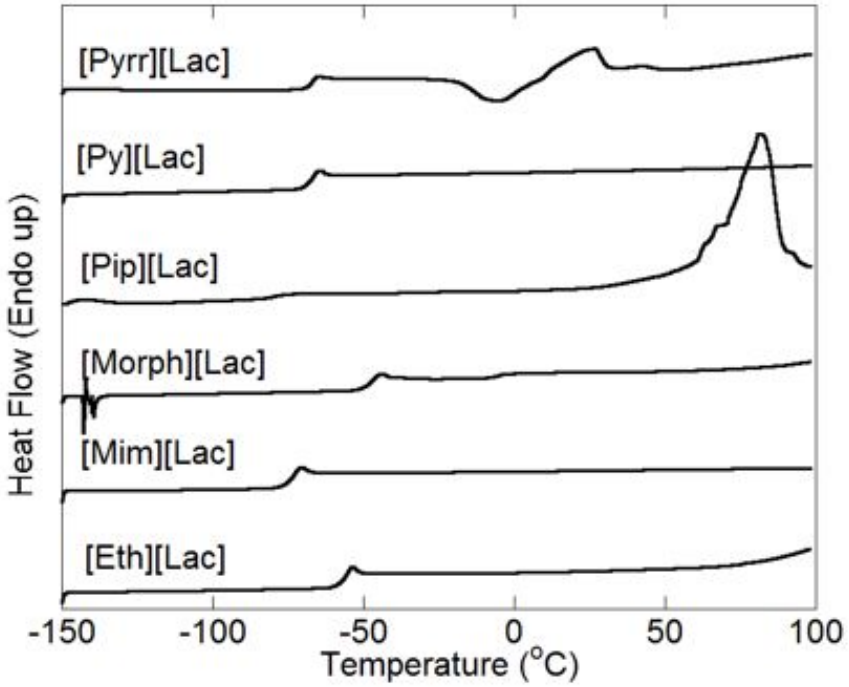

Figure E. 1. DSC heating traces of the lactate-based PILs used for this study.

E. 2. Biopolymer Solubility Tests

Figure E. 2. Images depicting the solubility of 5% w/w commercially available biomass components (Kraft lignin, microcrystalline cellulose and xylan) in the OAA PILs and reagents tested. The top depicts the solubility after stirring for 30 min at room temperature (25 °C) and the bottom shows after stirring for 24 h at 90 °C. Sample sizes were typically 10 g.

E. 3. Biopolymer Solubility Tests–with solvents.

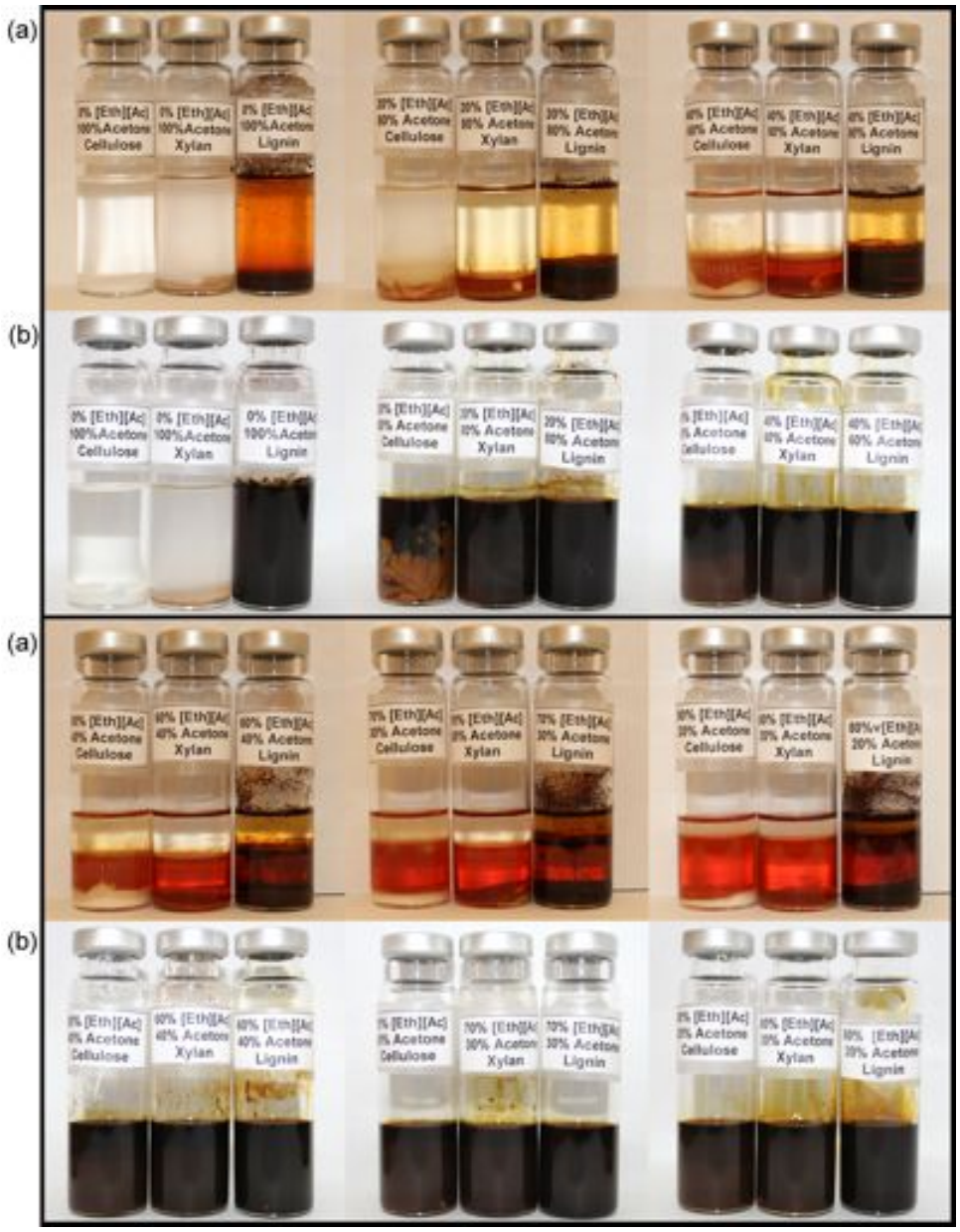

Figure E. 3. Images depicting the solubility of 5% w/w commercially available biomass components (Kraft lignin, microcrystalline cellulose and xylan) in the various concentrations of actetone mixtures,: (a) after stirring for 30 min at room temperature (25 °C) and (b) after stirring for 24 h at 90 °C (sample sizes were 10.0 g).

Figure E. 4. Images depicting the solubility of 5% w/w commercially available biomass components (Kraft lignin, microcrystalline cellulose and xylan) in the various concentrations of ethanol mixtures,: (a) after stirring for 30 min at room temperature (25 °C) and (b) after stirring for 24 h at 90 °C (sample sizes were 10.0 g).
Please note that the images for (b) are in a different order than (a).